

**The effects of long-term drainage on processes
governing CO₂ and CH₄ fluxes
on an Arctic floodplain in Siberia**

Dissertation

To Fulfill the
Requirements for the Degree of
„doctor rerum naturalium“ (Dr. rer. nat.)

**Submitted to the Council of the Faculty
of Biology and Pharmacy
of the Friedrich Schiller University Jena**

**by Minjung Kwon,
M.Sc. in Civil and Environmental Engineering**

born on April 16, 1986 in Seoul, Republic of Korea

Reviewers (Gutachter):

Prof. Dr. Kirsten Küsel	Aquatic Geomicrobiology, Institute of Ecology, Friedrich Schiller University, Jena, Germany
PD Dr. Gerd Gleixner	Max Planck Institute for Biogeochemistry, Jena, Germany
Prof. Dr. Lars Kutzbach	Institute of Soil Science, Department of Earth Sciences, University of Hamburg, Hamburg, Germany

Date of defense: November 23, 2016

Summary

Arctic ecosystems have acted as a carbon sink, having accumulated more than 1000 Pg of carbon in soils. As a part of global climate change, increasing atmospheric temperatures may thaw ice-rich permafrost in the Arctic, modifying soil topography and hydrology. Soil hydrology significantly affects carbon cycling, and thus, it needs to be considered when predicting Arctic ecosystems' response to climate change. This study investigates how long-term (>10 years) drainage, i.e., mimicking dry conditions following permafrost thaw, affects CO₂ and CH₄ fluxes in an Arctic floodplain in the growing and nongrowing seasons. In addition, the contributions of ecosystem properties, such as plant and microbial community structures and soil temperatures to variations in fluxes are examined. To answer these questions, a study site was set up on a floodplain in northeastern Siberia with two areas in parallel: one area that has been drained since 2004 and the other that has not been manipulated.

A decade-long drainage shifted dominant vegetation species from *E. angustifolium* to *C. appendiculata* and the abundance of shrubs increased. In addition, drainage considerably altered soil temperatures: temperatures were warmer at shallow layers due to lower heat capacity, but colder at deep layers due to lower thermal conductivity of dry organic soils above it. Moreover, reduced fractions of methanogens and methanotrophs were observed following drainage. These changes in ecosystem properties considerably affected CO₂ and CH₄ fluxes.

Drainage weakened CO₂ uptake strength, while accelerated emission rates in the growing season through plants and soil temperatures. *C. appendiculata* photosynthesized significantly less than *E. angustifolium* by up to 50%, but this decrease in CO₂ uptake was slightly offset by the increased abundance of shrubs. Warmer surface soils in drained areas resulted in increased CO₂ emission to the atmosphere, i.e., heterotrophic respiration, by up to 95%. $\Delta^{14}\text{C}$ of respired CO₂ revealed that decomposition of young, shallow soil organic matter was accelerated in the drained areas, confirming that the increased rates of ecosystem respiration is largely attributed to warmer soil temperatures at shallow layers.

Drainage considerably decreased CH₄ fluxes in the growing season as well. More oxic conditions substantially reduced CH₄ fluxes, and changes in ecosystem properties also contributed to this decrease. A decrease in the abundance of *E. angustifolium* contributed to lowered CH₄ emissions because *E. angustifolium* transported approximately 25% of the total CH₄ from soils to the atmosphere through aerenchyma structure in the control area. In addition, changes in soil temperatures reduced CH₄ fluxes in the drained areas, with potentially decreased rates of methanogenesis and increased rates of CH₄ oxidation. This was because CH₄ production and oxidation dominantly took place in deep and shallow soils, respectively. Furthermore, substantially reduced fractions of CH₄-associated microorganisms were coincided with lower CH₄ fluxes, implying CH₄ cycling can become less pronounced with drainage.

In the nongrowing season, although the magnitude of fluxes was lower compared to the growing season, CO₂ and CH₄ flux rates were higher in the drained area by four times and 10%, respectively. Considering roughly three times longer period and high sporadic fluxes, the contributions of CH₄ fluxes in the nongrowing season to the annual fluxes can be significant. Sporadically high fluxes were observed in the presence of *E. angustifolium* under decreasing air pressure, suggesting that while low air pressure promoted outgassing of CO₂ and CH₄ from soils, *E. angustifolium* could have acted as a path for gases in soils to the atmosphere.

Findings in this study revealed that ten years of drainage weakened CO₂ uptake strength, accelerated CO₂ emission rates, and significantly lowered CH₄ fluxes on an Arctic floodplain through modified plant and microbial communities, as well as soil temperatures. With warming temperatures, ice-rich permafrost thaw may considerably change soil hydrology and carbon cycling patterns in the Arctic. This study emphasizes the importance of considering drainage effects when predicting Arctic ecosystems' response to climate change, and the importance of long-term studies that investigate modifications in ecosystem properties that are closely linked to each other, and collectively affect CO₂ and CH₄ fluxes.

Zusammenfassung

Arktische Ökosysteme agierten in der Vergangenheit als Kohlenstoffsенke und haben im Laufe der Jahrtausende mehr als 1000 Pg Kohlenstoff im Boden angesammelt. Infolge steigender Temperaturen im Rahmen des globalen Klimawandels könnte eisreicher Permafrost in der Arktis abtauen, was zu Veränderungen in der Topographie und Hydrologie des Bodens führen kann. Die Bodenhydrologie hat bedeutenden Einfluss auf den Kohlenstoffkreislauf, weshalb sie berücksichtigt werden muss, wenn Einschätzungen zur Reaktion von arktischen Ökosystemen auf den Klimawandel gemacht werden. Diese Studie untersucht, wie sich eine langjährige (>10 Jahre) Entwässerung eines arktischen Überflutungsgebiets, welche trockenere Verhältnisse nach Permafrost-Degradation simuliert, auf die CO₂ und CH₄ Flüsse sowohl innerhalb als auch außerhalb der Vegetationsperiode auswirkt. Darüber hinaus werden die Einflüsse der Ökosystem-Eigenschaften, wie beispielsweise pflanzliche und mikrobielle Gemeinschaftsstrukturen und Bodentemperaturen, auf Schwankungen dieser Flüsse untersucht. Um diese Fragen zu beantworten, wurde ein Messprogramm mit zwei parallel betriebenen Untersuchungsflächen auf einer Überflutungsebene im Nordosten Sibiriens installiert: Eine dieser Teilflächen wird seit 2004 durch einen Drainagegraben entwässert, während der zweite Standort ungestörte Bedingungen repräsentiert.

Durch die langjährige Entwässerung wurde Wollgras (*E. angustifolium*) von Seggen (*C. appendiculata*) als dominante Vegetationsart abgelöst und der Bedeckungsgrad an Sträuchern erhöhte sich. Zudem veränderte sich die Bodentemperatur durch die Entwässerung deutlich: In oberflächennahen Schichten wurden erhöhte Temperaturen beobachtet, während die reduzierte thermische Leitfähigkeit von trockenem organischen Bodenmaterial zu einer Abkühlung in tieferen Schichten führte. Darüber hinaus zeigte sich, dass die Entwässerung die Population von sowohl methanogenen als auch methanotrophen Mikroorganismen reduzierte. Beide Veränderungen der Ökosystem-Eigenschaften beeinflussen die Flüsse von CO₂ und CH₄ erheblich.

Durch die weiter oben aufgeführten Änderungen von Vegetationsgemeinschaft und Bodentemperaturen reduzierte die Entwässerung die CO₂-Aufnahmekapazität durch Photosynthese, während gleichzeitig die Respirationsraten erhöht wurden. *C. appendiculata* haben eine um bis zu 50% niedrigere Photosyntheserate im Vergleich zu *E. angustifolium*,

wobei die Verringerung der CO₂-Aufnahme teilweise durch den höheren Bedeckungsgrad an Sträuchern ausgeglichen wurde. Aus den wärmeren Bedingungen in oberflächennahen Bodenschichten der trockeneren Standorte resultierte eine Zunahme der Ökosystem-Respiration von bis zu 95%. Eine Analyse des Radiokarbon ($\Delta^{14}\text{C}$) Signals von respiriertem CO₂ bestätigte, dass diese erhöhte Respiration vor allem dem beschleunigten Abbau von jungen organischen Substanzen im Oberboden zugeordnet werden konnte.

Eine Abnahme der Methanemissionen während der Vegetationsperiode konnte mit den veränderten Bodentemperaturen, verstärkt aeroben Bedingungen sowie der geringeren Verbreitung von *E. angustifolium* nach langfristiger Absenkung des Wasserspiegels in Verbindung gebracht werden. Der Transport von Methan durch die Hohlraumstrukturen von Wollgräsern kann bis zu 25% der Gesamtemissionen ausmachen. Reduzierte Temperaturen in tieferen Schichten als Folge von Entwässerung führen zu einer Abnahme der Methanbildung, gleichzeitig fördern jedoch warme und trockene Bedingungen im Oberboden die Methanoxidation. Zudem zeigte sich ein Zusammenhang zwischen verringerten Methanemissionen und der Gesamtpopulation der mit Methan assoziierten Mikroorganismen, woraus geschlossen werden kann, dass die Entwässerung zu einem insgesamt weniger ausgeprägten Methankreislauf führt.

Außerhalb der Vegetationsperiode waren die gemessenen Kohlenstoff-Flüsse generell geringer, jedoch zeigten sich im entwässerten Gebiet bis zu 4-mal bzw. 10% höhere Flüsse für CO₂ und CH₄ als in dem Kontrollgebiet. Aufgrund der etwa dreimal längeren Zeitspanne im Vergleich zur Wachstumsperiode können gerade die vereinzelt hohen Flussraten von Methan, die außerhalb der Vegetationsperiode beobachtet wurden, für die gesamte jährliche Bilanz relevant sein. Vereinzelt hohe Flüsse wurden vor allem an Standorten mit *E. angustifolium* und Zeiträumen mit fallendem Luftdruck beobachtet, was darauf hinweisen kann, dass *E. angustifolium* als Transportkanal für Gase aus dem Boden in die Atmosphäre dient, während der Druckunterschied zwischen Boden und Atmosphäre als Auslöser für Emissionen fungiert.

Die Ergebnisse dieser Studie zeigen, dass die langjährige Entwässerung eines arktischen Überschwemmungsgebiets zu einer verringerten Aufnahme von CO₂ durch Photosynthese, einer erhöhten Abgabe von CO₂ durch Respiration sowie zu deutlich verringerten Methanemissionen führt. Als dominante Kontrollfaktoren für diese systematischen Änderungen des Kohlenstoff-Kreislaufs wurden in diesem Zusammenhang die veränderten

Pflanzen- und Mikrobengemeinschaften, sowie modifizierte Bodentemperaturen identifiziert. Die Degradation von eisreichem Permafrostboden aufgrund von höheren Lufttemperaturen kann dazu führen, dass sich die Bodenhydrologie und der Kohlenstoffkreislauf in der Arktis in Zukunft deutlich verändern werden. Diese Studie verdeutlicht die Bedeutung von Entwässerungseffekten auf Permafrost-Ökosysteme und unterstreicht somit die Relevanz der Berücksichtigung von hydrologischen Bedingungen in Vorhersagemodellen zur Simulation arktischer Ökosysteme unter zukünftigen Klimawandel-Szenarien. Zudem konnte die Bedeutung von Langzeitstudien, die die Veränderungen der Ökosystemeigenschaften untersuchen, herausgestellt werden, da sich wichtige Einflussfaktoren auf die Kohlendioxid- und Methanflüsse teilweise nur sehr langsam an die neuen Umweltbedingungen anpassen.

Table of Contents

Summary	I
Zusammenfassung	III
List of Tables.....	IX
List of Figures	X
Chapter 1. Introduction.....	1
1.1 The carbon cycle between the atmosphere and the terrestrial ecosystem	1
1.2 Arctic tundra.....	3
1.3 Global climate change and its effects on the carbon cycle in the Arctic.....	3
1.4 Manipulation experiment to investigate climate change impacts on Arctic ecosystems.....	4
1.5 Objectives.....	7
Chapter 2. Methodology.....	10
2.1 Study site.....	10
2.1.1 Site description	10
2.1.2 Experiment setup.....	11
2.1.3 Field campaigns.....	12
2.2 Flux measurements.....	13
2.2.1 CO ₂ and CH ₄ flux rates.....	13
2.2.2 CH ₄ pathways	15
2.2.3 Interpolation of growing-season CO ₂ fluxes	16
2.2.4 R _h rates	19
2.3 R _{eco} partitioning.....	19
2.3.1 Radiocarbon signatures of R _{eco}	19
2.3.2 Radiocarbon signatures of sources	20
2.3.3 Source partitioning	20
2.4 WTD, TD, and T _{soil}	22
2.5 Plant community structure.....	22
2.6 Soil carbon content.....	23
2.7 Microbial community structure.....	23
2.7.1 DNA extraction	23

2.7.2 Illumina sequencing and data processing.....	24
2.7.3 Quantitative PCR	24
2.8 Data analysis	24
2.8.1 Ecosystem properties	24
2.8.2 Environmental effects on CO ₂ flux rates.....	25
2.8.3 Environmental effects on CH ₄ flux rates.....	26
Chapter 3. Results	28
3.1 Changes in ecosystem properties	28
3.1.1 WTD changes from drainage	28
3.1.2 Shifts in Tsoil and TD.....	28
3.1.3 Plant community structure	28
3.1.4 Microbial community structure.....	32
3.2 Growing-season CO ₂ fluxes.....	35
3.2.1 Tsoil effects on growing-season CO ₂ fluxes	35
3.2.2 Plant effects on growing-season CO ₂ fluxes	36
3.2.3 Gap-filled growing-season CO ₂ flux rates	38
3.2.4 Model error from interpolation	39
3.3 R _{eco} partitioning.....	40
3.3.1 Δ ¹⁴ C of R _{eco} and sources.....	40
3.3.2 Drainage effects on R _{eco} and its patterns	41
3.4 Growing-season CH ₄ fluxes.....	44
3.4.1 Tsoil effects on growing-season CH ₄ fluxes	44
3.4.2 Plant effects on growing-season CH ₄ fluxes	45
3.4.3 Microbial effects on growing-season CH ₄ fluxes.....	46
3.4.4 Growing-season CH ₄ flux rates.....	46
3.5 Nongrowing-season CO ₂ and CH ₄ fluxes	49
Chapter 4. Discussion.....	52
4.1 Drainage effects on ecosystem properties.....	52
4.1.1 Changes in WTD following drainage.....	52
4.1.2 Changes in Tsoil following drainage	52
4.2 Growing-season CO ₂ fluxes.....	53
4.2.1 Tsoil effects on growing-season CO ₂ fluxes	53

4.2.2 Plant effects on growing-season CO ₂ fluxes	54
4.2.3 The source of the increase in R _{eco} rates	55
4.3 Growing-season CH ₄ fluxes	57
4.3.1 Tsoil effects on growing-season CH ₄ fluxes	57
4.3.2 Plant effects on growing-season CH ₄ fluxes	58
4.3.3 Microbial effects on growing-season CH ₄ fluxes.....	59
4.4 Nongrowing-season CO ₂ and CH ₄ fluxes.....	60
4.5 Assessment of methodology.....	61
4.5.1 Flux measurements with chamber systems	61
4.5.2 Application of isotopes in the carbon cycle studies	63
4.5.3 Microorganisms in the carbon cycle studies	64
Chapter 5. Synthesis and Conclusion.....	65
5.1 Drainage effects on ecosystem properties, and CO ₂ and CH ₄ fluxes	65
5.2 Drainage effects on ecosystems' sensitivity to climate.....	67
5.3 Interactions among ecosystem properties.....	69
5.4 Conclusions and outlook	70
References	72
Acknowledgement.....	89
Declaration of independent completion of dissertation.....	91
Published or pending manuscripts.....	92

List of Tables

Table 1.1 CO ₂ flux changes (g C-CO ₂ m ⁻² day ⁻¹) in response to a decrease in water table depth (WTD) in the Arctic.	6
Table 1.2 CH ₄ flux changes (mg CH ₄ m ⁻² day ⁻¹) in response to a decrease in water table depth (WTD) in the Arctic.	7
Table 2.1 Water table depth (WTD) and vegetation characteristics of each plot.	13
Table 2.2 Δ ¹⁴ C (mean ± standard error) of three sources, i.e., surface soil, deep soil, and autotrophs.	21
Table 2.3 The settings used for CMAGEP runs.	27
Table 3.1 Groups of methanogens found and substrates each group uses.	34
Table 3.2 Groups of methanotrophic bacteria, and enzymes that each group possesses.	34
Table 3.3 Average daily flux (g C-CO ₂ m ⁻² day ⁻¹) from interpolation for the period of 22 July to 10 August (20 days) in both 2013 and 2014.	39
Table 3.4 Root mean squared error (RMSE) and mean bias error (MBE) of the observed and interpolated fluxes (mg C-CO ₂ m ⁻² s ⁻¹).	40
Table 3.5 Multiple linear regressions with Δ ¹⁴ C of ecosystem respiration (R _{eco}) as the dependent variable.	42
Table 3.6 Multiple linear regressions with contributions of surface soil (SS) and deep soil (DS) as the dependent variable.	43
Table 3.7 Daily and cumulative CH ₄ fluxes.	46
Table 3.8 Contribution of plant-mediated CH ₄ transport and ebullition to the total CH ₄ fluxes.	48

List of Figures

Figure 1.1 A schematic describing the environmental factors, as well as CO ₂ and CH ₄ fluxes that will be investigated in this study.	9
Figure 2.1 Maps of the study site in Chersky, northeastern Siberia.	10
Figure 2.2 Examples of the measured CH ₄ concentration ([CH ₄]) change.	16
Figure 2.3 One example of distributions of possible f values (i.e., source contributions) derived from partitioning.	21
Figure 3.1 Spatial and temporal variability in water table depth (WTD).	29
Figure 3.2 Soil temperatures (T _{soil}) and thaw depths (TD) against water table depths (WTD).	30
Figure 3.3 The abundance of vegetation species observed across the transects in 2003 and 2013.	31
Figure 3.4 The fractions of CH ₄ -related microorganisms, (a) methanogenic groups and (b) methanotrophic groups by depth.	33
Figure 3.5 Gene copy numbers of archaea and bacteria by depth.	35
Figure 3.6 Links between average soil temperatures at 5 cm and gross primary production (GPP) and ecosystem respiration (R _{eco}) rates.	36
Figure 3.7 Growing-season CO ₂ fluxes by vegetation type in 2013.	37
Figure 3.8 Logarithmic relations between photosynthetically active radiation (PAR, X axis) and gross primary production (GPP, Y axis) by transect (columns), vegetation type (color) and year (rows).	38
Figure 3.9 $\Delta^{14}\text{C}$ of ecosystem respiration (R _{eco}) and contributions of surface soil (SS), deep soil (DS), and autotrophs (AT) to R _{eco}	41
Figure 3.10 Relationships between $\Delta^{14}\text{C}$ of ecosystem respiration and the <i>Eriophorum angustifolium</i> abundance that is abundant in wet areas.	42
Figure 3.11 Relationships between source contributions and the <i>Eriophorum angustifolium</i> abundance that is abundant in wet areas.	42

Figure 3.12 Ecosystem respiration (R_{eco}) with partitioned sources (mean \pm standard error).	43
Figure 3.13 Relationships between soil temperatures and growing-season CH_4 fluxes.	44
Figure 3.14 The abundance of <i>Eriophorum angustifolium</i> and its relationship with CH_4 fluxes.	45
Figure 3.15 CH_4 fluxes during the growing season of 2013 and 2014.	47
Figure 3.16 CO_2 and CH_4 fluxes in the nongrowing season against the changes in air pressure.	50
Figure 4.1 The total aboveground dry biomass (mean \pm standard deviation) of standing dead and living plants, measured in 2003 ($N = 20$) and 2013 ($N = 4$).	55
Figure 4.2 Positive correlations between CO_2 and CH_4 that are transported through <i>Eriophorum angustifolium</i> in the growing season.	57
Figure 5.1 Ten years of drainage altered ecosystem characteristics, and, subsequently, (a) CO_2 and (b) CH_4 fluxes.	66

Chapter 1. Introduction

1.1 The carbon cycle between the atmosphere and the terrestrial ecosystem

The term ‘carbon cycle’ refers to the biogeochemical cycle that exchanges carbon between different compartments of the Earth system, i.e., biosphere, pedosphere, geosphere, hydrosphere and atmosphere. The presented research will focus on the relatively fast processes between the terrestrial ecosystems and the atmosphere. The most noticeable carbon flow from the atmosphere to the terrestrial ecosystem is the carbon dioxide (CO₂) uptake by vegetation (i.e., photosynthesis). The total amount of CO₂ that is assimilated by primary producers during the photosynthesis at the ecosystem level is termed *gross primary production (GPP)*¹. Approximately 40–52% of the total fixed carbon is used by the primary producers for building structures and synthesizing organic compounds (*net primary production, NPP*)^{2,3}, and the rest is respired back to the atmosphere (*autotrophic respiration, R_a*).

Carbon that has been accumulated in the terrestrial ecosystem through photosynthesis can be decomposed by a series of degradation processes. During these degradation processes, carbon can enter or leave the system laterally in various forms^{4,5}, as well as by leaching in the event of precipitation or continuously in inundated soils^{1,6,7}. In addition, carbon can leave the terrestrial ecosystem to the atmosphere, as final gaseous product of decomposition processes: soil carbon can be completely oxidized to CO₂ in the presence of sufficient oxygen (O₂), e.g., in shallow soil layers. When O₂ is absent or present in low concentrations, e.g., in inundated soils or in deep anoxic soil layers, soil carbon is decomposed anaerobically. Anaerobic processes include anaerobic respiration, e.g., fermentation, that produces CO₂ and methanogenesis that produces methane (CH₄)^{8,9} as final gaseous product. In inundated soils, such as in wetlands, CH₄ takes a large part in the carbon cycle¹⁰⁻¹³, and is produced by mainly two types of methanogens, i.e., hydrogenotrophic and acetoclastic methanogens. The former utilizes H₂ as electron donors and reduces CO₂ to produce CH₄, while the latter ferments acetate and produces CH₄ and CO₂. Hydrogenotrophic methanogenesis occurs when CO₂ is the only terminal electron acceptor after O₂, NO₃⁻, SO₄²⁻, Fe³⁺, and Mn⁴⁺ are depleted or

limiting, so that they are not outcompeted for H_2 by dissimilatory reducing bacteria^{9,14,15}. Acetoclastic methanogens yields much less energy than hydrogentrophic methanogens through acetate fermentation, and they are also outcompeted by acetate-using sulfate reducers¹⁶.

Aerobically and anaerobically produced CO_2 and CH_4 predominantly leave the terrestrial ecosystem through vertical exchange with the atmosphere, while carbon export as dissolved gas through lateral water flow plays a role in a few ecosystem types¹⁷. The sum of CO_2 that is produced through decomposition processes and leaves from the terrestrial ecosystem to the atmosphere is termed *heterotrophic respiration* (R_h), and the total amount of CO_2 emitted to the atmosphere, the sum of R_a and R_h , in ecosystem level is termed *ecosystem respiration* (R_{eco}). While CH_4 moves upward from deep anaerobic soil layers to the atmosphere, it can be oxidized to CO_2 in upper aerated soils^{18,19}. In aerated surface soils atmospheric CH_4 can be also oxidized to CO_2 by methanotrophic bacteria²⁰⁻²², which further influence CH_4 and CO_2 fluxes between atmosphere and the terrestrial ecosystems.

At the ecosystem level, GPP is primarily controlled by the length of the growing season²³⁻²⁵, leaf area index (LAI)²⁶, water and nutrient availability, and local climate conditions such as air temperature (T_a) and solar radiation¹. The environmental parameters that influence GPP primarily have an effect on R_a rates because autotrophs utilize approximately 50% of NPP and respire the rest^{2,3}, although the ratio of GPP to autotrophic respiration can vary with environmental conditions, such as temperature and nitrogen availability^{27,28}. Factors that affect R_h include temperature²⁹⁻³¹, litter quantity and quality^{32,33}, and soil conditions, such as moisture, oxygen, and acidity^{30,31,34}. Highly anoxic soil conditions with redox potential below -250 mV are essential for CH_4 production⁹, and water levels in wetlands can be used as a proxy for anaerobic conditions^{13,35}. Conversely, CH_4 oxidation rates increase with oxic conditions^{18,19}. The depletion of terminal electron acceptors, such as O_2 , NO_3^- , SO_4^{2-} , Fe^{3+} , and Mn^{4+} , is necessary for CH_4 production, so that CO_2 can be the only electron acceptors for methanogens^{9,14,15}. Plant community composition also plays a critical role in CH_4 fluxes³⁶⁻⁴², mainly because aerenchymatous plant species promote CH_4 emissions by providing effective transport pathways for CH_4 from deep soils to the atmosphere^{37,39,40,42}, while mosses significantly reduce CH_4 emission by oxidizing CH_4 ⁴². Temperatures positively influence both CH_4 production⁴³⁻⁴⁵ and oxidation^{43,46} until optimal temperature thresholds are reached.

1.2 Arctic tundra

The Arctic is a region located within the north of the Arctic Circle (i.e., 66° 33' N). Tundra is the most common type of biome in the Arctic, and it covers approximately 8% of the global land cover⁴⁷. The Arctic tundra is characterized by limited growth of trees due to low T_a and the existence of permafrost belowground⁴⁸. Permafrost refers to soil, whose temperature remains at or below 0 °C for two or more consecutive years. Permafrost covers most of the Arctic, and 24% of the exposed land surface of the Northern Hemisphere⁴⁹. Permafrost can be 100–500 m thick in North America and >500 m thick in Siberia⁵⁰. Arctic tundra can be divided into four categories depending on soil moisture conditions: aquatic, wet, moist, and dry tundra⁵¹. Except for dry tundra that occurs on the slope of mountain ranges where water drains well, Arctic tundra is characterized by predominantly wet soil conditions because surface water cannot drain to deeper soil layers due to the presence of permafrost.

In the Arctic tundra, the mean annual NPP is estimated to be 180 g dry mass m^{-2} ⁵², which is lower than that of other ecosystems, e.g., 380 dry mass $g m^{-2}$ in boreal forests which are affected by similar climate conditions⁵². Low temperatures and the frozen ground that limits water availability also inhibit decomposition processes in permafrost regions. As a result, more than 1000 Pg of carbon has accumulated in the upper 3 m of soils within the permafrost regions^{53–55}, which corresponds to approximately 40% of the global soil organic carbon^{56,57}.

1.3 Global climate change and its effects on the carbon cycle in the Arctic

The average global surface temperature has increased *ca.* 0.25 °C per decade since the late 20th century⁵⁸, and the increase rate in the Arctic is higher than in other regions. These pronounced temperature gradients at high northern latitudes are called Arctic amplification, and it is dominantly caused by changes in surface properties linked to the ice-albedo-feedback and the shallow Arctic atmosphere^{59,60}. The increase in global temperatures, including the Arctic, is forecast to continue in the future^{61–63}. Under warmer conditions, permafrost may become subject to degradation through increased thawing of previously frozen soil layers, which alters soil topography and soil hydrology depending on the ice content of permafrost. Thawing of ice-rich permafrost, e.g., permafrost with abundant ice wedges and ice lenses⁶⁴, may result in local ground subsidence and wetter soil conditions^{65–69}. At the same time, areas surrounding the subsided ground will be subject to lateral drainage of water to the depressed areas, making soil surface drier. In addition to these spatial changes, soil hydrology varies

temporally. As permafrost thaw further progresses, water drainage can be promoted through connected troughs and to deeper soil layers, making surface soils drier^{67,70,71}. In an extended spatial and temporal scale, thermokarst lakes develop from extensive thawing of permafrost and they can be drained depending on local hydrological and topographical condition⁷², increasing⁶⁵ or decreasing⁷³ the number of thermokarst lakes. Furthermore, temporally and spatially varying soil hydrology in the Arctic following warming and permafrost thaw can be amplified or alleviated by changing precipitation patterns. Overall, precipitation in the Arctic has increased over the last five decades⁷⁴, and is forecast to continue increasing in the future due to intensified hydrological cycles^{61,75,76}. However, precipitation patterns are difficult to predict and characterized by high spatiotemporal variability^{77,78}. Therefore, shifts towards wetter and drier soil conditions as a consequence of warming and permafrost thaw can significantly vary across multiple spatiotemporal scales.

Warming temperature and changing soil hydrology substantially modify ecosystem properties that influence the carbon cycle in the Arctic. Warmer temperature with deeper thaw depths (TD) may establish a favorable environment for shrubs and trees to grow⁷⁹⁻⁸², which consequently affect ecosystem properties, e.g., albedo, and carbon turnover rates. Moreover, a vast amount of carbon stored in the permafrost may become vulnerable to decomposition under warmer conditions, emitting CO₂ and CH₄ to the atmosphere⁵⁴. With ongoing global climate change and even greater changes forecast for the Arctic, observing the responses of the Arctic ecosystems is of great importance: whether continuing warming and changing soil hydrology in the Arctic change the ecosystems towards carbon sources, increasing the emission of CO₂ and CH₄ to atmospheric^{54,83-88}, or carbon sinks, amplifying photosynthetic rates that may compensate or exceed the elevated decomposition rates⁸⁹⁻⁹¹.

1.4 Manipulation experiment to investigate climate change impacts on Arctic ecosystems

Previous manipulation studies have focused on warming effects on the carbon cycle in the Arctic: warmer air as well as soil temperatures (T_{soil}) and the consequent permafrost thaw increased the rates of both GPP and R_{eco}⁹²⁻⁹⁴, including degradation of old soil carbon in deeper soil⁹⁵⁻⁹⁷. CH₄ emissions have been also observed to increase due to warming and permafrost thaw that are followed by wetter conditions⁹⁸. Yet, little is known about the effects of drying in the Arctic.

Some manipulation studies and comparison studies with varying water table depth (WTD) in the Arctic have shown that drier conditions generally increase the rates of GPP and R_{eco} ^{41,98–104}, and decrease CH_4 emissions^{98,100,105–108} in the growing season (Table 1.1 & Table 1.2). Increasing rates of R_{eco} can be attributed to elevated rates of R_{h} in more oxic conditions that is more efficient than in anoxic conditions¹⁰⁹. Plant productivity generally increases as well in drier conditions^{98,101,102}, implying R_{a} may also increase. Reduced rates of CH_4 emissions can be attributed to more oxic conditions^{98,100,105–108}. Although changes in GPP, R_{eco} and CH_4 fluxes generally showed similar patterns, the combined effects of the increased GPP and R_{eco} , as well as the magnitude of the reduction in CH_4 fluxes differed from ecosystem to ecosystem, due to varying observation period, vegetation types, and soil moisture conditions before and after the drying manipulation (Table 1.1 & Table 1.2).

Previous drying manipulation studies were restricted to short-term observations. Although short-term manipulation studies are capable of investigating the immediate effects of drying on CO_2 and CH_4 fluxes, they do not include changes in ecosystem properties, such as plant and microbial community composition, that may considerably modify CO_2 and CH_4 flux rates in the long term. Furthermore, despite the fact that nongrowing season CO_2 and CH_4 fluxes may considerably contribute to the annual carbon budget^{110–120}, observations in the nongrowing season have been limited in these studies. Because of the insulation provided by snow, T_{soil} remain warmer compared to T_{a} , and biological processes may continue throughout the nongrowing season^{111,113–115}. In addition, unlike in the growing season, CO_2 and CH_4 fluxes in the nongrowing season are often affected by physical factors, e.g., air pressure (P_{a}) gradients, because frozen state of soil water can hinder rates of soil processes and gas exchange between the terrestrial ecosystem and the atmosphere. While soil freezes, some waterlogged areas showed sporadically¹¹⁶ or constantly^{117–119} high CH_4 fluxes, partly due to variations in dominant plant species and WTD. However, higher CH_4 fluxes can be observed in drier tundra ecosystems¹²⁰. Due to limited number of studies, it is, yet, unclear how WTD variability affects CO_2 and CH_4 fluxes during the nongrowing season in the Arctic. To date, no studies have yet compared nongrowing-season CO_2 and CH_4 fluxes between wet and dry sites.

Table 1.1 CO₂ flux changes (g C-CO₂ m⁻² day⁻¹) in response to a water table depth (WTD) decrease. Changes are expressed as either flux_{control} – flux_{lower-WTD} or flux_{higher-WTD} – flux_{lower-WTD}. Negative net CO₂ flux rates represent a net increase in terrestrial CO₂ uptake; positive changes denote a decrease in net CO₂ uptake by the terrestrial ecosystem or an increase in terrestrial CO₂ emissions to the atmosphere. The ranges of these changes are partly due to different years, soil types, and study sites. Numbers in parentheses represent percent change compared to the original (control, WTD condition) flux rates.

Sites	WTD change	Net CO ₂ flux change		Ref.
Coastal plain	Drawdown	+0.59	(+160%)	104
	3 cm lower	+0.23	(+87%)	102 (1)
	Up to 3.6 cm lower ⁽⁶⁾	+1.17	(+63%)	99 (2)
	7–7.5cm lower	+0.36 to +0.4	(+450% to +500%)	101
	8.5 cm lower	+2.99	(+365%)	100 (3)
	11.9 cm lower ⁽⁶⁾	+0.41	(+67%)	103 (3)
	20 cm lower ⁽⁶⁾	+0.72	(+37%)	41
Floodplain	20–35 cm lower	-0.06	(-47%)	105 (4)
Moist tundra	2.5 cm lower	-0.02	(-3%)	98 (5)
Laboratory	Saturated vs. field capacity	-2.63 to -1.41	(-1716 to -344%)	121
	5 cm lower	-0.61 to +0.96	(-59 to +72%)	122
	10 cm lower	+2.21	(+184%)	123

⁽¹⁾ Only data from 2008 were used, as this was the only time when the WTD of the drained area was lower than that of the control area.

⁽²⁾ Only from grassland data.

⁽³⁾ Only ecosystem respiration was considered (no gross primary production).

⁽⁴⁾ Only data from 2003 and 2005 were used, as these were the only years when climate conditions were similar.

⁽⁵⁾ Only data from 2013 were used, as this was the only time when the WTD of the drained area was lower than that of the control area.

⁽⁶⁾ WTD difference from natural variation instead of manipulation.

Table 1.2 CH₄ flux changes (mg CH₄ m⁻² day⁻¹) in response to a water table depth (WTD) decrease in the Arctic. Numbers in WTD are displayed relative to the soil surface, with positive values indicating standing water above the soil surface, and negative values indicating water level below the soil surface. Positive values of CH₄ fluxes denote net CH₄ emissions to the atmosphere, while negative values denote net CH₄ uptake by the terrestrial ecosystem. Presented flux rates are mean values of the observation period, and ranges come from spatial or temporal variability.

WTD (cm)			CH ₄ flux (mg CH ₄ m ⁻² day ⁻¹)			Location (lat., long.)	Ref.
Control	Dry, drained	Change	Control	Dry, drained	Change (%)		
Wet (-20 – 0)	Dry ⁽¹⁾ (-57 – -56)	46 – 57	5.4	-1.5	-129	69N, 52W	124
Wet (12)	Dry ⁽¹⁾ (-16 – -15)	27 – 28	271.0 – 290.2	-0.7 – -0.5	-100	68N, 161E	125
Wet (7)	Dry ⁽¹⁾ (-13)	20	144.6	69.4	-52	71N, 156W	41
Wet (5 – 20)	Dry ⁽¹⁾ (0)	5 – 20	26.2 – 177.1	-0.2 – 11.0	-101 – -94	70N, 147E	107 (2)
Wet (5)	Dry ⁽¹⁾ (-5)	10	73.2 – 165.5	-1.9	-103 – -101	68N, 161E	38
Wet	Dry ⁽¹⁾	NA	35.0 – 210	0	-100	68N, 18E	126
Wet	Dry ⁽¹⁾	NA	46.3	0.3	-99	71N, 130E	125
Wet	Dry ⁽¹⁾	NA	2.3 – 2198.4	-0.1 – 1.0	-103 – -100	78N, 11E; 78N, 15–16E	127 (3)
Wet	Drained	20 – 35	266.7	8	-97	69N, 161E	105 (4)
Wet (2.5)	Drained (-6)	8.5 – 15.9	48	31.9	-33	71N, 156W	100,108
Wet	Mesic ⁽¹⁾	NA	46.7	2.3	-95	66–77N	128
Flooded/wet/moist	Dry ⁽¹⁾	NA	6.4 – 67.2	-3.2 – 9.6	-109 – -86	71N, 157W	106
Flooded/wet/moist	Dry ⁽¹⁾	NA	20 – 85.3	4.1	-95 – -79	71N, 156W	40
Above/at Center (-5 – 0)	Below ⁽¹⁾ Rim ⁽¹⁾ (-40 – -35)	NA	44.3 – 78.8	11.4	-85 – -74	70N, 148W	36
Center	Rim ⁽¹⁾	40	28	4.3	-85	72N, 126E	39
Center	Rim ⁽¹⁾	NA	53.2	4.7	-91	72N, 126E	129

⁽¹⁾ Natural variations in WTD.

⁽²⁾ Only data from floodplain were used, and CH₄ fluxes were gap-filled.

⁽³⁾ Only data from the wettest and the driest were used.

⁽⁴⁾ Only data from 2003 and 2005 were used, as these were the only years when climate conditions were similar.

NA: Not available.

1.5 Objectives

As described in Section 1.1, CO₂ and CH₄ fluxes are affected by numerous environmental factors. Some critical factors include soil moisture conditions, temperature, vegetation, and microorganisms. To investigate the effects of changes in these factors on CO₂ and CH₄ fluxes, a study site that has been drained for 10 years was selected in northeastern Siberia¹⁰⁵. This study also aims at filling a regional data gap: Although permafrost regions in Eurasia cover roughly twice the area and contain twice the amount of carbon as compared to North America⁵⁵, most studies have been carried out in North America, and Siberia has been under-represented in Arctic research. In addition, field manipulation studies are rare in the Arctic, so the results of this study can be a great addition to Arctic research.

One year after the drainage ditch was installed, CH₄ emission rates significantly decreased, while net CO₂ fluxes did not show considerable changes¹⁰⁵. These observations effectively showed the short-term drying effects on CO₂ and CH₄ fluxes, but were not able to take the changed ecosystem properties into account due to the limited observation period¹⁰⁵. As a continuation of hydrological manipulation initiated a decade ago and with a unique setup of long-term drying manipulation in northeastern Siberia¹⁰⁵, (i) the changes in ecosystem properties, i.e., T_{soil} as well as vegetation and microbial community structure, following a decade-long drainage will be addressed (Figure 1.1). In addition, (ii) the roles of modified ecosystem properties in CO₂ and CH₄ fluxes in the Arctic will be described, focusing on GPP, R_{eco}, and CH₄ production, transport, and oxidation in the growing and nongrowing seasons (Figure 1.1). By including the contributions of modified ecosystem properties to changes in CO₂ and CH₄ fluxes, the response of Arctic ecosystems to long-term drainage in terms of CO₂ and CH₄ can be investigated in depth. These findings can also serve as a basis for predicting Arctic ecosystems' feedback to climate changes.

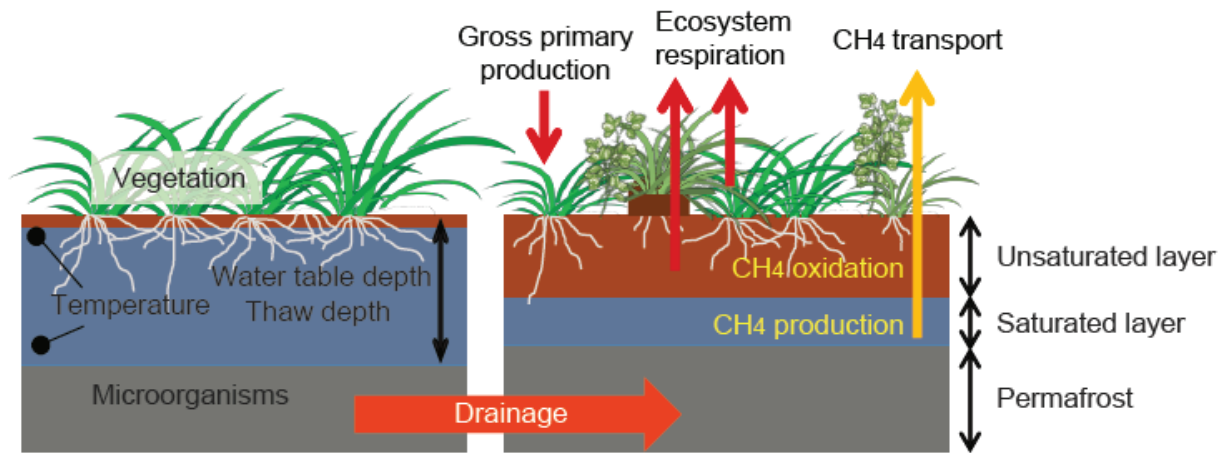


Figure 1.1 A schematic describing the environmental factors as well as CO₂ and CH₄ fluxes that will be investigated in this study. Drainage may alter ecosystem properties, such as soil temperatures and, subsequently, thaw depth, as well as plant and microbial community structure. They may affect CO₂ and CH₄ fluxes by modifying gross primary production and ecosystem respiration, as well as CH₄ production, oxidation, and transport.

Chapter 2. Methodology

2.1 Study site

2.1.1 Site description

A floodplain located near the town of Chersky (also written as Cherskii or Cherskiy) in northeastern Siberia (Figure 2.1a) was selected to investigate the long-term effects of drainage on ecosystem properties as well as CO₂ and CH₄ fluxes. The dominant vegetation species are tussock-forming *Carex appendiculata*, and *Eriophorum angustifolium*. An organic peat layer (15–20 cm deep) has accumulated on top of alluvial material soils (composed of

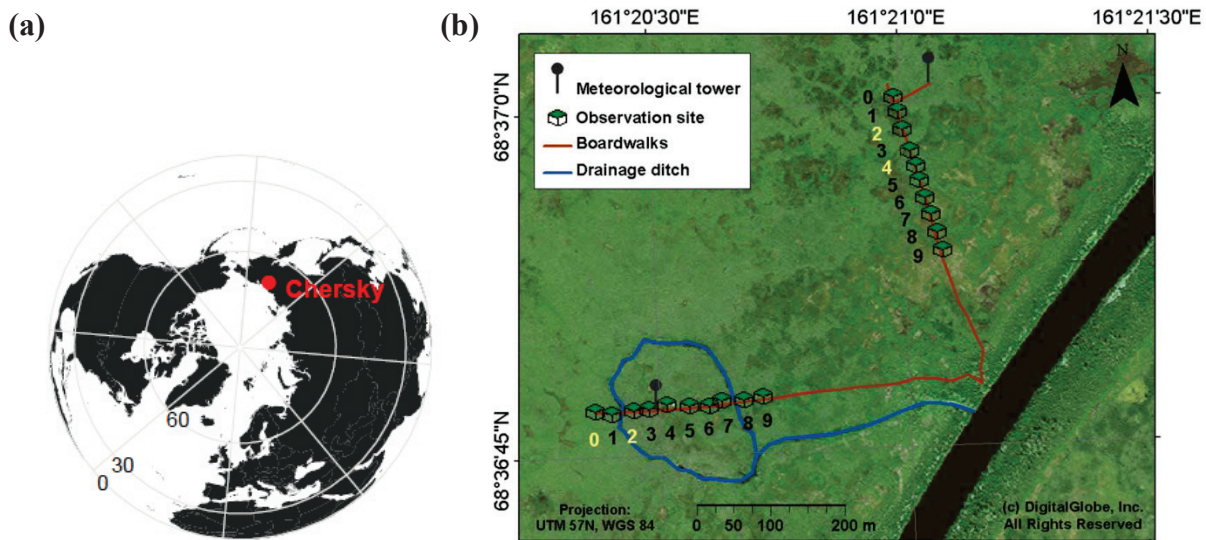


Figure 2.1 Maps of the study site in Chersky, northeastern Siberia. (a) The study site (68° 36' 47" N, 161° 20' 29" E) is located near Chersky within the Arctic Circle (66° 33' N). (b) Aerial photograph of the site, including schematics of the drained (bottom left; 68° 36' 47" N, 161° 20' 29" E) and the control (top right; 68° 37' 00" N, 161° 20' 59" E) transects. Each area consists of a meteorological tower, where air temperature, relative humidity, and air pressure are observed continuously and recorded half-hourly, and ten flux plots, where CO₂ and CH₄ fluxes as well as ecosystem properties are observed. Names of plots are written with numbers and two core plots for more frequent flux measurements are highlighted in yellow in each transect.

silty clay), although some organic peat materials can be found within alluvial layers due to cryoturbation.

Based on the record filtered by the Berkeley Earth project (berkeleyearth.org, Station ID 169921) for the period 1960–2013, mean monthly temperatures at the Chersky weather station range between -33 °C in January and +13 °C in July, and the annual mean temperature was -11 °C. World meteorological organization (WMO) records for the period 1950–1999 indicate a total annual precipitation of 197 mm, with about half of this falling as rain in summer. Snowmelt at the site and in the surrounding river basin usually results in a spring flood. This flooding brings an increased water level of up to 50 cm above the soil surface in late May or early June, followed by a gradual decrease in the water level starting in early July. After the flood waters have receded, the primary water source is precipitation.

2.1.2 Experiment setup

A drainage ring with a ~200 m diameter and minimum depth of 50 cm was constructed in Fall 2004¹⁰⁵, to drain water into the nearest river channel (Ambolikha). As a result, WTD in this drained area is lowered by 20 cm on average and by up to 30 cm in the growing season compared to control areas¹⁰⁵. While the spatial range of drainage effects varies by soil topography, high-resolution land cover classification (Worldview with 2 m resolution)¹³⁰ has indicated a high abundance of vegetation groups dominant in dry areas to only within 200 m on both sides of the ditch (Ina Burjack, unpublished data); therefore, the drainage effect can be limited to this maximum distance.

Starting Summer 2013, ecosystem properties as well as CO₂ and CH₄ fluxes were measured at two sites in parallel (Figure 2.1b): the drained area affected by the ditch since 2004 (68° 36' 47" N, 161° 20' 29" E), and a control area (68° 37' 00" N, 161° 20' 59" E) approximately 600 m away from the drained area that is not affected by the drainage ditch. Despite some short-term diurnal fluctuations of up to a few cm following evapotranspiration, as well as precipitation events and water supply from thawing permafrost, distinct differences in WTD between these treatment areas persist over the growing season. To investigate ecosystem properties and flux rates at microsite level, a transect of ten plots was established within both the drained and control areas (henceforth referred to as drained and control transects, respectively), using a stratified systematic sampling method. First, ten approximate positions

were selected with 25 m intervals along the boardwalks or transects; then the final plots were selected by considering representative vegetation groups of the selected positions, and by selecting specimens small enough to fit within flux chambers (Figure 2.1b). All plots were located within *ca.* 2 m of boardwalks to minimize disturbances.

2.1.3 Field campaigns

Three field campaigns were conducted within the context of the presented study. The first was 3 weeks, starting on 20 July 2013 (representing the mid-growing season); the second was 4 weeks, starting on 1 November 2013 (representing the nongrowing fall season); and third was 10 weeks, starting on 15 June 2014 (representing the growing season). The nongrowing season was defined as the time period when the average daily T_a was below 0 °C.

Although WTD of the drained transect was generally lower by 20 cm than that of the control transect after the spring flood in both years, heterogeneous soil topography rendered varying WTD within each transect: One plot in the drained transect had an average WTD close to that of wet plots in the control transect, and two plots in the control transect had an average WTD close to that of dry plots in the drained transect. Since our objective was to analyze how a decade-long drainage disturbance affects CO₂ fluxes and its links to environmental parameters, 20 plots were categorized into four groups—drained(D)_wet, drained_dry, control(C)_wet, and control_dry—according to transect and WTD category (Table 2.1). Plots were classified as ‘dry’ when the average WTD of the growing season was lower than -10 cm.

In 2013, all 20 plots were observed with equal frequency to investigate spatial variability among plots; in 2014, four core plots (i.e., one plot from each group) were more frequently observed to highlight temporal variability over the growing season (Figure 2.1b & Table 2.1). Due to different lengths of the observation periods between the two years, data from 2014 were divided into four sub-seasons to distinguish seasonal variability: (2014.1) from 15 June to 30 June, (2014.2) from 1 July to 15 July, (2014.3) from 16 July to 31 July, and (2014.4) from 1 August to 20 August. Sub-season 2014.4 and the 2013 field campaign covered similar periods, based on an analysis of plant phenology with the normalized difference vegetation index (NDVI), and both periods included peak growing season (i.e., when the NDVI of the site was the highest).

Table 2.1 Water table depth (WTD) and vegetation characteristics of plots. Average WTD was calculated by pooling all WTD measurements from both years by each vegetation group (mean \pm standard deviation), except the period where the whole area was flooded from snowmelt. When the average WTD of the growing season was larger than -10 cm, plots were classified as ‘wet’ group. Vegetation groups were created by taking into account only *C. appendiculata*, *E. angustifolium*, and shrubs when the relative abundance of each species exceeded 10%. The relative abundance of consisting plant species (mean \pm standard deviation) are separately presented.

Transect	Plot ID Number	WTD group	Group abbr.	Average WTD (cm)	Vegetation group	Vegetation abundance (%)
Drained	0	Wet	Drained_wet	4.6 \pm 2.2	EriophorumShrub	90, 10
	1, 2, 4	Dry	Drained_dry	-14.1 \pm 8.4	CarexEriophorum	31 \pm 23, 64 \pm 21
	3, 5, 6, 7, 8, 9	Dry	Drained_dry	-19.2 \pm 6.1	Carex	82 \pm 30
Control	0	Wet	Control_wet	-1.3 \pm 2.3	CarexShrub	85, 15
	1, 3, 6, 7, 8, 9	Wet	Control_wet	4.3 \pm 2.4	Eriophorum	79 \pm 33
	2	Wet	Conrol_wet	3.9 \pm 2.1	EriophorumShrub	80, 20
	4, 5	Dry	Control_dry	-18.5 \pm 4.1	CarexShrub	71 \pm 12, 27 \pm 15

2.2 Flux measurements

2.2.1 CO₂ and CH₄ flux rates

At each plot a 60 \times 60 cm² polyvinyl chloride (PVC) collar was inserted 15 cm into the ground in late June 2013, three weeks before the first flux measurements. No noticeable plant damage was identified around the collars after installation, and three weeks was expected to provide enough buffer time for any stabilization needed in the event of minor belowground damage^{131,132}. To take the flux measurements, a cubic transparent chamber (60 cm side length, made of 4 mm-thick plexiglass) was placed on the collar. The chamber had an opening valve on the top to avoid pressure effects when the chamber was placed onto the collars. Sensors for T_a, relative air humidity, P_a, and photosynthetically active radiation (PAR) were attached to one side of the chamber and all parameters were measured in parallel with fluxes. These sensors—along with three small fans on a vertical pole attached in one of the corners, for the purpose of mixing the air inside—were placed such that their shadows would not bias incoming solar radiation. CO₂ and CH₄ flux was measured with non-steady-state flow-through (i.e., closed dynamic) method using an Ultra-Portable Greenhouse Gas Analyzer (UGGA, Los

Gatos Research, USA), and all data were recorded at 1 Hz with a CR1000 data logger (Campbell, USA).

Each flux measurement was restricted to a maximum of 2 minutes to minimize saturation effects (i.e., warming and pressurized effects) within the chamber. In the event of strong incoming radiation, which can cause temperature to increase more than 1 °C per minute, ice packs were placed on the collar rims inside the chamber to keep temperatures constant while measuring fluxes. The number of ice packs was adjusted by observing the temperature changes at 1 Hz frequency. In addition to measuring NEE using the transparent chamber, in summer R_{eco} was also measured by covering the chamber with a tarp that blocked incoming solar radiation. The transparent and dark chambers did not result in variations in CH_4 flux rates, and, thus, all measured CH_4 fluxes were used regardless of light conditions. In the nongrowing season, no significant differences were found between NEE and R_{eco} for CO_2 fluxes, probably due to the role of low temperatures, low solar radiation, and snow cover in limiting photosynthesis; therefore only NEE was measured with a transparent chamber.

To calculate the CO_2 and CH_4 flux from the observed changes in CO_2 and CH_4 concentrations ($[\text{CO}_2]$ and $[\text{CH}_4]$, respectively) within the sampling time of 2 minutes, median values of the $[\text{CO}_2]$ and $[\text{CH}_4]$ slopes were computed selecting multiple time windows based on a bootstrapping approach, and fluxes (in units of $\text{mg C-CO}_2 \text{ m}^{-2} \text{ s}^{-1}$ and $\text{mg CH}_4 \text{ m}^{-2} \text{ s}^{-1}$) were calculated by taking into account T_a , P_a , and the volume and area of the chamber¹³³. Flux rates that fell outside of the range of seasonal mean $\pm 3 \sigma$ (i.e., standard deviation) were removed as outliers. GPP and R_{eco} are expressed in positive values, indicating the amount of CO_2 assimilated and respired, respectively. Negative values for NEE and CH_4 fluxes denote net CO_2 and CH_4 uptake by the terrestrial ecosystem, while positive values denote net CO_2 and CH_4 emission to the atmosphere. To produce net CO_2 flux budgets for selected periods, the available flux observations were interpolated based on a process modeling approach (see Section 2.2.3). CH_4 fluxes were interpolated to daily CH_4 fluxes because diurnal variations were negligible (data not shown). Then, daily CH_4 fluxes of each plot were linearly interpolated to acquire growing-season CH_4 fluxes, assuming that not-measured CH_4 fluxes between measurement days fell in the range of CH_4 fluxes measured. Nongrowing-season CH_4 fluxes were not linearly interpolated because of sporadic high fluxes. For CO_2 flux interpolation, see Section 2.2.3.

2.2.2 CH₄ pathways

Net methane emissions to the atmosphere are based on three major transport pathways: plant-mediated transport through aerenchymatous plants, release of bubbles (i.e., ebullition), and diffusion. To estimate how much CH₄ was transported through the aerenchymatous plants, with cotton grasses (*E. angustifolium*) as the target species at the study site, a single plant was placed into a cylindrical dark chamber (ø 10 cm × 50 cm height) and sealed the base with gas-tight cap that enclosed the plant. Diverse sizes of plants (stem diameters range from 0.3 to 1.5 cm and the green leaf lengths from 21 to 97 cm) were selected near the chamber collars for these observations. Due to the small volume of the plant chamber, gas samples was drawn at three different heights of the chamber instead of having fans for mixing air, and recorded [CH₄] for 2 minutes with UGGA at 1 Hz time resolution. To calculate the fraction of the amount of CH₄ transported through *E. angustifolium*, the three following steps were applied: (1) correlation analyses were carried out between the green leaf lengths and the amounts of CH₄ transported by a single plant, yielding a linear function that estimates flux rates based on plant height, (2) the average green leaf length of *E. angustifolium* inside the chamber collars was measured, and calculated the expected amount of CH₄ transported by a single plant (mean and standard deviation) with the functions derived from (1), and (3) the number of plants found inside the chamber collars was multiplied with the mean flux per plant from (2) to yield the total plant-mediated flux within the chamber area. The uncertainty ranges for this estimate were computed by modifying the green leaf lengths by 10 cm and the number of plants by 5. In step (1) green leaf length was chosen because it showed the strongest positive correlations with the amount of CH₄ emitted through *E. angustifolium* compared to other plant traits, such as stem diameter, the number of green leaves.

Ebullition events were detected by examining the trajectories of [CH₄] plotted over time during 2-minute flux measurements. When [CH₄] increased linearly within 2 minutes, the CH₄ transport was regarded as a mixture of diffusion and plant-mediated transport (Figure 2.2a). However, when an abrupt increase in [CH₄] was detected between two linear slopes, then this event was defined as ebullition (Figure 2.2b). For all 2-minute [CH₄] measurements over the growing season, the proportion of ebullition events to the total CH₄ fluxes—frequency and the amount of carbon emitted through ebullition—was calculated based on the equations below:

$$\text{frequency} = \frac{\text{the number of ebullition events}}{\text{the total number of flux measurement}} \quad (2.1)$$

$$\text{ebullition} = \frac{\text{the amount of CH}_4 \text{ through ebullition}}{\text{the total amount of CH}_4 \text{ flux}} \times \text{frequency} \times 100 (\%) \quad (2.2)$$

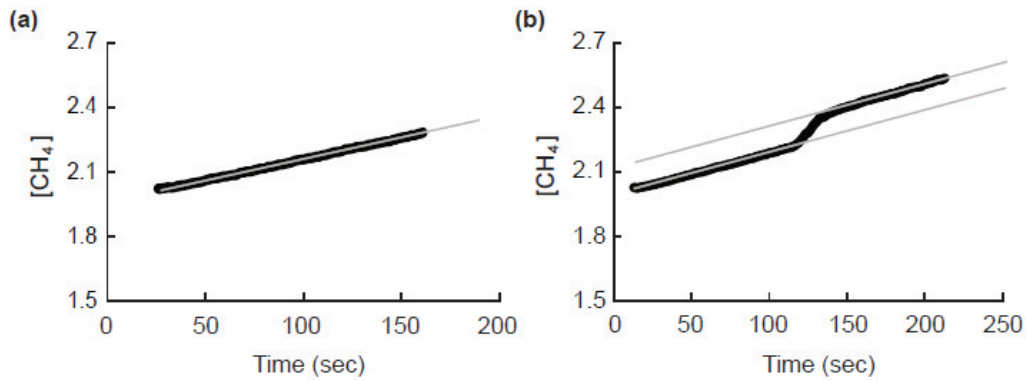


Figure 2.2 Examples of the measured CH₄ concentration ([CH₄]) change. (a) Diffusion and plant-mediated CH₄ transport with a constant increase in [CH₄], and (b) ebullition with an abrupt increase in [CH₄] between two linear slopes. Gray lines are example regression lines used for calculating CH₄ fluxes, and the differences in [CH₄] of the two gray lines in (b) are the amount of CH₄ through ebullition.

This estimation was based on the assumption that the frequency of ebullition within 2-minute measurements represents the natural conditions well, and diurnal variation in frequency and the size of ebullition events are negligible. Ebullition events that occurred within 30 sec after the chamber head was placed on the collar—it took *ca.* 20 sec for the gas from the chamber to travel to the analyzer—were evaluated separately because they may have been triggered by physical disturbance.

2.2.3 Interpolation of growing-season CO₂ fluxes

To compare flux variability among plots induced by temporal discrepancies in sampling, and to visualize the implications of these differences for net growing-season CO₂ uptake, CO₂ fluxes for each vegetation and WTD group were interpolated throughout the growing-season observation period. To simulate CO₂ flux rates a satellite-data-driven CO₂ flux model, the

Polar Vegetation Photosynthesis and Respiration Model (PolarVPRM), was adopted which calculates high-latitude NEE by subtracting GPP from R_{eco} ¹³⁴:

$$GPP = (\lambda \times T_{scale} \times W_{scale}) \times FAPAR_{PAV} \times \left(\frac{1}{1 + \frac{PAR}{PAR_0}} \right) \times PAR \quad (2.3)$$

$$T_{scale} = \frac{(T_a - T_{min}) \times (T_a - T_{max})}{(T_a - T_{min}) \times (T_a - T_{max}) - (T_a - T_{opt})^2} \quad (2.4)$$

$$W_{scale} = \frac{a \times WTD}{WTD_{max} - WTD_{min}} + b \quad (0 < a < 1, a + b = 1) \quad (2.5)$$

where λ is a parameter representing maximum light use efficiency at low light levels, and PAR_0 represents the half-saturation value of PAR. T_{scale} and W_{scale} are scaling variables ranging between 0 and 1 that reflect the influence of T_a and water availability, respectively, on photosynthesis. The set of three parameters required for calculating T_{scale} , i.e., minimum (T_{min}), maximum (T_{max}) and optimum (T_{opt}) temperatures, were set to 0, 40 and 20 °C according to literature recommendations to avoid the parameter instability that would arise from empirically fitting these parameters, due to the strong positive correlations between T_a and PAR ¹³⁵. $FAPAR_{PAV}$ is the fraction of PAR absorbed by the vegetation, and is calculated using the Moderate Resolution Imaging Spectroradiometer (MODIS) Enhanced Vegetation Index (EVI).

Site-level meteorological observations of T_a and PAR were used as inputs for PolarVPRM; these observations were taken from sensors installed in the chamber system (for calibration) and from nearby meteorological towers (for temporal interpolation; Figure 2.1b). The influence of water availability on photosynthesis (W_{scale}) was calculated based on WTD determined next to each plot at the time of flux measurement, with an optimized scaling factor (a, b) to obtain the best fits between $GPP_{modeled}$ and $GPP_{observed}$.

Both parameters (λ and PAR_0) were optimized empirically in R¹³⁶. PAR_0 was obtained from the curve fit between GPP and PAR measured with flux observations using the nonlinear least squares curve fitting in R¹³⁶; λ was calculated as the slope of the linear regression of observed GPP, and of GPP calculated from Eq. (2.3). GPP was estimated excluding PAR terms for *CarexEriophorum* in 2013 because no positive relationship between GPP and PAR was found

(see Section 3.2.2). GPP was then computed half-hourly using linearly interpolated WTD and EVI, as well as half-hourly measured T_a and PAR from the meteorological station.

R_{eco} was calculated using an empirical Q_{10} model:

$$R_{eco} = \alpha \times e^{k \times T_a} \quad (2.6)$$

The two free parameters in this exponential relationship between R_{eco} and T_a , i.e., α and k , were empirically calculated from chamber-based measurements of R_{eco} and T_a using nonlinear least squares curve fitting in R¹³⁶. Once these coefficients were calculated, R_{eco} was calculated at half-hourly intervals with half-hourly-averaged T_a from the meteorological station at each transect.

Parameter optimization and flux interpolation were carried out separately across four core plots for the year 2014, while 10 plots from each transect were categorized into three vegetation groups and pooled for the year 2013. These vegetation categories took into account only *C. appendiculata*, *E. angustifolium*, and shrubs when the relative abundance of each species exceeded 10% (Table 2.1). The categorized vegetation groups of the drained transect were EriophorumShrub, CarexEriophorum and Carex, while those of the control transect were CarexShrub, Eriophorum and EriophorumShrub (Table 2.1). The period of interpolation was restricted to the observation periods within each year because WTD (W_{scale}) was not measured continuously outside of this period. The discrepancies between the observed and modeled fluxes were calculated using root mean squared error (RMSE) and mean bias error (MBE). All data points that were used for calibration were utilized for the error estimates due to the limited number of data points.

Uncertainty ranges of the interpolated fluxes were calculated using cross validation by creating 2000 data subsets consisting of randomly selected data points (bootstrapping, 80% of the total dataset). To obtain an error range of R_{eco} , the 2000 resulting pairs of parameters, and, subsequently, $R_{eco} \pm 2 \sigma$ were computed for each 1 °C temperature bin. Similarly, 2000 pairs of PAR_0 and λ were estimated for binned PAR. The range of GPP was subsequently estimated by including the rest of the terms from Eq. (2.3). To constrain the uncertainty ranges of the interpolated fluxes, the GPP and R_{eco} error ranges were taken at each point from the corresponding PAR and temperature bin, respectively, that reflected the current condition. Because NEE is calculated as the difference of GPP and R_{eco} , uncertainty ranges were also

determined by adding the two error ranges of GPP and R_{eco} . For CarexEriophorum and EriophorumShrub groups in 2013—for which no positive relationship between GPP and PAR was found (see Section 3.2.2) or the number of data points was not enough to produce uncertainty ranges, respectively—the bootstrapping step was skipped.

2.2.4 R_h rates

To investigate the effect of T_{soil} on R_h , respiration rates of soils at 0–15 cm and 15–30 cm depths were measured by aerobically incubating soils at 15 °C in the laboratory ($N = 6$ for each depth). Respiration rates were corrected for bulk density and average growing-season T_{soil} at each 0–15 cm and 15–30 cm depth of both the wet and dry plots by assuming a Q_{10} value of 2 as the mean for tundra ecosystems¹³⁷. The relative heterotrophic respiration rates between the wet and the dry plots were subsequently compared, and were linked to changes in T_{soil} .

2.3 R_{eco} partitioning

To investigate the effects of drainage on the components of R_{eco} , R_{eco} was partitioned into three sources, i.e., surface soil (SS), deep soil (DS), and autotrophs (AT), by employing a radiocarbon tool.

2.3.1 Radiocarbon signatures of R_{eco}

CO_2 gases to analyze radiocarbon signals were collected by placing the chamber on the permanently installed collars (see Section 2.2.1). After an increase in CO_2 concentrations was determined at 1 Hz frequency to calculate R_{eco} , headspace CO_2 was scrubbed for 50 minutes with soda lime at a rate similar to that of R_{eco} to keep the headspace CO_2 concentration constant. This scrubbing replaced a quarter of the headspace CO_2 . Then, headspace gas was circulated through molecular sieve (Alltech 13x, Alltech Associates, USA) to collect 1.5 mg C- CO_2 . CO_2 was desorbed from molecular sieves by heating them at 500 °C¹³⁸. Extracted CO_2 was purified with liquid nitrogen on a vacuum line and the remaining CO_2 was reduced to graphite by Fe reduction in H_2 . Radiocarbon analysis was carried out at the ^{14}C Analytics lab at the Max Planck Institute for Biogeochemistry in Jena, Germany (precision $\pm 2.8\%$, $N = 49$). $\Delta^{14}\text{C}$ data were reported after normalized for $\delta^{13}\text{C}$ and corrected for the decay between the year 1950 and the measurement time:

$$\Delta^{14}\text{C} (\text{‰}) = [F^{14}\text{C} \times e^{\frac{\text{year}-1950}{8267}} - 1] \times 1000 \quad (2.7)$$

where $F^{14}\text{C}$ is fraction modern as given by Reimer et al. (2004)¹³⁹ and year is the year of sampling. In order to correct for atmospheric contamination, $\Delta^{14}\text{C}$ values of atmospheric air were removed by using of $\delta^{13}\text{C}$ values with a two-pool mixing model¹⁴⁰.

2.3.2 Radiocarbon signatures of sources

Six thawed soil cores were taken from each transect in July 2014 and two cores were combined to make three sets per transect. Each set of cores was divided into 3–4 increments at 7.5 cm intervals. Roots (>1 mm) were removed, and 80 grams of soils were transferred into beakers and then into 1 L glass jars with distilled water to keep the moisture constant. Soils were incubated at room temperature for five days to minimize the effects of respiration by remaining roots and mycorrhizae¹³². Then, the headspace air was scrubbed with soda lime, and incubation continued at room temperature. R_h rates of each depth were measured at the beginning of the incubation and incubation lasted for up to 4 weeks until the amount of carbon accumulated in the jar reached 1.5 mg. Headspace CO_2 was subsequently collected with molecular sieves (Alltech 13x, Alltech Associates, USA) and $\Delta^{14}\text{C}$ values were acquired at Max-Planck Institute in Jena, as described in the previous section.

To get $\Delta^{14}\text{C}$ of autotrophic respiration ($\Delta^{14}\text{C-AT}$), 1‰ was added to the $\Delta^{14}\text{C}$ values of the atmosphere measured in the year of sampling because $\Delta^{14}\text{C-AT}$ have been shown to be 1‰ more enriched compared to those of atmosphere⁹⁵.

2.3.3 Source partitioning

For input data for partitioning, mean and standard deviation values of each source's $\Delta^{14}\text{C}$ were calculated. SS (0–15 cm) and DS (below 15 cm) were divided based on the age of the respired CO_2 . $\Delta^{14}\text{C-SS}$ were enriched due to the “bomb effect” since 1960s, while $\Delta^{14}\text{C-DS}$ were depleted. To calculate $\Delta^{14}\text{C-SS}$ and $\Delta^{14}\text{C-DS}$ from a single core, $\Delta^{14}\text{C}$ values of each soil depth were weighted by its respiration rate that was corrected for average monthly T_{soil} using a Q_{10} value of 2.5^{95,141,142}, and then averaged $\Delta^{14}\text{C}$ values of all depths. Mean and standard deviation were acquired from soil core replicates (Table 2.2). The standard deviations were obtained from plant incubation conducted in Hicks Pries et al. (2013)⁹⁵ (Table 2.2).

Table 2.2 $\Delta^{14}\text{C}$ (mean \pm standard error) of three sources, i.e., surface soil, deep soil, and autotrophs. Numbers in parentheses indicate the number of replicates. $\Delta^{14}\text{C}$ values of surface and deep soil are weighted by each depth's respiration rate and corrected for average monthly soil temperatures. $\Delta^{14}\text{C}$ values of autotrophs were acquired from atmospheric air (mean) and plant incubation (standard error).

Site	Treatment	Surface soil (6)	Deep soil (6)	Autotrophs (16)
Chersky				
2014	Control	35.86 \pm 5.34	-55.48 \pm 4.22	21.83 \pm 2.27
	Drained	39.37 \pm 5.13	-55.40 \pm 4.23	21.83 \pm 2.27

Stable Isotope Analysis in R (SIAR) was used to partition $\Delta^{14}\text{C-R}_{\text{eco}}$ to its three sources, i.e., SS, DS, and AT¹⁴³. The partitioning was performed with each plot (each $\Delta^{14}\text{C-R}_{\text{eco}}$ value) separately and with non-informative prior. The SIAR method uses Markov chain Monte Carlo approach to produce probable solutions of each source's contribution. To estimate the contributions of SS, DS, and AT to R_{eco} , the following two equations were used:

$$^{14}\text{C}_{\text{Ecosystem}} = f_{\text{SS}} \times ^{14}\text{C}_{\text{SS}} + f_{\text{DS}} \times ^{14}\text{C}_{\text{DS}} + f_{\text{AT}} \times ^{14}\text{C}_{\text{AT}} \quad (2.8)$$

$$1 = f_{\text{SS}} + f_{\text{DS}} + f_{\text{AT}} \quad (0 < f_{\text{SS}}, f_{\text{DS}}, f_{\text{AT}}) \quad (2.9)$$

where ^{14}C is $\Delta^{14}\text{C}$ values of R_{eco} and each source, and f is contribution of each source to R_{eco} . The mean values of 10,000 possible f values were taken for source contributions (Figure 2.3).

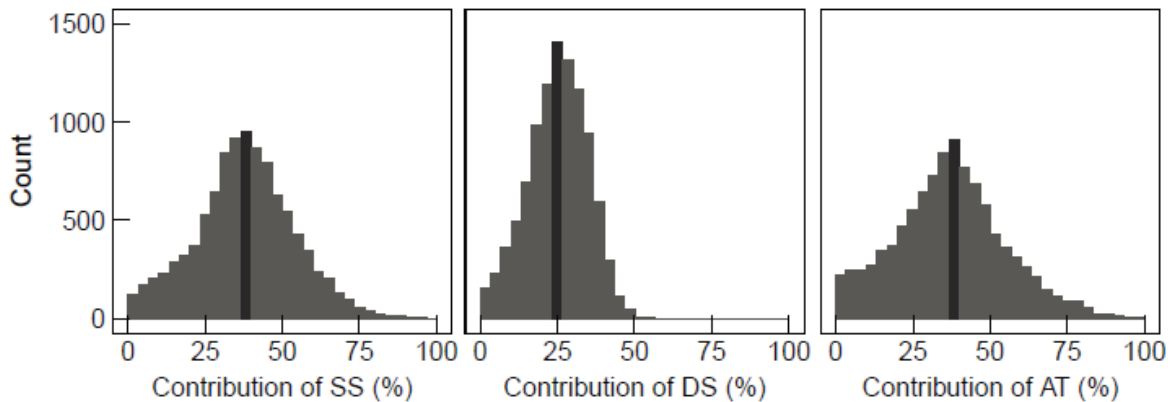


Figure 2.3 One example of distributions of possible f values (i.e., source contributions) derived from partitioning. Black bars indicate the bins where mean value of each distribution belongs to.

Using one type of isotope to obtain three unknown f values may produce uncertain results but the range of uncertainty depends on the similarity of source isotopic signatures¹⁴⁴. The three source signatures used in partitioning were distinct (Table 2.2), and the previous study that utilized this model produced robust results¹⁴².

2.4 WTD, TD, and Tsoil

WTD was measured during each flux measurement using perforated PVC pipes (\varnothing 25 mm), which were installed at each plot. WTD was measured relative to soil surface, with values larger than 0 cm denoting water standing above the soil surface. TD was estimated by pushing a measuring pole into the ground. At even-numbered plots Tsoil probes were installed at 5, 15, 25 and 35 cm (Th3-s, UMS, Germany), and data were recorded while fluxes were measured.

2.5 Plant community structure

Changes in plant community structure between 2003 (before the drainage ditch was installed) and 2013 (nine years after the drainage ditch was installed) were examined using historical data collected in 2003 through the Terrestrial Carbon Observation System Siberia project (TCOS Siberia)¹². Plant community structure was then identified in 2013 along the same transect as in 2003 (which had not been drained in 2003, but was drained in 2013), as well as in the control transect (newly selected in 2013). Identification was carried out using the same harvest method in all transects. All living vegetation inside a $1 \times 1 \text{ m}^2$ quadrat ($N = 4$ per transect) was harvested. Collected vegetation was sorted by species, completely dried at $40 \text{ }^\circ\text{C}$, and then weighed ($\text{g dry biomass m}^{-2}$). Relative abundance of each species (%) was calculated based on the dry biomass to avoid potential biases linked to the water content of plants.

To correlate abundance of plant species with CO_2 and CH_4 fluxes without destroying plots for further flux observations, a non-destructive point-intercept method was applied using a $60 \times 60 \text{ cm}^2$ quadrat that was divided into $10 \times 10 \text{ cm}^2$ sub-grids in 2014. After creating this grid, the plant species that a laser pointer hit when pointed downward at each sub-grid intersection were recorded, and calculated the percentage of each species' cover. This analysis was performed within each collar, so that plant community structure of each plot could be linked directly to CO_2 and CH_4 fluxes. As plots were selected using a stratified method (see Section 2.1.2), this analysis was also performed at a spot 10 m away from each plot, to confirm that the plant community structure of each plot accurately represented the transects.

2.6 Soil carbon content

Five soil cores of thawed layers were taken in each transect in July 2013. Each core was divided into an organic peat layer and an alluvial soil layer, and then each layer was further divided in 7.5 cm increments, leading to 3–4 increments per core. Soils were transferred directly after sampling to the laboratory and stored at 4 °C until analysis. Subsamples of soils were dried at 105 °C for 24 hours to derive gravimetric soil moisture (%), and then ashed at 450 °C to get organic carbon content (%). Total carbon and nitrogen (%) were estimated after drying peat soils at 70 °C and alluvial soils at 40 °C (varioEL, Elementar, Germany).

2.7 Microbial community structure

2.7.1 DNA extraction

Soil samples from core plots were selected for microbial analysis. Subsamples of soils were conserved in soil preservation solution (Life Guard Soil Preservation Solution, Mo Bio, USA) and kept frozen at -20 °C until extraction. Each sample was split into three as triplicates. Total genomic DNA was extracted through the following sequence: (1) 0.5 g of soil was mixed with 0.5 g of Zirconia Beads (\emptyset 0.1 mm), 0.75 ml sodium phosphate buffer solution (112.9 mM Na₂HPO₄, 7.1 mM NaH₂PO₄), and 0.25 ml sodium dodecyl sulfate (SDS) buffer solution (500 mM Tris-HCl, 100 mM NaCl, 10% w/v SDS, pH 8.0), (2) the mixture was subsequently lysed for 45 sec with 6.5 m/s speed (FastPrep-24, MP-Biomedicals, USA), (3) supernatant after centrifugation at 18,000 \times g for 5 minutes was extracted with equal volumes of phenol:chloroform:isoamylalcohol (25:24:1 v:v:v; Sigma Aldrich), followed by chloroform:isoamylalcohol (24:1 v:v; Sigma Aldrich, USA), (4) nucleic acids were precipitated from 0.5 ml of extract with 1 ml poly(ethylene glycol) 8,000 (Sigma Aldrich, USA) by incubation at 4 °C overnight and centrifugation at 19,000 \times g for 30 minutes. (5) The precipitate from step was washed with 0.4 ml ice cold ethanol solution (70% v/v) and dissolved in 500 μ l TE buffer (10 mM Tris, 1 mM EDTA, pH 8.0). (6) The extract was filtered to remove co-extracted organic contaminants (OneStep™ PCR Inhibitor Removal Kit, Zymo research, USA) and samples with remaining contamination (detected with ND-1000 Spectrophotometer, Thermo, USA) were purified again by repeating the steps from (3) to (6).

2.7.2 Illumina sequencing and data processing

The diversity and composition of prokaryotic communities was determined by applying a high-throughput sequencing-based protocol that targets PCR-generated amplicons from V4 variable regions of the 16S rRNA gene using the bacterial primer set 515F (5'-GTGCCAGCMGCCGCGGTAA-3') and 806R (5'-GGACTACHVGGGTWTCTAAT-3')¹⁴⁵. Amplicons were barcoded and sequencing was conducted on an Illumina MiSeq2000 platform at the Research Resources Center (RRC) of the University of Illinois at Chicago following standard protocols¹⁴⁶⁻¹⁴⁸. MiSeq paired-end raw reads were de-multiplexed and then processed using the program MOTHUR version 1.33¹⁴⁹, with the following criteria: (1) the 300-bp reads were truncated at any site that obtained an average quality score of <20 over a 50-bp sliding window, and the truncated reads <50 bp were discarded; (2) reads with any mismatch in barcode, more than two nucleotide mismatch in primer or containing ambiguous characters were removed; (3) overlapping sequences <10 bp or with a mismatch ratio of more than 0.2 within the overlap region were eliminated; (4) sequences were trimmed to a common length of 250 bp; (5) chimeric sequences were filtered out by UCHIME¹⁵⁰; (6) to ensure a better comparison of samples differing in the number of sequence reads, read numbers of each sample were normalized to the size of the smallest data set (14,670); (7) OTUs were classified with 97% similarity level (SILVA database). Sequencing coverage was 92% on average and minimum 84%. To investigate whether drainage affects the community structures of CH₄-associated microorganisms, the fractions and the compositions of methanogens and methanotrophs were investigated.

2.7.3 Quantitative PCR

Bacterial and archaeal 16S rRNA copies in DNA extracts were quantified by quantitative PCR (qPCR) on a Mx3000P instrument (Agilent, USA) by using the primer combinations A-806F and A-958R (V5 region)^{151,152} and B-28F and B-338R (V1-V2 region)^{153,154}, as described in previous literature¹⁵⁵.

2.8 Data analysis

2.8.1 Ecosystem properties

Spatial differences in the 2013 WTD and TD between the two transects were tested using an independent *t*-test. A two-way analysis of variance (ANOVA) was performed to investigate

total carbon and nitrogen content differences by transect and WTD. Regression analyses were performed for each transect with WTD as the independent variable and Tsoil at 5 cm and 35 cm, and TD as the dependent variable to investigate whether Tsoil and TD were affected by WTD.

A permutational multivariate ANOVA (PERMANOVA) was performed to compare plant community structure between the drained and the control transects of 2013 and 2003. Data from 2014 were not compared with those from 2003 due to the different experimental methods employed. The abundance of *E. angustifolium* among the four groups as well as 2003 was compared with one-way ANOVA. When the abundance was significantly different by group, Tukey's post hoc test was performed.

Two-way ANOVA was performed to find out whether the fractions of methanogens and methanotrophs varied by transect and WTD category. Two-way PERMANOVA was carried out with the communities of methanogens and methanotrophs as the dependent variables to see whether microbial community structures differed with transect and WTD category.

2.8.2 Environmental effects on CO₂ flux rates

To investigate whether vegetation groups affected the 2013 CO₂ fluxes, all fluxes were aggregated by vegetation group (see Section 3.2.2; Table 2.1) and one-way ANOVA was performed for each vegetation group as an independent variable. When independent variables significantly influenced dependent variables, Tukey's post hoc test was applied. To investigate whether vegetation group and Tsoil significantly affected the nongrowing season CO₂ fluxes, one-way ANOVA and multiple linear regressions were performed, respectively. A multiple linear regression analysis was also performed to identify additional major environmental drivers for cold-season CO₂ fluxes. For multiple linear regression analyses, significant variables were defined based on Bayesian information criteria (BIC); with these selected variables the best-fit regression models were identified, based on the Akaike information criterion (AIC).

To investigate which environmental parameters significantly affect $\Delta^{14}\text{C-R}_{\text{eco}}$ and the contributions of each source to R_{eco} , multiple linear regression analyses were carried out in R. Due to the small number of data points ($N = 20$), normality was not fully achieved for the contributions of DS and AT. However, data were analyzed without transformation because no

outliers were found and transformation did not improve the normality. The independent variables included WTD, TD, abundance of *E. angustifolium*, and Tsoil at 5, 15, 25, and 35 cm. Among all the independent variables, significantly explaining variables were selected including interactions of any two variables using the `regsubsets` command in `leaps` package in R¹⁵⁶. With these selected variables, the best fitting models were selected based on AIC and with stepwise method¹⁵⁷. The residuals were visually checked to ensure that they did not vary with random factors. All assumptions of linear regression were tested as well.

2.8.3 Environmental effects on CH₄ flux rates

Regression analyses were carried out for each transect to test the dependencies between CH₄ fluxes and the abundance of *E. angustifolium*, CH₄ fluxes of the dry plots and Tsoil at 5 cm, and CH₄ fluxes of the wet plots and Tsoil at 35 cm. All statistical analyses were carried out using R¹³⁶.

To compare the major environmental drivers for the growing- and the nongrowing-season CH₄ fluxes, a machine learning method that yields a symbolic regression was employed. The latter is a regression approach, where a variety of transformations and their multiplicative and additive interactions are tested. Methods of this kind are deployed to derive complex models in a purely data driven way that allow data interpretation beyond linear statistics. Here, gene expression programming (GEP) was used¹⁵⁸, but combined with a covariance matrix adaptation evolution strategy (CMAES)¹⁵⁹ to additionally identify optimal parameterizations of the identified models (hereafter, CMAGEP¹⁶⁰). The CMAGEP was applied to each transect as such: candidate driving variables included in this analysis were the absolute values and temporal derivatives of continuously measured T_a, P_a, and PAR, as well as Tsoil at 5 to 35 cm. In the array of candidate drivers for the CMAGEP derived models, the abundance of *E. angustifolium*, *C. appendiculata*, and *P. palustris*, and additionally WTD and TD in case of the growing season were included. The settings used for each CMAGEP run are described in the Table 2.3. For each transect, 100 subsets of randomly selected data points were generated. In each subset, 70% of the total number of data points is used for training 100 models. The rest is used for computing validation fit of all models. The model with the best fit at validation is finally selected. Model evaluation and selection considered the AIC values computed between the observed and modeled flux rates for all 100 data subsets. For interpretability, the RMSE and MBE were also computed across the entire dataset.

Table 2.3 The settings used for CMAGEP runs.

Parameter	Value
Number of chromosomes	1000
Number of genes in a chromosome	3
Head length	5
Functional transformation	+, -, ×, ÷, power, square root, natural logarithm, exponential
Link function	+
Fitness function	Akaike information criterion
Selection method	Tournament ¹⁶¹
Mutation probability	0.05
Insertion (IS) and root insertion (RIS) transposition probabilities	0.1
Inversion probability	0.05
Recombination probability	0.8

Chapter 3. Results

3.1 Changes in ecosystem properties

3.1.1 WTD changes from drainage

Following spring floods due to snowmelt in early June, the drainage ditch effectively lowered WTD in the drained transect. Average differences in WTD between the two transects were significant with a mean drop of approximately 20 cm, and a maximum difference of up to 30 cm during a three-week period in Summer 2013 (independent t -test, $P < 0.001$, $t = -4.55$, $df = 17.91$; Figure 3.1a). Approximately the same difference in mean WTD was observed in the middle of the 2014 growing season. However, several significant rainfall events from late July of 2014 triggered an increase in WTD in the dry plots, especially in the drained transect (Figure 3.1b).

3.1.2 Shifts in Tsoil and TD

The dry plots generally showed higher fluctuating Tsoil at shallow layers, thus warmer temperatures during the daytime (linear regressions for the sub-season 2014.4; drained transect, adj. $R^2 = 0.12$, $P < 0.01$; control transect, adj. $R^2 = 0.06$, $P < 0.01$; Figure 3.2a), but colder temperatures at deep layers (linear regressions for the sub-season 2014.4; drained transect, adj. $R^2 = 0.97$, $P < 0.001$; control transect, adj. $R^2 = 0.36$, $P < 0.001$; Figure 3.2b), and the consequent shallower TD compared to the wet plots (linear regressions for the sub-season 2014.4; drained transect, adj. $R^2 = 0.61$, $P < 0.001$; control transect, adj. $R^2 = 0.48$, $P < 0.001$; Figure 3.2c). These trends became more distinct in the later sub-seasons (Figure 3.2a–c).

3.1.3 Plant community structure

In its natural, undisturbed state, the plant community of this floodplain has historically been dominated by *Eriophorum angustifolium*, followed by *Carex appendiculata*. This plant community structure was reflected in the observations made in 2003¹²—that is, before the

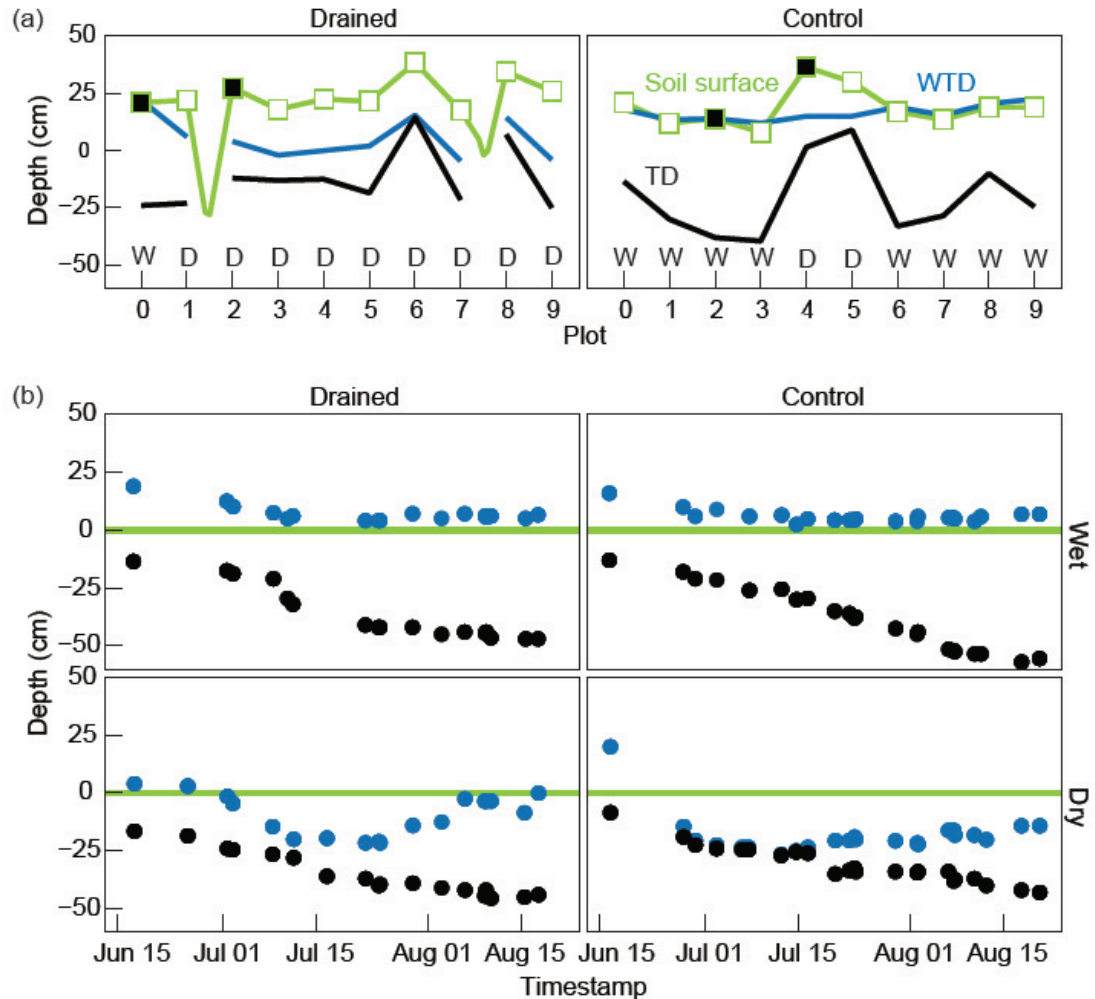


Figure 3.1 Spatial and temporal variability in water table depth (WTD). (a) Spatial variability in WTD (blue lines) and thaw depths (TD, black lines) measured across the two transects on 10 August, 2013. Green lines indicate terrain height, with plots indicated with squares (core plots = closed squares). The letters W and D indicate the wet and dry WTD category of each plot, respectively. (b) Temporal variability in WTD (blue points) and TD (black points) observed at the four core plots over the growing season of 2014, separated by transect (columns) and WTD category (rows). Green lines represent soil surface.

drainage ditch was constructed (Figure 3.3, black)—as well as in the control transect in 2013 (Figure 3.3, blue). After a decade of drainage, the abundance of *E. angustifolium* decreased, while shrubs (*Betula exilis*, and *Salix fuscescens* and *pulchra*) and *C. appendiculata* became the dominant species in the drained transect (Figure 3.3, red). While no statistically significant differences were found between the plant community structures in 2003 and in the control transect of 2013 (PERMANOVA, $F = 1.62$, $P = 0.19$), significant differences were found

between both the 2003 and the drained transect of 2013 (PERMANOVA, $F = 3.31$, $P < 0.05$) and between the two transects of 2013 (PERMANOVA, $F = 5.22$, $P < 0.05$). Although the two observation methods (see Section 2.5) were not experimentally compared, a qualitative comparison of results from 2013 (i.e., harvest) and 2014 (i.e., point intercept) showed a similar abundance of each species; this implies that these two different methods can be used to compare plant community structures.

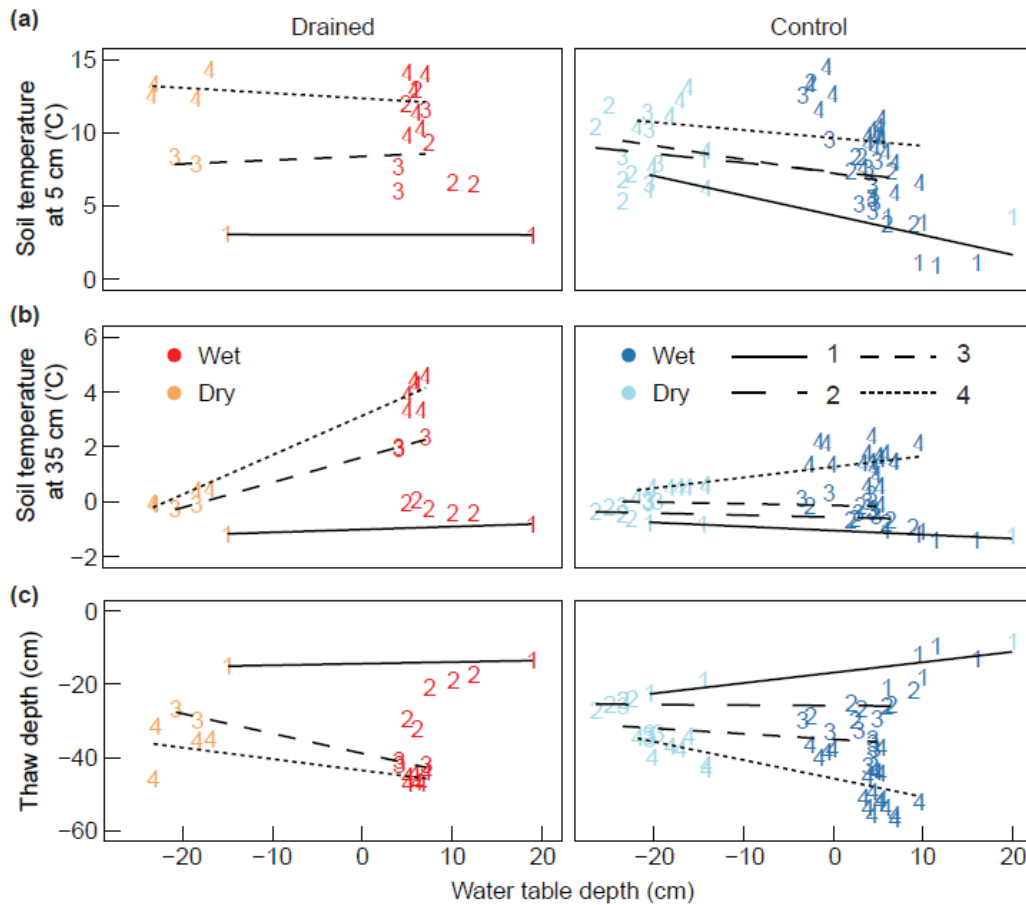


Figure 3.2 Soil temperatures (T_{soil}) and thaw depths (TD) against water table depths (WTD). T_{soil} at (a) 5 and (b) 35 cm, and (c) TD against WTD. Data are from 2014 only and those from the dry plots with rising WTD due to heavy precipitation were excluded. Regression lines were drawn by sub-season, and regression lines of the sub-season 2014.2 in the drained transect lacks due to limited information. Sub-season 2014.1 represent the period from 15 June to 30 June, sub-season 2014.2 from 1 July to 15 July, sub-season 2014.3 from 16 July to 31 July, and sub-season 2014.4 from 1 August to 20 August.

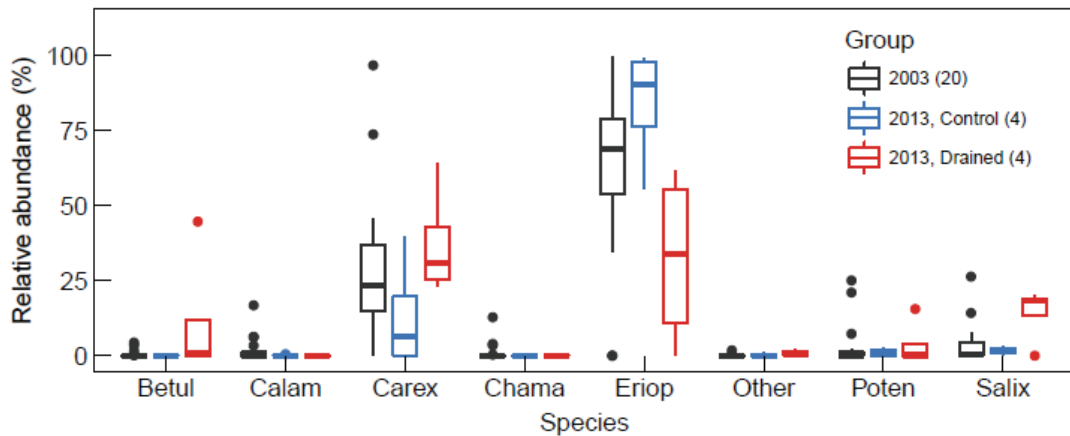


Figure 3.3 The abundance of vegetation species observed across the transects in 2003 and 2013. Numbers in parentheses are the number of replicates. Boxplot contains median, 25% and 75% quartiles, and ± 1.5 interquartile ranges. Betul: *Betula exilis*, Calam: *Calamagrostis purpurascens*, Carex: *C. appendiculata*, Chama: *Chamaedaphne calyculata*, Eriop: *Eriophorum angustifolium*, Poten: *Potentilla palustris*, Salix: *Salix* species.

In the control transect the plant community structures of the wet and the dry plots were dominated by *E. angustifolium* and *C. appendiculata*, respectively, but some dry plots within the drained transect showed a vegetation transition stage (Table 2.1). Plots in the drained transect that were categorized as CarexEriophorum (Table 2.1) showed a mixture of young *C. appendiculata* (without discrete tussock forms or small developing tussocks) and short and thin *E. angustifolium*. The presence of this mixture implies that these areas were formerly dominated by *E. angustifolium*, which is abundant in saturated areas, but whose abundance decreased due to drainage. The core plots that were selected based on drainage manipulation and WTD category represented this vegetation shift well; control_wet and drained_wet were dominated by *E. angustifolium*, control_dry was dominated by *C. appendiculata* and shrubs and drained_dry showed a transition stage from *E. angustifolium* to *C. appendiculata* (Table 2.1).

The abundance of shrubs (*Betula* and *Salix* sp.) was underestimated within the collars in the drained transect as a result of the methodological choice to exclude tall shrubs when selecting plots to ensure that all of the vegetation could fit into the chambers when measuring fluxes (Note that these results are presented to compare fluxes by vegetation group, see Section 2.5). The abundance of shrubs within the collars of the drained transect was 2% on average, while independently investigated average abundance along the transect was 20% on average. This

discrepancy will be taken into account in the following sections when interpreting the effects of shrubs on flux rates.

3.1.4 Microbial community structure

The fraction of methanogens was highest in control_wet and lowest in control_dry plots (Figure 3.4a). The two upper soil layers showed significant difference between four groups in the fractions (two-way ANOVA; drainage, $F = 4.67$, $P < 0.05$; WTD, $F = 6.50$, $P < 0.05$; drainage×WTD, $F = 6.31$, $P < 0.05$) as well as in the community composition (two-way PERMANOVA; drainage, $F = 9.41$, $P < 0.001$; WTD, $F = 6.37$, $P < 0.001$; drainage×WTD, $F = 8.80$, $P < 0.001$). *Methanobacterium* was prevalent in the control transect, while Rice Cluster II was dominant in the drained transect especially in deeper soil layers (Table 3.1 & Figure 3.4a).

Methanotrophs also showed the greatest fraction in control_wet and the smallest fraction in control_dry plots (Figure 3.4b). This difference was substantial by WTD when the fractions of the two uppermost soil layers were compared (two-way ANOVA; drainage, $F = 0.09$, $P = 0.76$; WTD, $F = 44.34$, $P < 0.001$; drainage×WTD, $F = 4.22$, $P = 0.06$). Significant difference was also found in community composition by WTD (two-way PERMANOVA; drainage, $F = 1.66$, $P = 0.19$; WTD, $F = 16.93$, $P < 0.001$; drainage×WTD, $F = 2.37$, $P = 0.10$). *Methylobacter* was most abundant in all depths of all plots and the fractions of *Methylocystis* were higher at the surface layers (Table 3.2 & Figure 3.4b).

The quantity of bacteria were 85% and 75% higher under dry conditions in the drained and the control transects, respectively (two-way ANOVA; drainage, $F = 26.75$, $P < 0.001$; WTD, $F = 23.81$, $P < 0.001$; drainage×WTD, $F = 2.76$, $P = 0.11$; Figure 3.5), but the abundance of archaea did not change (two-way ANOVA; drainage, $F = 2.11$, $P = 0.16$; WTD, $F = 0.50$, $P = 0.49$; drainage×WTD, $F = 9.33$, $P < 0.01$; Figure 3.5).

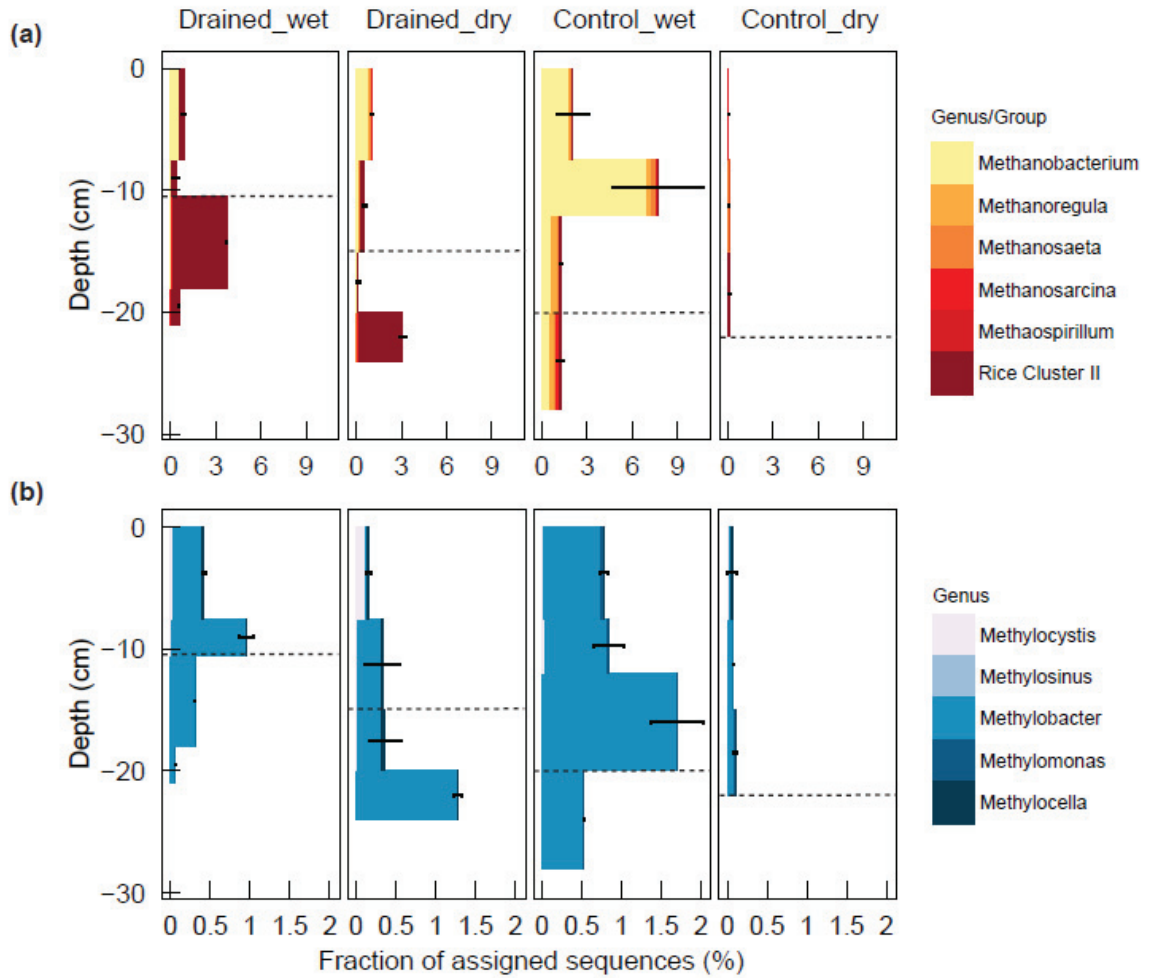


Figure 3.4 The fractions of CH₄-related microorganisms, (a) methanogenic groups and (b) methanotrophic groups by depth. Dashed lines indicate the borders between organic and mineral soil layers.

Table 3.1 Groups of methanogens found and substrates they use. Temperature and pH ranges are based on the investigations in species level, and the range may vary.

Genus/group	Substrates	Temp range	pH range	Ref.
Methanobacterium	H ₂ , (formate, alcohols)	20–70	5–9	162–164
Methanoregula ⁽¹⁾	H ₂ , formate	5–45	4–5.8	165
Methanosaeta	Acetate	10–70	5.5–8.4	163,164,166
Methanosarcina	Methylamines, methanol, (acetate, H ₂ , DMS ⁽³⁾)	1–55	4–8.5	163,164,166
Methanospirillum	H ₂ , formate, (alcohols)	30–45	6.6–7.4	164,167
Rice Cluster II ⁽²⁾	(H ₂)	NA	NA	168,169

⁽¹⁾ Candidatus Methanoregula, belonged to the order Methanomicrobiales

⁽²⁾ Uncultured group

⁽³⁾ Dimethylsulfide

NA: Not available

Table 3.2 Groups of methanotrophic bacteria, and enzymes that each group possesses. Temperature and pH ranges are based on the investigations in species level, and the range may vary.

Genus	Type	Enzyme genes (affinity to CH ₄)	Temp range	pH range	Ref.
Methylocystis	Type II	pmoA1 (low), pmoA2 (high)	10–40	6–9	170–174
Methylosinus	Type II	pmoA1 (low), pmoA2 (high)	10–40	5.5–9	171–174
Methylobacter	Type I	pmoA1 (low)	15–40	5.5–9.0	171,173,174
Methylomonas	Type I	pmoA1 (low)	10–42	3.8–8.5	171,173–175
Methylocella	-	mmoX (low)	4–30	4.2–7.5	176–178

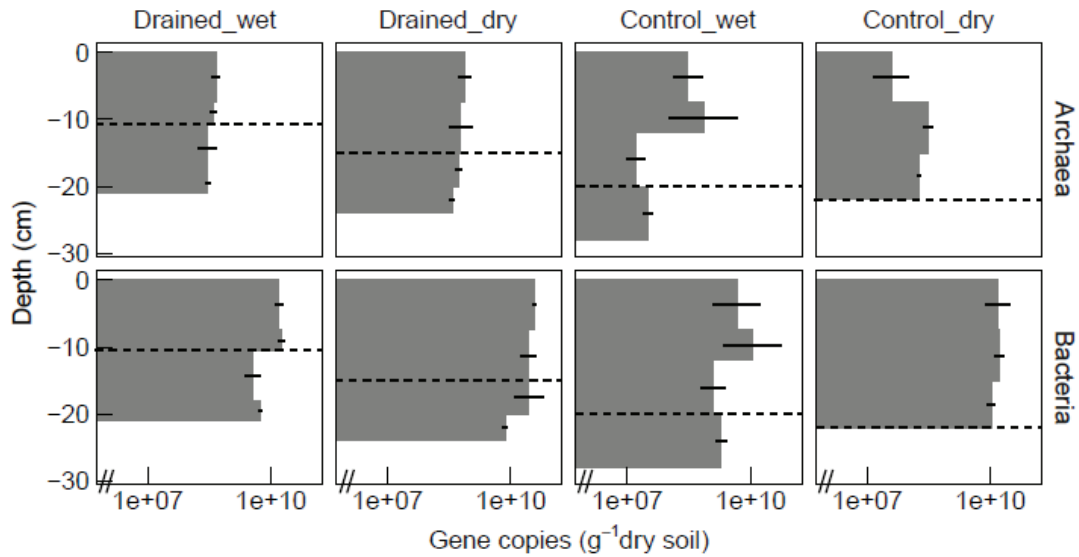


Figure 3.5 Gene copy numbers of archaea and bacteria by depth. Dashed lines indicate the borders between organic and mineral soil layers. Note that the X-axis is in log scale and has breaks.

3.2 Growing-season CO₂ fluxes

3.2.1 Tsoil effects on growing-season CO₂ fluxes

GPP and R_{eco} rates increased with T_{soil} at shallow layers (Figure 3.6) because warmer T_{soil} generally accelerate both photosynthesis^{179,180} and root respiration¹⁸¹. The average R_{eco} rates of the dry plots were 25% higher than those of the wet plots in 2013 (independent t -test, $P < 0.001$, $t = -5.70$, $df = 532$) despite the fact that GPP rates were found to be lower in the dry plots, meaning that lower R_a rates would have been expected (Figure 3.6).

Modifications in T_{soil} at shallow layers had greater impacts on R_h than those in T_{soil} at deep layers: The warmer T_{soil} at shallow layers of the dry plots increased R_h by 240%, while colder T_{soil} at deep layers reduced R_h only marginally as compared to the wet plots. Combining these two contrasting effects, R_h rates in dry plots were elevated by 95% as a result of the stronger effects of T_{soil} at shallow layers as compared to T_{soil} at deep layers on compacted peat soils.

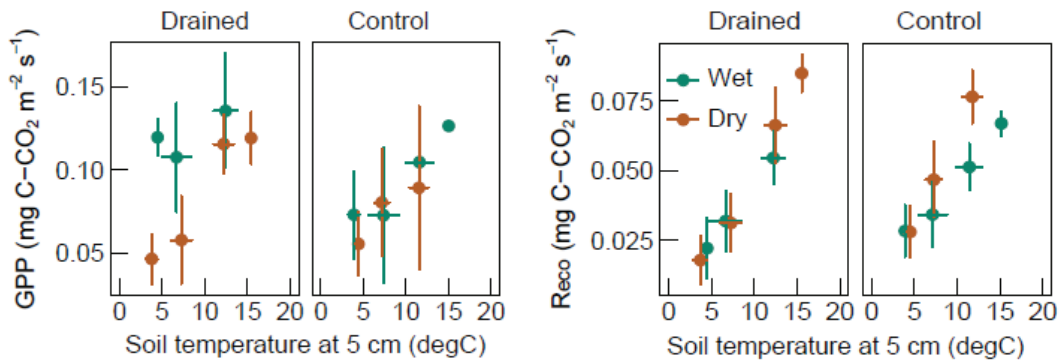


Figure 3.6 Links between average soil temperatures at 5 cm and gross primary production (GPP) and ecosystem respiration (R_{eco}) rates. Green color indicates wet plots and brown indicates dry plots. Data are from 2013 (20 July to 10 August) and sub-season 2014.4 (1 August to 20 August); both cover similar phenological periods. Data were grouped into temperature bins of 5 °C.

3.2.2 Plant effects on growing-season CO_2 fluxes

CO_2 flux measurements during the 2013 growing season showed similar mean and standard deviations of NEE, GPP, and R_{eco} rates between the two transects (Figure 3.7). However, fluxes showed a large variability across plots within each transect (each of which was *ca.* 225 m), which results from one-way ANOVA indicated to be closely linked to the dominant vegetation groups (NEE: $F = 24.99$, $P < 0.001$; Figure 3.7a). R_{eco} also differed by dominant vegetation group, but this difference was not as pronounced as it was for GPP (GPP: $F = 11.23$, $P < 0.001$, R_{eco} : $F = 3.63$, $P < 0.01$; Figure 3.7b & 3.7c).

One of the vegetation effects on CO_2 fluxes was that, *Eriophorum*-dominated plots in both transects had higher rates of photosynthetic uptake than *Carex*-dominated plots. GPP rates of *Eriophorum*Shrub were 55% higher than those of *Carex* in the drained transect, and those of *Eriophorum*Shrub and *Eriophorum* were 20% higher than those of *Carex*Shrub in the control transect in 2013 (Figure 3.7b). *Carex**Eriophorum* plots in the drained transect—which represent a vegetation transition from *E. angustifolium* to *C. appendiculata* following drainage—showed the lowest GPP rates in both years, despite the presence of *E. angustifolium* (Figure 3.7b). In addition, these plots showed decreasing GPP rates along with increasing PAR (Figure 3.8). Increasing shrub abundance slightly compensated for lowered GPP rates in drained areas following a reduction in *E. angustifolium* coverage. *Eriophorum*Shrub of the

control transect, which had 10% shrub coverage, had, on average, 4% higher GPP rates than Eriophorum in 2013 although this difference was not significant (Figure 3.7b).

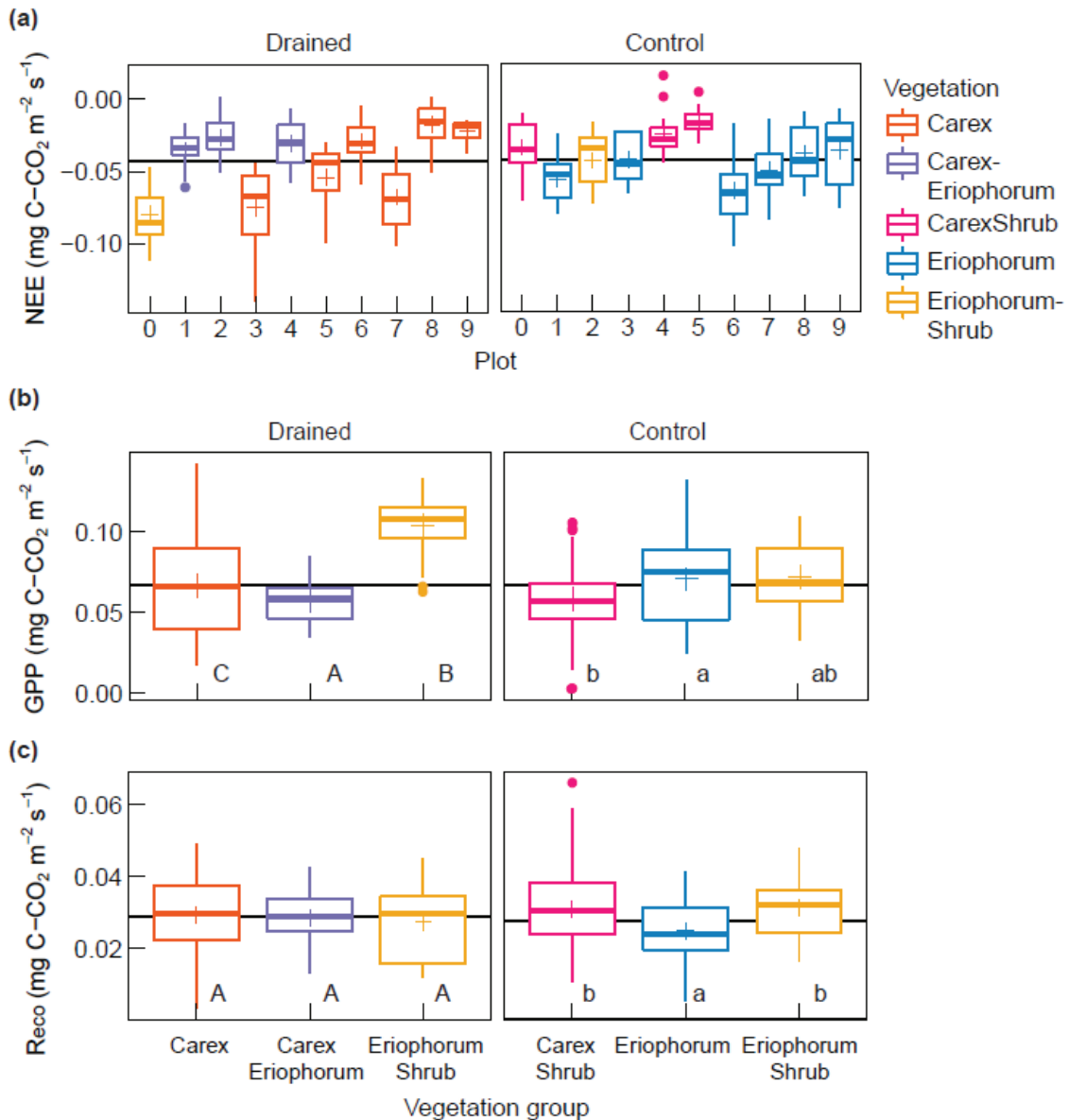


Figure 3.7 Growing-season CO₂ fluxes by vegetation type in 2013. (a) Variability of net ecosystem exchange (NEE) among individual plots during the 2013 growing season. Boxplot contains median, 25% and 75% quartiles, ± 1.5 interquartile ranges, as well as mean values with cross points per plot, with colors indicating the dominant vegetation species. The black horizontal bars show the mean flux rates averaged for the entire transect. (b) Gross primary production (GPP) and (c) ecosystem respiration (R_{eco}) rates aggregated by vegetation group. Significance of differences between groups, determined by one-way ANOVA and Tukey's post hoc test, is indicated by the letters. Different letters indicate significant differences between groups while the same letters indicate significant similarities.

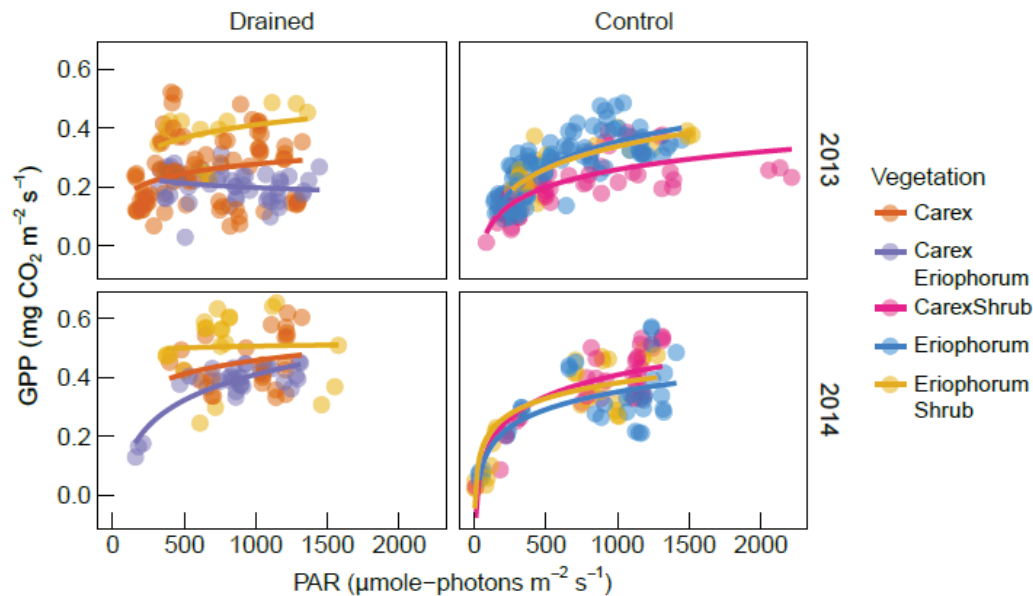


Figure 3.8 Logarithmic relations between photosynthetically active radiation (PAR, X axis) and gross primary production (GPP, Y axis) by transect (columns), vegetation type (color) and year (rows). Data points are only from August when vegetation activity was high enough to minimize seasonality.

3.2.3 Gap-filled growing-season CO_2 flux rates

The modeled fluxes for both 2013 and 2014 had similar patterns to the observed fluxes: *Eriophorum*-dominated plots (i.e., wet plots) generally showed higher GPP rates than *Carex*-dominated plots (i.e., dry plots) in both transects (Table 3.3). In addition, the 10% difference in shrub cover between *Eriophorum* and *EriophorumShrub* from the control transect did not significantly affect GPP rates (Table 3.3). R_{eco} rates were consistently greater in the dry plots, in part due to increased R_h rates, and the cumulative R_{eco} increased with drainage by 5% in 2013 and by 10% in 2014 (Table 3.3). Combining the effects of T_{soil} and vegetation on R_{eco} and GPP rates, the net effects of drainage on CO_2 fluxes (NEE) was $-0.3 \text{ g C-CO}_2 \text{ m}^{-2} \text{ day}^{-1}$ (i.e., 25% more CO_2 uptake) in 2013 and $+0.98 \text{ g C-CO}_2 \text{ m}^{-2} \text{ day}^{-1}$ (i.e., 35% less CO_2 uptake) in 2014 when daily CO_2 fluxes of 20 days, weighted by the number of plots of each group, were compared (Table 3.3). Despite the variability between years for transect level, patterns of underlying processes were consistent: After 10 years of drying manipulation, the replacement of *E. angustifolium* by *C. appendiculata*, more aerobic conditions, and increased T_{soil} at shallow layers all weakened CO_2 uptake and increased CO_2 emission (Table 3.3).

Table 3.3 Average daily flux ($\text{g C-CO}_2 \text{ m}^{-2} \text{ day}^{-1}$) from interpolation for the period of 22 July to 10 August (20 days) in both 2013 and 2014. Values in parentheses are cumulative flux ($\text{g C-CO}_2 \text{ m}^{-2}$) for the period of 22 July to 10 August (20 days) in 2013 and 16 June to 20 August (66 days) in 2014. Results from 2013 represent the fits of all data points \pm standard deviation from bootstrapping, and those of 2014 represent mean \pm standard deviation from bootstrapping. Net ecosystem exchange (NEE) was calculated by subtracting gross primary production (GPP) from ecosystem respiration (R_{eco}): positive values are CO_2 emission to the atmosphere, and negative values are CO_2 uptake by the terrestrial ecosystem.

Year	Group	R_{eco}	GPP	NEE
2013	D_Carex	2.03 ± 0.10 (41 \pm 2)	3.42 ± 0.00 (68 \pm 0)	-1.38 ± 0.09 (-28 \pm 2)
	D_CarexEriophorum	1.89 ± 0.16 (38 \pm 3)	3.30 (66) ¹	-1.41 ± 0.24 (-28 \pm 5) ¹
	D_EriophorumShrub	1.88 ± 0.53 (38 \pm 11)	4.81 (96) ¹	-2.93 ± 0.34 (-59 \pm 7) ¹
	C_CarexShrub	2.04 ± 0.08 (41 \pm 2)	2.55 ± 0.02 (51 \pm 0)	-0.51 ± 0.05 (-10 \pm 1)
	C_Eriophorum	1.76 ± 0.05 (35 \pm 1)	3.41 ± 0.01 (68 \pm 0)	-1.65 ± 0.04 (-33 \pm 1)
	C_EriophorumShrub	2.34 ± 0.17 (47 \pm 3)	3.32 ± 0.00 (66 \pm 0)	-0.98 ± 0.14 (-20 \pm 3)
2014	D_wet (EriophorumShrub)	3.27 ± 0.16 (184 \pm 9)	7.59 ± 0.11 (404 \pm 6)	-4.31 ± 0.05 (-221 \pm 3)
	D_dry (CarexEriophorum)	3.51 ± 0.19 (200 \pm 9)	5.14 ± 0.07 (274 \pm 4)	-1.64 ± 0.11 (-74 \pm 5)
	C_wet (EriophorumShrub)	2.81 ± 0.24 (162 \pm 14)	5.85 ± 0.03 (312 \pm 1)	-3.05 ± 0.21 (-150 \pm 13)
	C_dry (CarexShrub)	3.98 ± 0.21 (222 \pm 12)	6.20 ± 0.03 (331 \pm 2)	-2.22 ± 0.18 (-109 \pm 10)

¹ As no bootstrapping was conducted on data for GPP, error range in NEE is only from R_{eco} .

3.2.4 Model error from interpolation

Comparing observed against modeled flux rates for all individual measurements in the database, the mean RMSE of R_{eco} was 0.009 and 0.007 $\text{mg C-CO}_2 \text{ m}^{-2} \text{ s}^{-1}$ for 2013 and 2014, respectively, and that of GPP was 0.021 and 0.016 $\text{mg C-CO}_2 \text{ m}^{-2} \text{ s}^{-1}$ for 2013 and 2014, respectively (Table 3.4). Low uncertainty ranges imply that variations in R_{eco} and GPP can be mainly explained by T_a and PAR, respectively. The uncertainty ranges of R_{eco} were large compared to those of GPP (Table 3.4), suggesting that R_{eco} rates varied with factors other than T_a , while GPP rates mostly varied with PAR. Larger RMSE and MBE in the drained transect in 2013 compared to the control transect can be attributed to the pooling of data points by vegetation group, as well as to the limited number of data points; the large error in GPP for the Carex group of the drained transect can be attributed to varying standing biomass, and that of the EriophorumShrub in the drained transect stems from the small number of data points

(Table 3.4). In 2014, data points for each group came from only a single plot, but varying WTD and thickening TD over the growing season resulted in relatively large errors (Table 3.4).

Table 3.4 Root mean squared error (RMSE) and mean bias error (MBE) of the observed and interpolated fluxes ($\text{mg C-CO}_2 \text{ m}^{-2} \text{ s}^{-1}$). The observed fluxes indicate those used for calibration. Period of interpolation: 22 July to 10 August (20 days); values in parentheses for 2014: 16 June to 20 August (66 days).

Year	Group	Ecosystem respiration		Gross primary production	
		RMSE	MBE	RMSE	MBE
2013	D_Carex	0.009	0.00004	0.025	-0.035
	D_CarexEriophorum	0.007	-0.002	0.013	-0.001
	D_Eriophorumshrub	0.01	0.00005	0.026	-0.029
	C_CarexShrub	0.008	0.00002	0.016	-0.035
	C_Eriophorum	0.006	-0.00001	0.017	-0.027
	C_EriophorumShrub	0.007	0.000002	0.014	-0.034
	2014	D_wet (EriophorumShrub)	0.003 (0.007)	-0.0002 (-0.00004)	0.032 (0.03)
D_dry (CarexEriophorum)		0.008 (0.009)	0.003 (-0.00006)	0.02 (0.022)	0.003 (-0.054)
C_wet (EriophorumShrub)		0.01 (0.01)	-0.004 (-0.00002)	0.013 (0.023)	0.003 (-0.044)
C_dry (CarexShrub)		0.012 (0.011)	0.001 (0.0002)	0.023 (0.03)	0.002 (-0.091)

3.3 R_{eco} partitioning

3.3.1 $\Delta^{14}\text{C}$ of R_{eco} and sources

$\Delta^{14}\text{C-R}_{\text{eco}}$ significantly differed by treatment (ANOVA; $F = 5.35$, $P < 0.01$; Figure 3.9a). These shifts in signals can be explained by increased contributions of SS and decreased contributions of DS to R_{eco} following drainage (ANOVA; SS, $F = 5.28$, $P < 0.05$; DS, $F = 6.21$, $P < 0.01$; AT, $F = 2.03$, $P = 0.15$; Figure 3.9b). Soil cores were collected in the middle of July, and TD continued to increase until the middle of August when $\Delta^{14}\text{C-R}_{\text{eco}}$ was measured. This may have resulted in overestimation of $\Delta^{14}\text{C-DS}$ as well as the contributions of DS to R_{eco} . However, this discrepancy applied to all treatments, so the patterns found among treatments may remain the same.

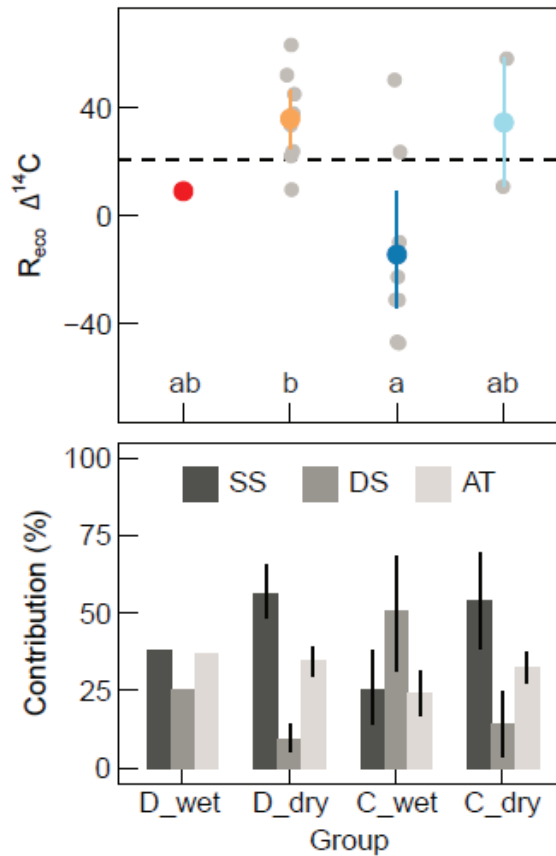


Figure 3.9 $\Delta^{14}\text{C}$ of ecosystem respiration (R_{eco}) and contributions of surface soil (SS), deep soil (DS), and autotrophs (AT) to R_{eco} . (a) $\Delta^{14}\text{C}-R_{\text{eco}}$ (mean \pm standard deviation) and individual measurements (gray points). Dashed lines are atmospheric $\Delta^{14}\text{C}$. Significance of differences by treatment, determined by one-way ANOVA and Tukey's post hoc test, is indicated by the letters. Different letters indicate significant difference among treatments, while the same letters indicate significant similarity. (b) Contributions of each source to R_{eco} (mean \pm standard deviation). SS: surface soil, DS: deep soil, AT: autotrophs.

3.3.2 Drainage effects on R_{eco} and its patterns

The abundance of *E. angustifolium* was found to be the major parameter negatively affecting $\Delta^{14}\text{C}-R_{\text{eco}}$ and the contributions of each source to R_{eco} (Figure 3.10 & Table 3.5). The abundance of *E. angustifolium* increased with WTD (correlation: $r = 0.77$, $P < 0.001$), and thus, drier soil conditions were also associated with higher $\Delta^{14}\text{C}-R_{\text{eco}}$. Consequently, contributions of SS decreased with higher abundance of *E. angustifolium*, i.e., wetter conditions, whereas those of DS increased (Figure 3.11 & Table 3.6). TD that is closely linked with WTD was also selected as the main explanatory factors for contributions of R_{h} to R_{eco} (Table 3.6).

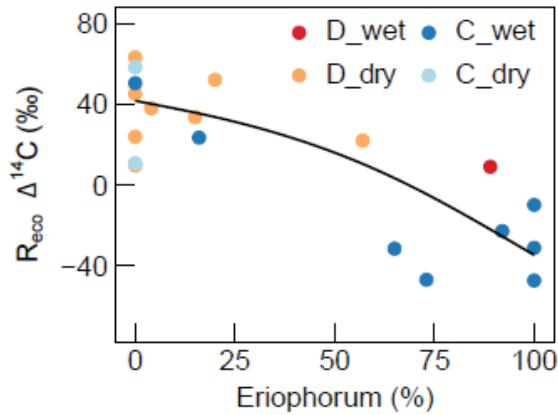


Figure 3.10 Relationships between $\Delta^{14}\text{C}$ of ecosystem respiration and the *Eriophorum angustifolium* abundance that is abundant in wet areas. The lines are drawn based on the predicted values from multiple linear regressions including the *E. angustifolium* abundance and water table depth, as described in Table 3.5.

Table 3.5 Multiple linear regressions with $\Delta^{14}\text{C}$ of ecosystem respiration (R_{eco}) as the dependent variable. WTD: water table depth.

Response	Parameters	Coefficients	SE	<i>t</i> value	<i>P</i> value	R^2	<i>P</i> value
$\Delta^{14}\text{C}-R_{\text{eco}}$	Intercept	51.81	8.39	6.17	< 0.001	0.67	< 0.001
	WTD	1.24	0.66	1.87	0.08		
	Eriophorum	-0.65	0.22	-2.96	< 0.01		
	WTD:Eriophorum	-0.05	0.03	-1.53	0.15		

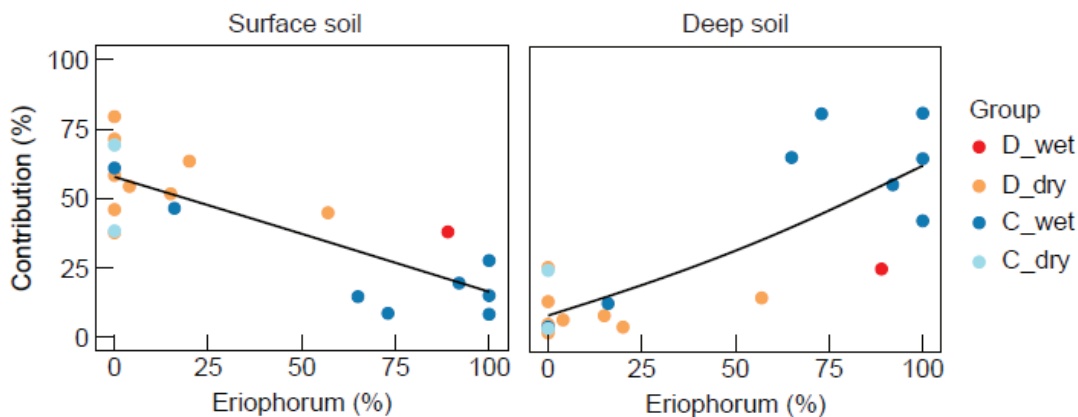


Figure 3.11 Relationships between source contributions and the *Eriophorum angustifolium* abundance that is abundant in wet areas. The lines are drawn based on the predicted values from multiple linear regression analyses including the *E. angustifolium* abundance, water table depth, and thaw depth, as described in Table 3.6.

Table 3.6 Multiple linear regressions with contributions of surface soil (SS) and deep soil (DS) as the dependent variable. Contributions of autotroph (AT) are not given because of insignificant regressions. WTD: water table depth, TD: thaw depth.

Response	Parameters	Coefficients	SE	<i>t</i> value	<i>P</i> value	<i>R</i> ²	<i>P</i> value
SS	Intercept	0.95	0.24	3.89	< 0.01	0.69	< 0.001
	WTD	0.01	0.04	2.26	< 0.05		
	TD	-0.01	0.01	-1.35	0.20		
	Eriophorum	-0.003	0.001	-2.69	< 0.05		
	WTD:Eriophorum	-0.0003	0.0002	-1.66	0.12		
DS	Intercept	-0.23	0.32	-0.71	0.49	0.66	< 0.001
	WTD	-0.01	0.01	-1.44	0.17		
	TD	0.01	0.01	0.86	0.40		
	Eriophorum	0.004	0.002	2.21	< 0.05		
	WTD:Eriophorum	0.0004	0.0002	1.82	0.09		

When R_{eco} rates and the source contributions were combined, drainage in wet tundra ecosystems increased R_{eco} rates, and this increase could largely be attributed to the enhanced decomposition of young soil carbon at shallow layers, while the contributions of old soil at deep layers were significantly reduced (Figure 3.12).

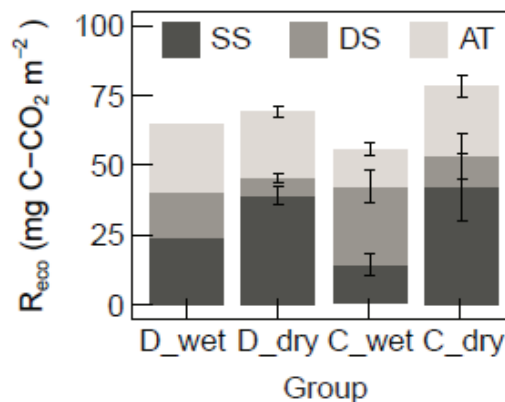


Figure 3.12 Ecosystem respiration (R_{eco}) with partitioned sources (mean \pm standard error). R_{eco} data are from 1–20 August 2014 and multiplied with the contributions of three sources, i.e., surface soil (SS), deep soil (DS), and autotrophs (AT).

3.4 Growing-season CH₄ fluxes

3.4.1 T_{soil} effects on growing-season CH₄ fluxes

T_{soil} at deep layers of the wet plots was positively related to growing-season CH₄ fluxes (linear regressions for August; drained transect, adj. $R^2 = 0.93$, $P < 0.001$; control transect, adj. $R^2 = 0.11$, $P < 0.001$; Figure 3.13a), while T_{soil} at shallow layers of the dry plots was negatively correlated with growing-season CH₄ fluxes (linear regressions for August; drained transect, adj. $R^2 = 0.04$, $P < 0.05$; control transect, adj. $R^2 = 0.00$, $P = 0.32$; Figure 3.13b). It should be noted that CH₄ production and oxidation rates were not determined in this study and these correlations were based on the assumption that (1) CH₄ production occurs actively at deep soil layers with more anoxic condition, while CH₄ oxidation happens more at shallow layers with more oxic condition, and (2) CH₄ fluxes of the wet plots are dominated by CH₄ production or less affected by CH₄ oxidation, and those of the dry plots are largely influenced by CH₄ oxidation.

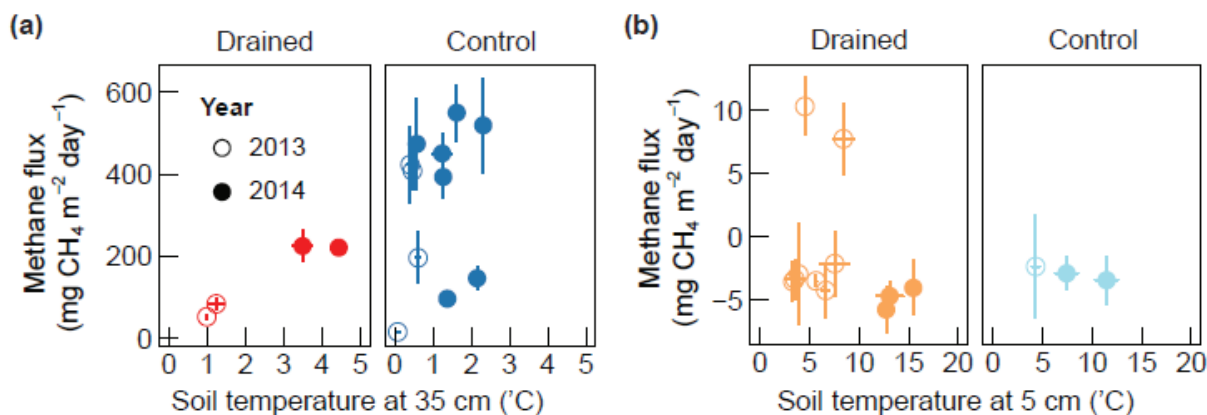


Figure 3.13 Relationships between soil temperatures (T_{soil}) and growing-season CH₄ fluxes. (a) Relationship between T_{soil} at 35 cm and CH₄ fluxes of the wet plots and (b) between T_{soil} at 5 cm and CH₄ fluxes of the dry plots. Data are from August to minimize seasonality and were grouped into temperature bins of 5 °C from 0 °C to 20 °C. Data from the dry plots with rising WTD due to heavy precipitation were excluded.

3.4.2 Plant effects on growing-season CH₄ fluxes

The abundance of *E. angustifolium* considerably decreased following drainage (one-way ANOVA; $F = 8.45$, $P < 0.001$; Figure 3.14a), and it was positively correlated with CH₄ fluxes, suggesting *E. angustifolium* may effectively transport CH₄ through aerenchyma (linear regressions for August; drained transect, adj. $R^2 = 0.72$, $P < 0.001$; control transect, adj. $R^2 = 0.55$, $P < 0.001$; Figure 3.14b). *C. appendiculata* showed negative correlations with CH₄ fluxes (linear regressions for August; drained transect, adj. $R^2 = 0.67$, $P < 0.001$; control transect, adj. $R^2 = 0.63$, $P < 0.001$) but it does not suggest “reverse” CH₄ transport through aerenchyma—CH₄ transport from the atmosphere to soils—but lower CH₄ fluxes with more abundant *C. appendiculata* that represent drier conditions. The other aerenchymatous species present in the site—*P. palustris*—did not show correlations with CH₄ fluxes (data not shown). When CH₄ transport through *P. palustris* was measured, its contribution was approximately 10 times lower than *E. angustifolium* (data not shown).

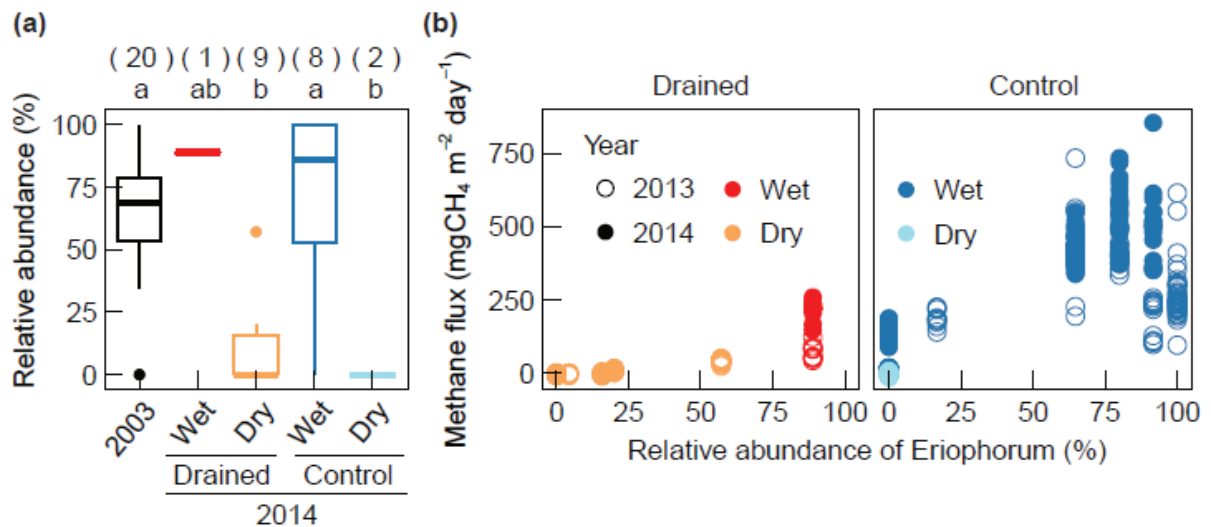


Figure 3.14 The abundance of *Eriophorum angustifolium* and its relationship with CH₄ fluxes. (a) Abundance of *E. angustifolium*, with 25% and 75% quartiles, and ± 1.5 interquartile ranges. Numbers in parentheses are the number of observations. Significance of differences between groups, determined by one-way ANOVA and Tukey’s post hoc test, is indicated by the letters. Different letters denote significant difference among groups, while the same letters indicate significant similarity. (b) Relation between the abundance of *E. angustifolium* and CH₄ fluxes. Data are from August to minimize temporal variability in fluxes. Colors indicate four groups and shapes indicate the observation year.

3.4.3 Microbial effects on growing-season CH₄ fluxes

Control_wet showed the highest CH₄ fluxes, drained_wet followed as the second highest, and the dry plots showed fluxes close to 0 (see Section 3.4.4). Given these patterns, CH₄ fluxes were coincided with higher fractions of methanogens and methanotrophs (Figure 3.4).

3.4.4 Growing-season CH₄ flux rates

CH₄ fluxes were significantly larger in the wet plots in both transects: Control_wet showed the highest daily CH₄ fluxes, drained_wet followed as the second highest, and the dry plots showed fluxes close to 0 (Table 3.7 & Figure 3.15a). Some of the dry plots showed negative net fluxes, suggesting oxidation rates exceed production rates (Table 3.7 & Figure 3.15). Fluxes of control_wet were about three times higher than those of drained_wet in both years despite similar WTD (Table 3.7 & Figure 3.15). Weighting the average daily fluxes with the number of wet and dry plots of each transect resulted in approximately 19 and 28 times lower CH₄ emission rates compared to the control transect in 2013 and 2014, respectively (Table 3.7).

Table 3.7 Daily and cumulative CH₄ fluxes. Daily: daily CH₄ fluxes (mean ± standard deviation) over 18 days (24 July to 10 August) in 2013 and over 62 days (20 June to 20 August) in 2014. Each group of data from 2013 consists of multiple plots, while that from 2014 consists of the core plots only. Therefore, the standard deviation values of 2013 are from both spatial and temporal variation whereas those of 2014 are from temporal variation only. Cumulative: cumulative CH₄ fluxes (mean ± standard deviation) of 18 days in 2013 and 62 days in 2014. Cumulative CH₄ fluxes were calculated from each plot, and the mean and standard deviation of those fluxes were calculated by group. Therefore, the groups that consist of a single plot are given without standard deviations.

Group	Daily (mg CH ₄ m ⁻² day ⁻¹)		Cumulative (mg CH ₄ m ⁻²)	
	2013	2014	2013	2014
Drained_wet	77 ± 13	105 ± 77	1392	6496
Drained_dry	4 ± 14	-1 ± 2	69 ± 272	-71
Control_wet	267 ± 141	332 ± 168	4803 ± 2437	20467
Control_dry	-2 ± 1	-3 ± 1	-33 ± 17	-177

One plot from drained_dry showed significantly higher cumulative fluxes compared to other plots of the same group (Figure 3.15b). It was coincided with abundant *E. angustifolium*

coverage. In addition, another plot from control_wet group showed considerably lower cumulative fluxes (Figure 3.15b), and it was dominated with *C. appendiculata*. These variations suggest that WTD is not the only factor that explains variations in CH₄ fluxes (Table 3.7 & Figure 3.15b).

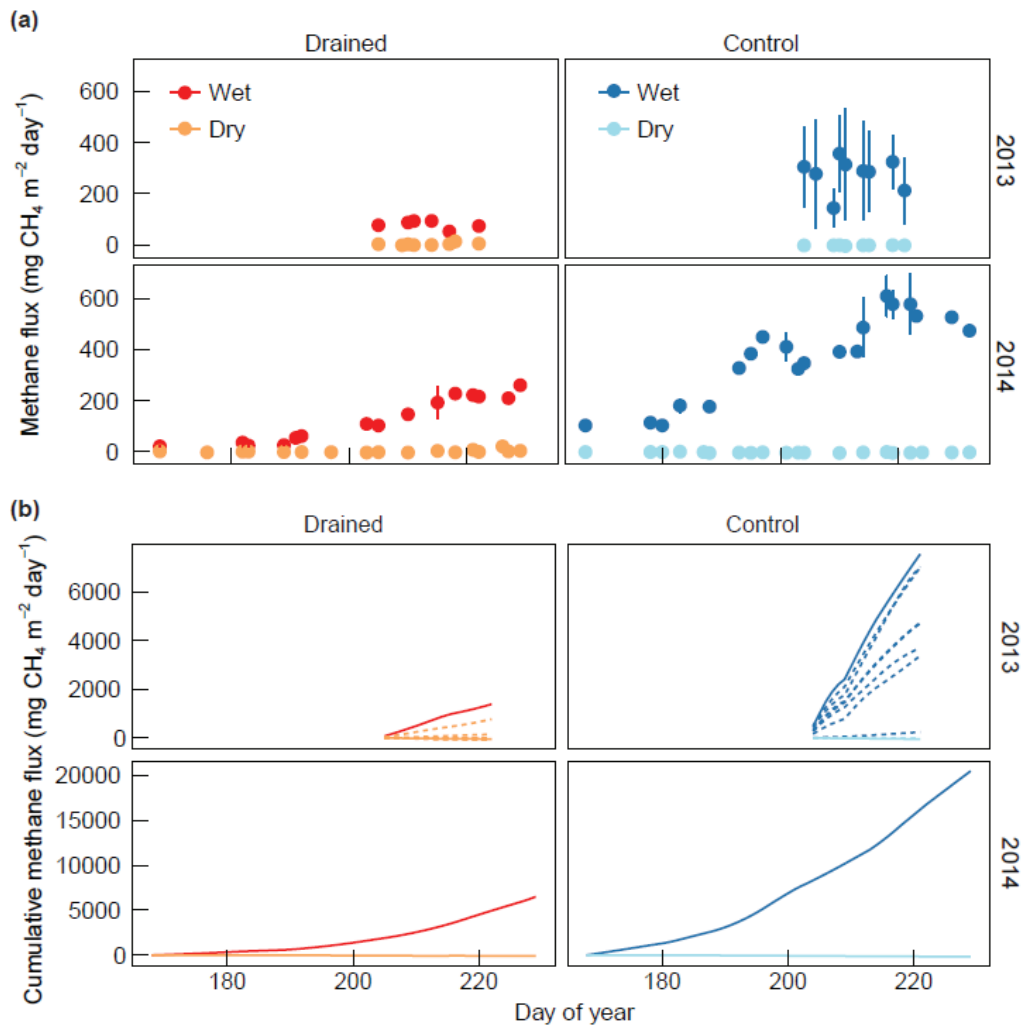


Figure 3.15 CH₄ fluxes during the growing season of 2013 and 2014. (a) Points represent average daily CH₄ fluxes of each group (2013) or plot (2014) and error bars represent standard deviations from multiple plots (2013) or multiple measurements from a single plot (2014). (b) Cumulative CH₄ fluxes are based on linear interpolation by plot. Data covered 18 days (24 July to 10 August) in 2013, and 62 days (20 June to 20 August) in 2014. Solid lines in 2013 indicate fluxes at core plots that correspond to lines in 2014. Note that the scale of 2013 and 2014 are different.

The contribution of aerenchyma to the total CH₄ flux varied among four categories: control_wet showed the highest contribution with 25% and drained_wet followed with 5% (Table 3.8). Control_dry had 0% contribution because it did not have *E. angustifolium* (Table 3.8). Drained_dry showed very high proportion of aerenchyma transport to the total CH₄ fluxes (i.e., 75%), while the absolute values of the total CH₄ fluxes were close to 0 (Table 3.7 & 3.8). CH₄ transport continued after clipping plants right above the water table, suggesting that plant-mediated CH₄ transport was not from active transport, but diffusive transport. Because plant-mediated CH₄ transport by *E. angustifolium* was passive diffusion, it can be considered to be independent from stomatal conductance and diurnal fluctuations¹⁸².

Control_wet emitted 2% of CH₄ through ebullition, while no ebullition events were observed in other plots (Table 3.8). When ebullition events that might come from disturbance are included, the percentage of control_wet increases to 4%, while drained_wet increases to 1% (Table 3.8). The dry plots did not show any ebullition events (Table 3.8).

Table 3.8 Contribution of plant-mediated CH₄ transport and ebullition to the total CH₄ fluxes. The percentage was calculated with the data acquired from 23 July to 20 August in 2014. For aerenchyma, numbers in parenthesis indicate sensitivity of this estimate when the green leaf lengths changes by 10 cm and the number of plants change by 5. For ebullition, numbers in parentheses indicate ebullition events that occurred within 30 sec after the chamber was placed on the collar, which may be resulted from physical disturbance.

	Aerenchyma (%)	Ebullition (%)
Drained_wet	5 ± 1 (± 5)	0 (+ 1)
Drained_dry	75 ± 300 (± 680) ¹	0
Control_wet	25 ± 10 (± 20)	2 (+ 2)
Control_dry	NA ²	0

¹ Higher than 100% values indicate the amount of plant-mediated CH₄ transport was higher than the total CH₄ fluxes, and the difference came from CH₄ oxidation.

² Not available data. No *Eriophorum angustifolium* existed.

Total carbon content was 20% higher in the drained transect in the organic soils (two-way ANOVA; drainage, $F = 25.40$, $P < 0.001$; WTD, $F = 0.56$, $P = 0.46$; drainage×WTD, $F = 1.83$, $P = 0.18$) and 45% higher in the mineral soils (two-way ANOVA; drainage, $F = 11.69$, $P < 0.01$; WTD, $F = 12.24$, $P < 0.01$; drainage×WTD, $F = 7.46$, $P < 0.05$). However, both

transects had high carbon content with 30% and 4% on average in organic and mineral soils, respectively, which is essential for CH₄ production.

3.5 Nongrowing-season CO₂ and CH₄ fluxes

Due to the low T_a and low PAR, GPP in the nongrowing season was negligible. Although a limited amount of photosynthetic activity could have theoretically taken place during this time¹⁸³, no significant differences were found between NEE and R_{eco}, implying that CO₂ fluxes consisted mostly of CO₂ released from the soil.

The drained transect emitted an average of four times more CO₂ and 10% more CH₄ than the control transect: If the observed flux pattern is representative for the entire month of November, the net CO₂ and CH₄ emission of this month would be 11 g C-CO₂ m⁻² and 330 mg CH₄ m⁻² in the drained transect and 3 g C-CO₂ m⁻² and 300 mg CH₄ m⁻² in the control transect.

CO₂ and CH₄ fluxes in the nongrowing season were generally lower compared to those in the growing-season, but some plots showed sporadically high fluxes, the rates of which were comparable to flux rates from the growing season (Figure 3.16). These high CO₂ fluxes in the drained transect could be linked to vegetation groups, especially the abundance of *E. angustifolium*, as well as to P_a and T_{soil} (multiple linear regression, adj. R² = 0.46, P < 0.001; P_a, P < 0.001; T_{soil} at 5 cm, P < 0.001; *Eriophorum*, P < 0.001; P_a × T_{soil} at 5 cm, P < 0.001; P_a × *Eriophorum*, P < 0.001). Similar factors influenced CH₄ fluxes in the nongrowing season as well: Fluxes were positively influenced by T_a and the abundance of *E. angustifolium*, and negatively influenced by P_a (drained, Equation 3.1; control, Equation 3.2). When P_a is decreasing, accumulated CH₄ in soils can be easily emitted to the atmosphere due to diminished P_a applied to soils^{184,185}.

$$\text{CH}_4 \text{ fluxes (mg CH}_4 \text{ m}^{-2} \text{ s}^{-1}) = 30.0 \times \text{Eriophorum (\%)} \times e^{1.302 \times T_a (\text{°C})} \quad (3.1)$$

Model evaluation: 0.11, R² = 0.43, P < 0.001, RMSE = 0.0004, MBE = -0.00003

$$\text{CH}_4 \text{ fluxes (mg CH}_4 \text{ m}^{-2} \text{ s}^{-1}) = \frac{0.093}{P_a \text{ (hPa)}} \quad (3.2)$$

Model evaluation: 0.00, R² = 0.08, P < 0.001, RMSE = 0.0005, MBE = -0.00003

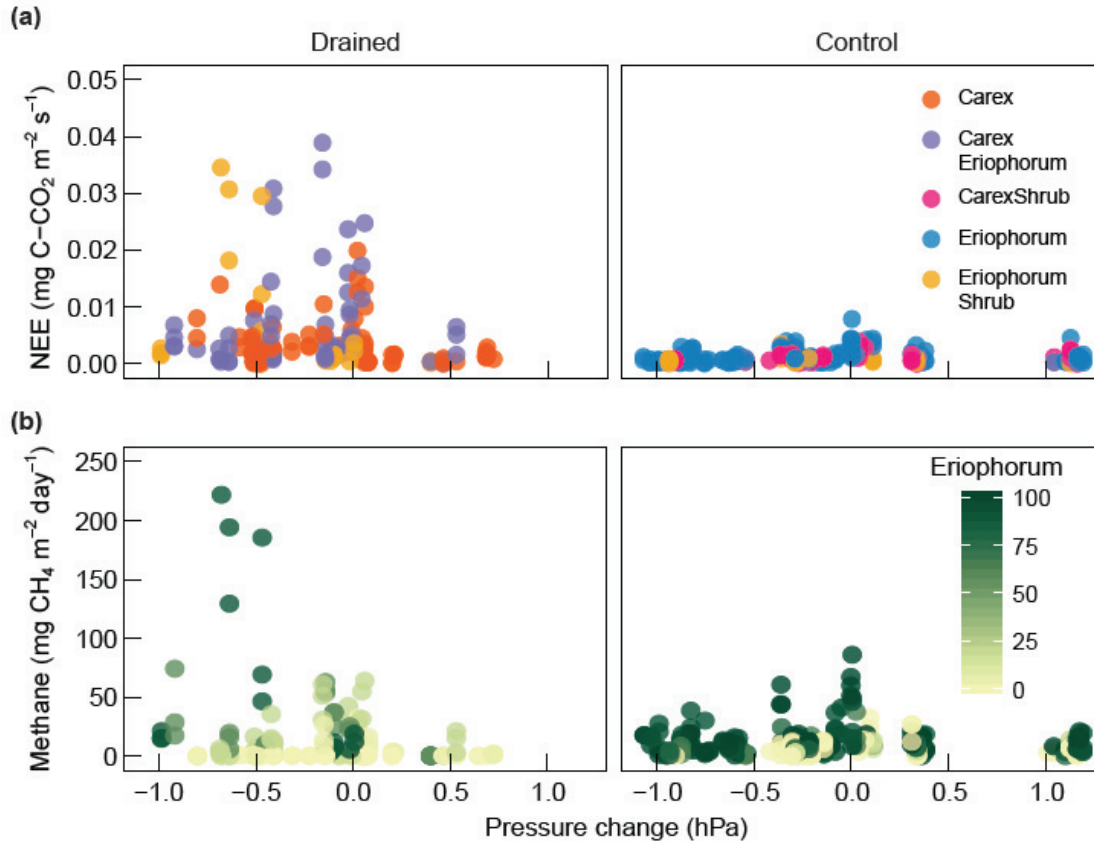


Figure 3.16 CO₂ and CH₄ fluxes in the nongrowing season against the changes in air pressure. Changes in air pressure refer to changes within 6 hours before individual flux was measured. (a) Net ecosystem exchange (NEE) by vegetation type (color), and (b) CH₄ fluxes by the abundance of *Eriophorum angustifolium*.

These parameters were found to be similar to those that affect growing-season CH₄ fluxes (drained, Equation 3.3; control, Equation 3.4), suggesting CH₄ fluxes are influenced by similar factors in the growing and nongrowing seasons.

$$\text{CH}_4 \text{ fluxes (mg CH}_4 \text{ m}^{-2} \text{ s}^{-1}) = \frac{0.091 \times T_{\text{soil at 35 cm (}^\circ\text{C)}}}{0.15 \times \text{Pa (hPa)} + 4.3 \times \text{Carex (\%)}} \quad (3.3)$$

Model evaluation: 0.88, $R^2 = 0.90$, $P < 0.001$, RMSE = 0.001, MBE = -0.00007

$$\text{CH}_4 \text{ fluxes (mg CH}_4 \text{ m}^{-2} \text{ s}^{-1}) = \frac{0.056 \times \text{Eriophorum (\%)}}{\text{Pa (hPa)}} \quad (3.4)$$

Model evaluation: 0.69, $R^2 = 0.70$, $P < 0.001$, RMSE = 0.007, MBE = -0.00007

However, growing-season CO₂ fluxes were not considerably influenced by these parameters because of much stronger signals of photosynthetic uptake as well as decomposition and respiration, which are affected by T_a, T_{soil}, and PAR, as described in Section 3.2.

Chapter 4. Discussion

4.1 Drainage effects on ecosystem properties

4.1.1 Changes in WTD following drainage

The amount of precipitation was similar at both transects, but WTD for some drained_dry plots was more susceptible to increase compared to the control_dry plots; this was because the width of the area within the drainage ring was three times larger than that of the elevated areas of control_dry plots, and, accordingly, pathways for lateral drainage of water into the nearest depression were considerably longer. In addition, drainage may slow when the water level rises within the drainage ditch due to the obstruction of water flow by taller vegetation—*E. angustifolium* and aquatic plants—at the end of the growing season^{186,187}. As a result, WTD in drained_dry plots stayed high longer than in the control transect following heavy rainfalls. Similar patterns were also observed in 2005, one year after the drainage ditch was installed¹⁰⁵. Nonetheless, WTD difference between the wet and the dry plots showed distinct patterns. In the long term, it can be speculated that new drainage pathways will be established within the drainage area, which will lead water away more effectively after precipitation events, and thus reduce the fluctuations in WTD related to rainfall events, which were observed at our site. Transferring our findings to a natural disturbance scenario (e.g., the formation of a connected system of troughs following ice-rich permafrost degradation), water drainage is expected to be more effective than our drainage manipulation, as thawing permafrost following persistently warmer conditions is likely to induce more pronounced topographical changes^{65,66,70}.

4.1.2 Changes in Tsoil following drainage

Following drainage, Tsoil was observed to be warmer at shallow soil layers but colder at deep soil layers. This finding highlights the important role of water content in the thermal properties of organic soils, with soils at shallow layers of the dry plots tending to heat up more easily during the daytime due to the reduced heat capacity of dry organic soil^{188–191}. At the same time, these dry organic soils also have lower thermal conductivity, limiting downward heat transfer; as a result, deeper soil layers remained colder than soils at the same depth in the wet plots¹⁹¹.

However, the relationship between soil moisture and temperature needs to be evaluated with caution, because the net effect depends on the balance of changes in both heat capacity and thermal conductivity, and the degree of changes in soil moisture in each organic and mineral soil layers¹⁹². In addition, the effects of physical structures of vegetation on T_{soil} need to be monitored as well. For example, increasing abundance of shrubs can reduce T_{soil} due to shade¹⁹³, while increase T_{soil} due to decreased albedo¹⁹⁴.

4.2 Growing-season CO_2 fluxes

4.2.1 T_{soil} effects on growing-season CO_2 fluxes

Increase in the R_{eco} rates in dry plots can be partly explained by the increased rates of R_{h} under more aerobic conditions following drainage: As anaerobic respiration is slower and less efficient than aerobic respiration, carbon release from both organic and mineral soils (surface and deep soil layers, respectively) under aerobic conditions can be 4–10 times higher than under anaerobic conditions¹⁰⁹. However, drier conditions altered T_{soil} regimes, and these effects further affected R_{h} rates.

Although colder T_{soil} at deep layers slightly decrease R_{h} rates in dry plots, warmer T_{soil} at shallow layers significantly elevated R_{h} rates. This increase was largely due to a greater amount of organic carbon—an increased total carbon content by 11% as well as more compacted soil with an increase in bulk density by 44% (data not shown)—in the dry plots affected by warmer T_{soil} at surface layers. Contrary to the accelerated respiration rates at the surface, colder T_{soil} at deep layers and reduced TD imply that carbon currently stored in permafrost can be preserved following drainage. In addition to these contrasting effects, another opposing influence of the physical structures of vegetation on T_{soil} (see Section 4.1.2) with continuously changing vegetation communities following drainage (see Section 4.2.2) need to be monitored over a longer period of time to gain further insight into the net impact of secondary drainage on carbon accumulation and CO_2 fluxes. Overall, the complex interactions among drainage severity, effects of soil type on T_{soil} shifts following drainage, and acclimation processes in the plant community call for the study of net drainage effects at multiple locations across the Arctic.

4.2.2 Plant effects on growing-season CO₂ fluxes

Drainage shifted the dominant plant species from *E. angustifolium* to *C. appendiculata*. Some drained_dry plots showed the transition stage of plant composition with a mixture of thinning *E. angustifolium* and young *C. appendiculata*. In this transition stage or in early succession stages, plants assimilate less CO₂ than they previously did due to lower biomass, and can be more susceptible to disturbances^{195,196}. The dry and warm year of 2013 was an especially good example of this process: These plots showed slightly decreased GPP rates along with increasing PAR (Figure 3.8), implying that the combination of high PAR and high T_a caused stress to plants. Under the same climate conditions, CarexShrub in the control transect—which can be considered to be the potential vegetation communities of CarexEriophorum groups in the longer term—took up significantly less CO₂ than in 2014, but did not show decreasing GPP rates (Figure 3.8). This implies that when *E. angustifolium* is fully replaced by *C. appendiculata* and shrubs, the current CarexEriophorum plots may not undergo stress as easily as they currently do although they can be still strongly influenced by climate. Taking into account such transition effects after 10 years of drainage is important given that the fraction of these areas of the total area—three out of ten plots—is not small. Moreover, this finding highlights the fact that ecosystem acclimation to new environmental conditions may take a long time, as 10 years was evidently not sufficient for this ecosystem to be resistant to disturbances, e.g., harsh climate conditions.

Higher abundance of shrubs was found to coincide with a slight increase in GPP rates. This difference is expected to be more pronounced than the observed data, since the abundance of shrubs was underestimated (see Section 3.1.3). Also, this compensation may become larger with increasing abundance and biomass of shrubs following continuing drainage. Increasing the abundance of shrubs not only changes carbon exchange rates between the atmosphere and the terrestrial ecosystem, but also carbon storage patterns within the terrestrial ecosystem¹⁹⁷. In the drained transect, living aboveground biomass was larger than in the control transect, and in 2003, while the biomass of green leaves decreased, that of stems increased, mostly due to the increased abundance of shrub species (Figure 4.1). When shrubs continue to expand, a large portion of carbon will be stored in plants, especially in shrubs' stems, and the proportion of litter added to the soil will decrease accordingly (Figure 4.1). The subsequent effects of

these changes, such as litter quantity and quality added to soils and its decomposability^{198,199}, need to be further investigated to better understand long-term vegetation effects on CO₂ fluxes.

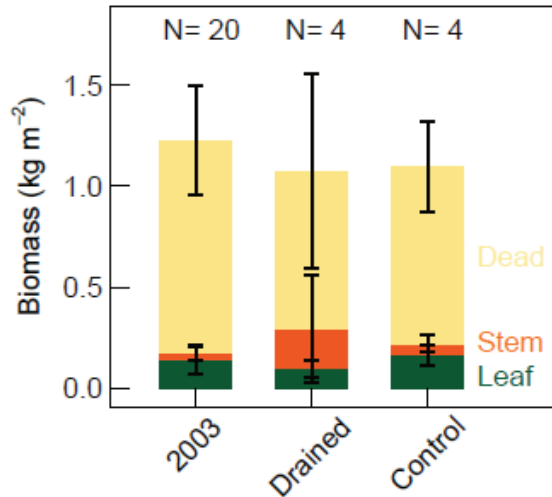


Figure 4.1 The total aboveground dry biomass (mean \pm standard deviation) of standing dead and living plants, measured in 2003 ($N = 20$) and 2013 ($N = 4$). Weights of dry biomass were not separated by species. Dead: standing dead materials, largely from *C. appendiculata* and *Eriophorum angustifolium*; stem: stems, mainly from shrub species; leaf: green leaves of all species.

4.2.3 The source of the increase in R_{eco} rates

Drainage in wet tundra ecosystems generally increased R_{eco} rates, and this increase was largely attributed to the enhanced decomposition of young soil carbon at shallow layers. These findings imply that drying soils in the Arctic may accelerate decomposition of carbon at shallow layers, while carbon pools in permafrost soils can be stabilized in response to colder T_{soil} in deep layers due to reduced thermal conductivity of dry organic soils. Our results are based on observations in August, when TD are *ca.* 5–10 cm thinner compared to maximum TD at the end of the growing season. Thus, the contributions of old soil carbon to R_{eco} presented in this study may have been underestimated as TD deepen over the growing season⁹⁵. Although this underestimation can be offset when lower contributions of old soil carbon to R_{eco} before August are considered, soil moisture status and T_{soil} also vary significantly over the course of the growing season, and our findings may be limited to the peak growing season. Furthermore, to examine the net effects of drainage on R_{eco} rates and the

source of the changes in R_{eco} rates, the nongrowing season should be considered as well. R_{eco} in the nongrowing season substantially contributes to the annual CO_2 flux budget^{110–115}, and, thus, further studies on comparing drainage effects on R_{eco} rates and its sources in different seasons will further improve our understanding of the stability of permafrost carbon pools under climate change.

Assuming only T_{soil} played a major role in changing R_{h} patterns, the time since drainage may not be important because heat capacity and thermal conductivity of soils instantaneously change with moisture conditions. However, T_{soil} and, subsequently, contributions of three sources to R_{eco} , can be indirectly influenced by soil moisture over time through changing vegetation composition following persistent dry conditions. The first potential effect may be altered vegetation composition and the consequently modified physical structures that may affect T_{soil} . For example, increased abundance of shrubs with higher vegetation canopy^{79–81} can decrease T_{soil} in summer by shading¹⁹³ or increase T_{soil} in spring by decreasing albedo, and subsequently, increase T_{soil} in summer¹⁹⁴. Consequently, contributions of surface soil decomposition to R_{eco} may decrease or increase with changing vegetation characteristics after long-term acclimation processes. The second vegetation effect on R_{eco} patterns can be through modified plant productivity. When moist or wet tundra becomes drier, plant productivity usually increases^{98,101,102}, and it can be accompanied with increasing abundance of plants with higher biomass, such as shrubs^{91,200,201}. Although there was neither considerable increase in plant productivity nor the subsequent increase in contributions of AT to R_{eco} following drainage, a slight increase in the contributions of AT to R_{eco} in drained plots implies that long-term drainage may enhance plants' contributions to R_{eco} through changes in plant productivity and composition. In the future, the potential effects of these changes in plant productivity and composition on the rates of R_{h} through shifts in quantity and quality of root exudates and litter need to be further investigated.

A negative correlation between $\Delta^{14}\text{C}-R_{\text{eco}}$ and *E. angustifolium* as well as a positive correlation between contributions of DS with *E. angustifolium* may not be only related to WTD gradients, but also *E. angustifolium* that creates a pathway for old CO_2 from deep soils to the atmosphere^{202,203}. Positive correlations between the amounts of CO_2 and CH_4 transported through *E. angustifolium* support this interpretation (Figure 4.2). As wet tundra was drained, the abundance of aerenchymatous plants decreased, which may have partly

contributed to a reduced amount of old CO₂ to net R_{eco}. However, this interpretation remains speculative because the amount of CO₂ measured with a plant chamber included both plant-mediated CO₂ transport and R_a. Separating these two CO₂ sources in future studies will elucidate the mechanisms more precisely. Again, the findings in this study highlight the role of plant composition to CO₂ fluxes.

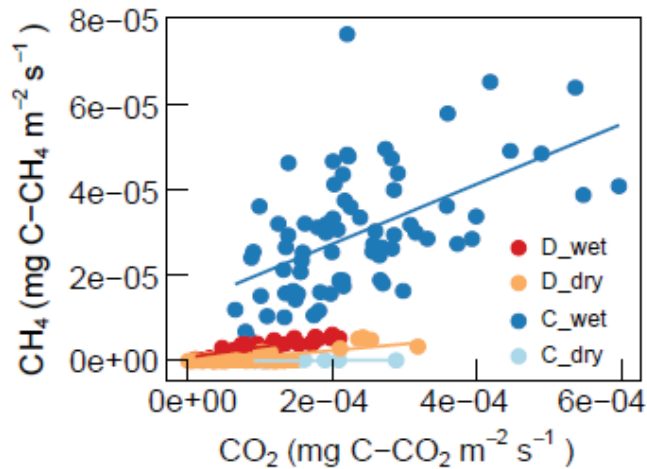


Figure 4.2 Positive correlations between CO₂ and CH₄ that are transported through *Eriophorum angustifolium* in the growing season.

4.3 Growing-season CH₄ fluxes

4.3.1 Tsoil effects on growing-season CH₄ fluxes

The divergent drainage effects across the vertical profile of Tsoil—warmer Tsoil at shallow layers and colder Tsoil at deep layers—were linked to CH₄ production and oxidation rates at deep and shallow layers, respectively, because both processes are thermodynamically influenced and the rates of them increase with rising temperatures up to optimal temperatures^{43,46,204,205}. Warmer Tsoil at shallow layers and colder Tsoil at deep layers in drained areas both contributed to a decrease in net CH₄ fluxes due to potentially increased rates of CH₄ oxidation and reduced rates of methanogenesis, respectively.

Different from plant and microbial community structure that require time to acclimate to a new condition, Tsoil can be instantaneously affected by soil moisture. Thus, constant changes in soil moisture due to variability in climate, e.g., precipitation, can intensify or dampen Tsoil

effects on CH₄ processes. However, modifications in plant community with the increased abundance of tussock-forming *C. appendiculata* and shrubs following long-term drainage might have indirectly offset the increased soil surface temperatures because of shadows of larger plants' physical structures¹⁹³. This may explain temporally and spatially more fluctuating soil surface temperatures in the drained_dry plots than in the control_dry plots (Figure 3.2a). At this study site, plant community structure has been undergoing changes for 10 years due to drainage, and will be further altered. Ongoing modifications in plant composition and their effects on T_{soil} and, consequently, CH₄ fluxes need to be further monitored.

4.3.2 Plant effects on growing-season CH₄ fluxes

Three aerenchymatous plant species exist in this study site: *C. appendiculata*, *P. palustris*, and *E. angustifolium*. Similar CH₄ flux rates were found in *Carex*-dominated and in *Eriophorum*- and *Potentilla*-dominated areas in saturated conditions¹², implying that three species potentially transport CH₄ through aerenchyma. However, the role of *E. angustifolium* in transporting CH₄ was considerably significant compared to *C. appendiculata* and *P. palustris* in this site. Even though the contribution of aerenchyma to CH₄ fluxes on this Arctic floodplain was lower than in other studies of Arctic tundra^{39,42}, *E. angustifolium* transported a significant amount of CH₄ from deep soils to the atmosphere in the naturally wet conditions, in strong agreement with previous findings^{39,40,42,206}. However, persistently low WTD—a consequence of drainage—for ten years decreased the abundance of *E. angustifolium*, and thus, the possibility to directly transporting CH₄ to the atmosphere. A large amount of CH₄ that used to reach the atmosphere through aerenchyma alternatively diffused through soil layers, leading to an increased probability of oxidation.

Plant community structures in the control transect represents plants' acclimation to WTD for more than a decade: *E. angustifolium* dominated in the wet plots, while no *E. angustifolium* was found in the dry plots. Several drained_dry plots that displayed the transition stage of plant community, featuring limited *E. angustifolium* cover and young *C. appendiculata* imply that drainage lowered the productivity of *E. angustifolium* that are abundant in inundated areas and less adaptive to dry conditions, and *C. appendiculata* gradually replaced the dominance. Despite their low abundance, a small amount of CH₄ was still transported through remaining thin *E. angustifolium* in drained_dry plots, but a further decrease in the abundance of *E.*

angustifolium is expected in these plots with continuing drainage. Subsequently, the amount of CH₄ that is transported through aerenchyma will be further reduced and net CH₄ fluxes may possibly become similar to those at control_dry plots.

4.3.3 Microbial effects on growing-season CH₄ fluxes

Relating DNA-based microbial fractions to their activities, e.g., fractions of CH₄-related microorganisms to CH₄ production or oxidation, is challenging. When such relations are made, results should be evaluated carefully because possessing DNA does not imply its activity. Nevertheless, microbial community structure acquired from DNA-based analysis often correlates with genes abundance or expression, and such information can be used to assess potential *in situ* activities of different microbial groups^{124,126,127,207,208}.

Increased fractions of CH₄-associated microorganisms were found to coincide with greater CH₄ fluxes, implying that CH₄ cycling was more pronounced under wetter conditions. It is speculated that the continuous supply of CH₄ in anoxic wet soils produced by a higher abundance of methanogens maintains closely-associated methanotrophic populations. In addition, larger fractions of these microbial groups in the drained transect were found at relatively deeper depths, mostly at or close to mineral soil layers, where carbon content was significantly lower compared to organic layers. Thus, although the fractions of both microbial groups in the drained transect were similar to control_wet, the smaller amount of carbon at deeper layers can potentially result in the reduced CH₄ cycling. Furthermore, with “hotspots” of CH₄ cycling existing at deeper layers in drained soils, higher proportion of CH₄ can be oxidized in the longer passage through aerated soil depths above, with potentially larger abundance of CH₄-oxidizers, which can be inferred from increased quantity of bacteria. Although it was not attempted to quantitatively relate microbial communities with CH₄ fluxes due to the limited number of samples, abundant fractions of CH₄-associated microorganisms at deeper soil layers may explain the reduced CH₄ fluxes in the drained transect, especially at drained_wet, despite similar WTD to that of control_wet.

Not only the fractions but the microbial composition also differed between the four groups of microsites differentiated in this study. Although it is challenging to assess how microbial composition contributes to CH₄ fluxes, due to the deficient information on physiology of all existing microorganisms in soils and their acclimation to changing environment²⁰⁹, processes

and possessing genes that dominant microbial groups adopt can give us hints how changed microbial community structure may affect CH₄ cycling. For instance, an increased proportion of *Methylocystis* genus at shallow layers of the dry plots, which can oxidize CH₄ at high and low concentrations (Table 3.2)²¹⁰, suggests that drainage expands layers or at least spatial niches in the soil where methanotrophs oxidize atmospheric CH₄. It potentially strengthens the CH₄ sink capacity of this ecosystem. Although quantitative relations between microbial communities and CH₄ fluxes could not be found, significantly changed abundance and composition of CH₄-related microorganisms following long-term drainage may have dramatic effects on CH₄ cycling in this ecosystem.

4.4 Nongrowing-season CO₂ and CH₄ fluxes

Large CO₂ and CH₄ fluxes in the nongrowing season may be to a large part induced by the physical processes, as outlined by Mastepanov et al. (2008, 2013)¹¹⁸: The freezing of soil in fall and the consequent reduction in soil pore space, pushes stored CO₂ and CH₄ gases from the soil to the atmosphere through cracks in soil or dead plant bodies. However, the fact that nongrowing season CO₂ and CH₄ fluxes presented in this study were partly influenced by T_{soil} implies that high CO₂ and CH₄ emissions were not exclusively triggered by the physical expression of existing CO₂ and CH₄ in soils, but also from ongoing respiration at relatively mild T_{soil} due to snow insulation^{111,113–115,211–213}. Although T_{soil} between 0–35 cm were consistently below zero, T_{soil} at 35 cm did not fall below -5 °C until the end of November. The mean T_{soil} at 35 cm during this observation period were -5 and -6 °C at the wet and dry plots, respectively, and they are approximately 17 °C warmer than the mean T_a with -22 °C. Ongoing freezing at greater depths than 35 cm and low P_a^{184,185} could have stimulated CO₂ and CH₄ emission from the soil to the atmosphere through dead *E. angustifolium*. The amount of CO₂ and CH₄ that can be produced under these temperatures is not trivial, especially considering approximately three times longer nongrowing season compared to the growing season in the Arctic.

In case of CH₄ fluxes, the controlling factors in the nongrowing season were similar to those in the growing season, but variability in fluxes during the nongrowing season was high. In addition, rates of CH₄ emission in the growing season and nongrowing season were not correlated to each other. This may be partly attributed to limited availability of liquid water and physical barrier of the frozen soils that restrained CH₄ production, oxidation, and transport

processes in the nongrowing season. These findings support that nongrowing-season CH₄ fluxes were more influenced by physical factors than biological factors, with sporadic fluxes as shown in other studies^{116–120}.

Although the CO₂ and CH₄ fluxes in the nongrowing season were partially explained by vegetation group, P_a, and T_{soil}, the amount of variation (R^2) together explained by these factors was low. What's more, these high CO₂ and CH₄ fluxes were more pronounced in the drained transect despite there being similar conditions in the control transect. High uncertainties and limitations in predicting both nongrowing-season CO₂ and CH₄ fluxes and possible high CO₂ and CH₄ fluxes during the thawing season²¹⁴ need to be addressed in follow-up studies to determine the net effects of drainage on the annual CO₂ and CH₄ fluxes of this site. Nevertheless, the observed considerably higher CO₂ and CH₄ fluxes in the drained area during the nongrowing season imply that drainage not only affects growing-season CO₂ and CH₄ fluxes, but also has the potential to alter nongrowing-season fluxes significantly. Furthermore, very different CH₄ fluxes between the growing and nongrowing seasons despite the fact that similar controlling factors are involved highlight the importance of effects of physical factors on nongrowing-season CH₄ fluxes.

4.5 Assessment of methodology

4.5.1 Flux measurements with chamber systems

Chamber systems have been widely used to investigate gas exchange between the atmosphere and the terrestrial ecosystems^{215–217}. Compared to other techniques, chambers are easy to build and handle with low cost and energy consumption, and thus, can be utilized in diverse conditions. Also, small size allows directly targeting specific ecosystem elements. For example, measuring flux rates and correlating them with ecosystem properties in highly heterogeneous ecosystems can be efficiently carried out, compared to eddy-covariance systems—that is another widely-used flux measuring tool—that usually capture a mixed signal from a larger source area.

One of the shortcomings of a closed dynamic chamber system is perturbing natural conditions, such as increasing gas concentrations and pressure, that may result in “saturation effects” and underestimation of flux rates^{218–220}. If the headspace temperature increases, an increase in water vapor due to evaporation aggravates these effects. By employing a non-steady-state

flow-through system, i.e., closed dynamic chamber system, saturation effects were minimized, because the changes in gas concentrations were constantly monitored with a directly connected gas analyzer, so that measuring time was restricted to a maximum of two minutes. In addition, the temperature inside the chamber was regulated by placing icepacks on the chamber rims. In addition, the slopes of gas concentration changes were checked to ensure the “saturation effects” were negligible.

Another limitation of closed-chamber techniques is the restriction to infrequent observations, especially in non-automated systems, compared to other high-frequency flux measuring tools, such as eddy covariance. A number of environmental factors affect fluxes. As these environmental parameters change diurnally and seasonally, fluxes drastically alter as well. To overcome this limitation, to compare flux variability among plots induced by temporal discrepancies in sampling, and to estimate continuous flux rates of this ecosystem for each observation period, measured CO₂ fluxes need to be interpolated based on functional relationships that link flux rates to continuously monitored environmental parameters. The model equations used in this study, i.e., polarVPRM, consider the environmental parameters that are expected to affect GPP and R_{eco}, and the observed and the modeled fluxes were generally aligned well. However, any model can only represent a simplified version of the real conditions, and particularly the use of simple model configurations as used within this study bears the risk of excluding important control parameters. Accordingly, the variance that was not fully explained by these model equations, mainly due to varying conditions over the season, can be reduced in potential future studies. For example, WTD fluctuated during the 2014 growing season due to several heavy precipitation events and the addition of water from permafrost thaw over time, and temporally changing soil moisture may have influenced the rates of R_{eco}. However, varying soil moisture conditions were not considered when interpolating R_{eco}, because adding another term in the equation requires the larger number of data points to produce robust relationships among parameters as well as between parameters and flux rates. Due to the limited number of data points, flux was not extrapolated in this study. Usually, with the large number of data points, half of the observed flux data can be used for parameterizing and the other half for validating the model parameters. However, due to the limited number of data points, the same data set was used for both parameterization and validation, and fluxes could not be extrapolated beyond the observation periods. After the larger number of data points are collected, and the clear and robust relationships between

62

parameters and fluxes are explained under varying climate conditions, fluxes can be extrapolated with continuously monitored environmental parameters. In this study, the interpolated fluxes successfully minimized one of the drawbacks of non-automated chamber systems, i.e., non-continuous data coverage, but it can be further improved with continuing observations.

Despite several potential shortcomings described in the preceding paragraphs, chamber systems can be a strong tool for flux measurements. Floodplains are characterized by highly heterogeneous environment, and correlating environmental factors with flux rates in fine-scale level can be challenging with other tools that are commonly used in flux measurements, e.g., eddy covariance. By investigating environmental factors temporally and spatially in parallel with fluxes, finding significant controlling factors of CO₂ and CH₄ fluxes was effectively achieved with chamber systems while most of drawbacks were minimized. By reducing the potential bias inherently related to chamber systems and combining chamber systems with other tools that can continuously observe fluxes in site level, such as eddy covariance flux observations, chamber technique can be more effectively utilized in the future studies.

4.5.2 Application of isotopes in the carbon cycle studies

Determining the fractions of stable and radioactive isotopes provides a strong tool for understanding carbon cycle processes in depth. The net direction and rates of processes can be determined by observing flux rates between the atmosphere and the terrestrial ecosystems, and the origins and the ages of the sources can be additionally revealed by analyzing the fractions of isotopes^{221,222}. $\Delta^{14}\text{C}$ of R_{eco} was used to partition R_{eco} into three sources, i.e., SS, DS, and AT. The results presented in this dissertation were robust because the three sources' signatures were well separated from one another. However, employing one isotopic signature to partition into three sources may increase uncertainty, when source signatures are similar to each other¹⁴⁴. This potential drawback can be overcome by applying additional isotopic signatures, e.g., $\delta^{13}\text{C}$. $\delta^{13}\text{C}$ of soils increases with depth^{223–225}. In addition, $\delta^{13}\text{C}$ of plants is highly influenced by water availability^{226,227}, so employing additional isotope ^{13}C to partition the R_{eco} sources in drying manipulation experiments can reduce the uncertainty more effectively in the future studies. Moreover, extending this analysis into the nongrowing season and investigating the development of $\Delta^{14}\text{C}$ of R_{eco} over the year can help us understand how R_{eco} patterns vary by season. Furthermore, analyzing the $\delta^{13}\text{C}$ and $\delta^2\text{H}$ of CH₄ along with flux rates may provide

evidence of the relative rates of hydrogenotrophic and acetoclastic CH₄ production as well as CH₄ oxidation²²⁸.

4.5.3 Microorganisms in the carbon cycle studies

Relationships between CH₄-associated microorganisms and CH₄ fluxes were based on the DNA analysis. DNA-based microbial analysis does not imply the activity of those microorganisms that can be related to the final product of the processes, as mentioned in Section 4.3.3. In addition, investigating microbial community structure and activities from four representative locations in terms of water regime history may well represent the combined ecosystem properties, i.e., soil moisture, plant community structure, and T_{soil}, but not effects of individual factors. This is because the studied floodplain is a highly heterogeneous ecosystem, and microbial community structure and the activities of each functional group can significantly vary spatially and temporally with a combination of numerous factors^{229,230}. For example, altered microbial community structure following drainage may be not only due to the altered soil moisture conditions, but also due to modified plant community structure that produce different quantity and quality of root exudates^{231,232}. Because of these limitations, the relationships between CH₄ fluxes and microbial results were evaluated only qualitatively. To better understand the direction of changing microbial community structure and each functional group's activity in terms of CH₄ fluxes following drainage, a larger number of replicates with diverse soil moisture conditions and dominant vegetation types are needed. In this way, qualitative assessment of the relationships between CH₄ fluxes and microbial parameters can be feasible.

The relationships between microorganisms and CO₂ fluxes were not created in this study. Previous studies have attempted to relate microbial parameters, such as microbial biomass^{233–236}, extracellular enzymatic activities²³⁵, and microbial community structures²³⁶, with the rates of R_h. However, the relationships between microbial parameters and R_h rates were generally found in incubation studies, where other environmental factors were well controlled. In addition, given that R_a and R_h were not separately measured and R_a took a large part of R_{eco}, finding solid relationships between microbial parameters and R_{eco} would not have given any significant results.

Chapter 5. Synthesis and Conclusion

5.1 Drainage effects on ecosystem properties, and CO₂ and CH₄ fluxes

Drainage of a floodplain near Chersky resulted in an average WTD drop of 20 cm. This substantially altered both biogeophysical and biogeochemical ecosystem properties over the span of a decade, with profound net impacts on CO₂ and CH₄ fluxes. The first change important for CO₂ and CH₄ processes was that WTD variation led to divergent vertical T_{soil} profiles, with drained areas showing greater fluctuations in T_{soil} at shallow layers due to the low heat capacity of dry organic soils, and colder T_{soil} at deep layers due to the low thermal conductivity of the dry organic soils above it. Consequently, the drained areas had shallower TD compared to the control areas. The second change was that plant community structure in drained areas shifted significantly toward an increased abundance of *C. appendiculata* and shrub species (*Betula* and *Salix* sp.), but a decreased abundance of *E. angustifolium*, which was previously dominated. The third change was that the fractions of CH₄-associated microorganisms decreased following drainage.

These aboveground and belowground changes significantly affected CO₂ fluxes in the growing season (Figure 5.1a). The drained areas showed higher R_{eco} rates due to more aerobic conditions, with a greater amount of organic carbon affected by warmer T_{soil} close to the surface. Increased contribution of surface soil decomposition to R_{eco} was confirmed by radiocarbon signals. Dominant plant species in the drained areas took up less CO₂ (i.e., *C. appendiculata* engaged in less GPP) than *E. angustifolium*, which is dominated in the wet control areas. Overall, drainage increased net CO₂ uptake (NEE) by 25% in 2013 but decreased it by 35% in 2014 during the 20 days of the growing season when the two transects were compared. The opposite patterns of the two years can be attributed to the pronounced sensitivity of the dry plots in the control area to variations in climate. Despite the inter-annual variability in net drainage effects on CO₂ fluxes, both years had consistent trends toward the replacement of *E. angustifolium* with *C. appendiculata*, more aerobic conditions, and increased T_{soil} at shallow layers, all of which weakened net CO₂ uptake (NEE).

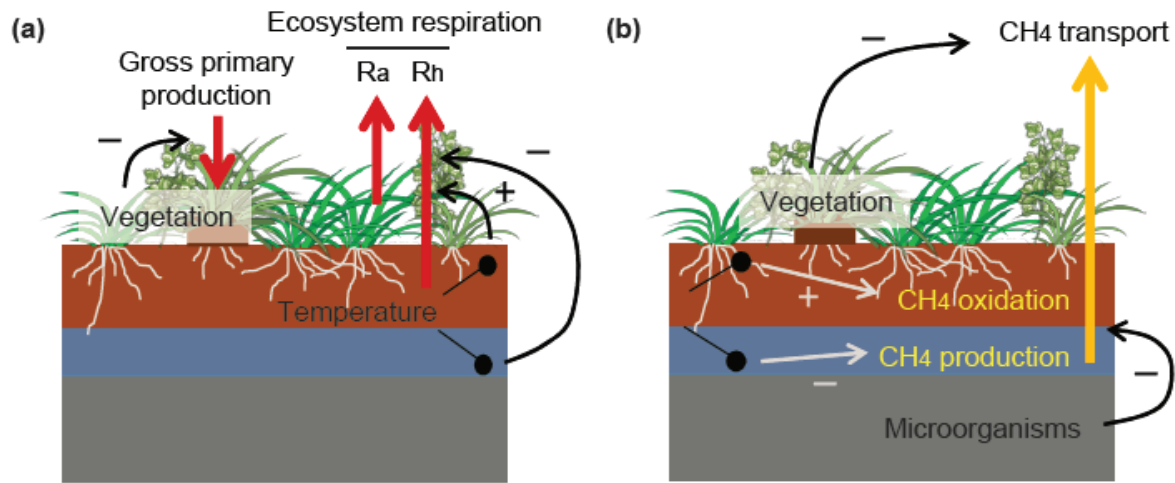


Figure 5.1 Ten years of drainage altered ecosystem characteristics, and, subsequently, (a) CO₂ and (b) CH₄ fluxes. R_a and R_h refer to autotrophic and heterotrophic respiration, respectively. The plus and minus signs indicate enhanced and reduced processes, respectively, following drainage disturbance.

A decade-long drainage considerably reduced CH₄ emission rates by 20 times on average. Significant reduction in CH₄ fluxes one year after the installation of drainage ditch¹⁰⁵ implies that a decrease in WTD—more aerobic condition—considerably affects growing-season CH₄ fluxes¹⁰⁵. However, without changes in ecosystem properties, growing-season CH₄ fluxes would have risen to the previous level when WTD was raised, e.g., due to heavy precipitation²³⁷. Ten years after the drainage installation, the decreased growing-season CH₄ flux rates remained at similar level, but this reduction was to a large part based on altered ecosystem characteristics—the abundance of aerenchymatous plants, the fractions of CH₄-associated microorganisms, and T_{soil}, as well as modified CH₄ production, oxidation, and transport processes (Figure 5.1b). With these modified ecosystem properties included, instant rise in WTD would not elevate the CH₄ flux rates to the original high rates^{238,239}.

In the nongrowing season, CO₂ and CH₄ emission was four times and 10%, respectively, higher in the drained than in the control areas. These shifts could partially be attributed to differences in the abundance of *E. angustifolium* and T_{soil} between the drained and control areas, while P_a gradients appeared to be an important trigger for high emission rates overall. These factors were found to be critical for growing-season CH₄ fluxes as well, but the variability in flux rates was much larger in the nongrowing season, and the net CH₄ emission

rates were higher in the drained area compared to the control area, unlike in the growing season. These findings imply that nongrowing-season fluxes are largely determined by physical factors that affect transport, and not much by biological factors that influence production and oxidation processes. In addition, the findings emphasize the importance of monitoring the contributions of nongrowing season CO₂ and CH₄ fluxes to net annual budget in Arctic ecosystems, and investigating the underlying processes that changes in ecosystem properties are involved.

To summarize the core findings of this study, ecosystem changes after 10 years of drainage in an Arctic floodplain decreased photosynthetic CO₂ uptake, increased CO₂ emissions through respiration, and reduced CH₄ emissions. These findings in this study emphasize the role of plants, microorganisms, and T_{soil} in CH₄ fluxes in addition to WTD, and the importance of long-term studies that can capture such relatively slow shifts in ecosystem properties when investigating CO₂ and CH₄ fluxes in response to global climate changes. As ongoing global climate change holds the potential to degrade ice-rich permafrost and make large regions within the Arctic significantly drier, current Arctic wetlands may accumulate less carbon in the terrestrial ecosystem, respire more CO₂ from shallow soil layers, but also preserve carbon in deep soil layers in the future, counterbalancing effects under warmer and wetter conditions^{84,240,241}. Therefore, re-distribution of surface water needs to be taken into account to better predict how Arctic ecosystems will respond to climate change, and how susceptible carbon pools at different layers are to mineralization under future climate scenarios. Given that vegetation communities continue changing even 10 years after the disturbance initiated, with different microsites responding individually to altered environmental conditions, longer-term observations of this site, as well as of other ecosystems in the Arctic, are needed to better predict the fate of the Arctic in the face of global climate change.

5.2 Drainage effects on ecosystems' sensitivity to climate

Despite variations in optimum temperature ranges among species or ecosystems due to their adaptation to different climate conditions^{242–244}, increasing temperature can be expected to stimulate photosynthesis and respiration rates. Thus, the rates of both GPP and R_{eco} are likely to increase with warmer temperatures, under future climate scenario^{79–82,245}. Depending on the individual rate of changes in GPP and R_{eco}, warming can result in decreased or increased net CO₂ fluxes of the ecosystem because the two processes act in the opposite directions.

Combining warming effects with the impact of long-term drainage is likely to result in complex changes in the carbon cycle, where several ecosystem characteristics play an important role. In this study, the replacement of *E. angustifolium* with *C. appendiculata* in combination with warmer T_{soil} at shallow depths consistently decreased net CO_2 flux rates, i.e., reduced photosynthetic uptake capacity and increased R_{eco} rates.

In addition to this general reduction in photosynthetic capacity due to long-term dry conditions, changing from *E. angustifolium* to *C. appendiculata* also altered the ecosystems' sensitivity to short-term climate conditions. For example, plots where the dominant plant species was *C. appendiculata* showed particularly reduced GPP rates under warm and dry conditions. In the meantime, *Eriophorum*-dominated plots appeared to be less sensitive to short-term climate variability. Because of these altered sensitivity of ecosystem to climate conditions, net CO_2 fluxes of the two observation years, which were characterized by different temperature and precipitation patterns, showed opposite trends; significantly reduced GPP rates in the dry plots within the control area in the warm and dry year 2013 resulted in lower net CO_2 uptake. Despite the opposite patterns in net CO_2 fluxes between the two observation years, all underlying processes displayed similar trends in both years: decreased GPP due to the replacement of *E. angustifolium* to *C. appendiculata* and increased R_{eco} rates due to warmer T_{soil} at shallow layers. This implies that when floodplains or wetlands in the Arctic are converted to moist or dry tundra due to warming and permafrost degradation, the ecosystems' carbon uptake capacity as well as their sensitivity to climate, particularly drought, may be altered. These findings in this study highlight the fact that it may not be sufficient to investigate the links between carbon cycle processes and individual ecosystem properties. Instead, complex interactions among multiple ecosystem properties and their relationships to CO_2 and CH_4 fluxes need to be observed under different climate conditions. Thus, the findings highlight the importance of observing underlying processes in multiple years in addition to the role of ecosystems' sensitivity to climate conditions when it comes to investigating ecosystems' response, e.g., CO_2 and CH_4 fluxes, to climate change.

The changes in CO_2 flux rates in this study site following drainage were found to be in a similar range compared to other sites in the Arctic. Also, increased R_{eco} rates due to more oxic condition following drainage were aligned with other studies^{98,100–102,104}. However, decreased GPP rates due to drainage in this site were different from what was generally observed at other

sites^{98,100–102,104}. This may be in part linked to more pronounced changes in WTD in this study site than in other studies, leading to decreased photosynthetic rates of wetland plants, which was also observed one year after drainage¹⁰⁵. In addition, changed plant composition following long-term drainage has contributed to a decrease in GPP, which was not considered in other short-term studies. These results highlight that ecosystems do not consistently respond to drainage, but the original characteristics of the ecosystems and the magnitude of change have to be taken into account to better understand the effects of drainage in the Arctic.

5.3 Interactions among ecosystem properties

Not a single ecosystem property performs independently. For example, shifting plant community structure not only alter CO₂ flux rates due to photosynthetic uptake capacity but R_h as well as R_a rates indirectly, by modifying quality and quantity of litter and root exudates, as well as T_{soil}. In addition, CH₄ emission rates were reduced directly from drainage, but the decreased abundance of *E. angustifolium*, an aerenchymatous plant species, reduced fractions of CH₄-associated microorganisms, and warmer T_{soil} at shallow layers but colder T_{soil} at deep layers all contributed to the reduction in CH₄ fluxes (Figure 5.1b). Although it was attempted to quantify the individual effects of plants and T_{soil} on CO₂ and CH₄ fluxes, estimating each factor's contribution to the net CO₂ and CH₄ fluxes could not be achieved because of close interactions among the numerous factors involved. Nevertheless, this study monitored the altered ecosystem characteristics and their contributions to changes in CO₂ and CH₄ fluxes that have not been observed in other short-term manipulation studies. The results presented herein emphasize that the combination of drainage severity and selected ecosystem properties is a key element for more precise quantification of future changes in flux rates. Identifying these factors, and the role they play in the carbon cycle processes, remains as an important challenge to improve predictions how much CO₂ and CH₄ fluxes can be modified by drainage.

In the nongrowing season, high sporadic CO₂ and CH₄ fluxes were observed. These high CO₂ and CH₄ fluxes were correlated to each other (Figure 3.16), implying that they could be derived from the same source and emitted to the atmosphere simultaneously¹¹⁸. Furthermore, these high fluxes were both partly promoted by physical factors, such as decreasing P_a, as well as the abundance of *E. angustifolium*, suggesting that *E. angustifolium* may have acted as a path for gases in soils to the atmosphere, as described in Section 4.4. It was the first attempt to

investigate the nongrowing-season CO₂ and CH₄ fluxes in a drainage manipulation experiment in the Arctic. These findings emphasize that *E. angustifolium* can be an effective pathway for gases to be emitted to the atmosphere both in the growing and nongrowing seasons, but the existence of this pathway alone does not yield high CH₄ emissions. Instead, other factors such as decreasing P_a over time are also required to trigger high short-term flux rates. These results again stress multiple factors being involved: soil moisture conditions, plant community structure, climate, and their influence on CO₂ and CH₄ flux rates. Other studies have observed high fluxes in wet areas^{116–118}, but not in all cases^{119,120}. Physical factors play a significant role in CH₄ emission in all seasons. However, these results were not sufficient to reveal the sources of these high CO₂ and CH₄ fluxes in the nongrowing season. As Δ¹⁴C was applied to investigate the sources of respired CO₂, it can be employed in the nongrowing season to find out the sources of high CO₂ and CH₄ fluxes.

5.4 Conclusions and outlook

In the Arctic, both GPP and R_{eco} have increased for the last several decades^{89,246–248}, due to “Arctic greening” and increased decomposition rates under warmer temperatures. Warming has been expected to increase mineralization rates of old carbon currently stored in permafrost as well^{95–97}. GPP has been found to react more strongly to warming than R_{eco}⁸⁹, yet, over longer timeframes carbon losses to the atmosphere are expected to be larger than the increased uptake by the terrestrial ecosystem⁸⁷, and it is not clear whether the Arctic would act as a carbon sink or source in the future. To date, many studies carried out in the Arctic focused on the direct impact of warming on CO₂ and CH₄ flux exchange patterns. However, the results presented within this study emphasize that it is vital to discuss warming effects in combination with hydrological effects: The isolated treatment of warming can provide only limited insights, since virtually any substantial change in temperature regimes would be accompanied by shifts in the hydrological cycle and water availability^{61,75,76}. In addition, water availability itself has been shown to play an equally important role as compared to temperature²⁴⁹. Therefore, a comprehensive assessment of combined temperature and soil hydrology effects in future studies is crucial to improve the accuracy of forecast for the sustainability of Arctic carbon pools under future climate change.

As warming degrades ice-rich permafrost, soil topography and hydrology in the Arctic may undergo severe changes spatially and temporally, creating both wetter or drier areas. This

study aimed to investigate the effects of drainage on ecosystem properties, and subsequently, on CO₂ and CH₄ fluxes in the growing and nongrowing seasons. The observed changes in CO₂ and CH₄ fluxes as well as shifts in sensitivity to climate highlight the complex interplay among ecosystem properties, climate and carbon cycle dynamics. Still, some of these effects could not be investigated in depth. For example, the increasing abundance of shrubs influenced CO₂ fluxes only slightly, but at the same time more carbon has accumulated in aboveground biomass, suggesting that not only flux rates have changed between the atmosphere and the terrestrial ecosystems, but carbon pools may change. Also, in the nongrowing season, high sporadic CO₂ and CH₄ fluxes were observed, which were promoted by physical factors such as decreasing P_a, but the data was not sufficient to clearly identify the sources of these emissions. To examine this mechanism in detail, radiocarbon analysis would be a promising tool, and $\Delta^{14}\text{C}$ of emitted CO₂ can be compared over seasons.

Previous studies have investigated the effects of short-term drainage manipulation on CO₂ and CH₄ fluxes in the Arctic^{98,100–102,104,105,108}. These studies investigated the differences in CO₂ and CH₄ fluxes that were induced solely by WTD alterations, but could not include modified ecosystem characteristics following persistent dry conditions, which may considerably contribute to variations in CO₂ and CH₄ fluxes. Taking these factors into account is crucial for understanding ecosystems' response to WTD over longer timeframes. To date, this is the first study demonstrating the impact of modified ecosystem properties in CO₂ and CH₄ fluxes following long-term drainage manipulation in the Arctic. Although not all relationships among ecosystem characteristics, i.e., vegetation, T_{soil}, and microorganisms, could be monitored in detail in this study, it provided insights on closely-linked ecosystem components, and their interactive relations to CO₂ and CH₄ fluxes. Future studies should be designed that build on these findings, and explore such interactions in depth, including observations in other ecosystem types, and other regions. In particular, more observations in northeastern Siberia, which has been under-represented in the Arctic research despite the fact that the Arctic in Eurasia is two times larger than that in North America⁵⁵, would be a valuable addition to closing important knowledge gaps in Arctic ecosystem research. Considering ongoing shifts in plant community structure, the Chersky floodplain site also needs to be further monitored to better understand long-term drainage effects on wet Arctic ecosystems' response to warming and permafrost thaw.

References

1. Chapin, F. S., Matson, P. A. & Vitousek, P. M. in *Princ. Terr. Ecosyst. Ecol.* 123–156 (Springer New York, 2012). doi:10.1007/978-1-4419-9504-9
2. Waring, R. H., Landsberg, J. J. & Williams, M. Net primary production of forests: a constant fraction of gross primary production? *Tree Physiol.* **18**, 129–134 (1998).
3. Chapin, F. S., Matson, P. A. & Vitousek, P. M. in *Princ. Terr. Ecosyst. Ecol.* 157–182 (Springer New York, 2012). doi:10.1007/978-1-4419-9504-9
4. Zhang, H. *et al.* Inclusion of soil carbon lateral movement alters terrestrial carbon budget in China. *Sci. Rep.* **4**, 7247 (2014).
5. Ciais, P. *et al.* The impact of lateral carbon fluxes on the European carbon balance. *Biogeosciences* **5**, 1259–1271 (2008).
6. Kling, G. W., Kipphut, G. W. & Miller, M. C. Arctic lakes and streams as gas conduits to the atmosphere: implications for tundra carbon budgets. *Science* **251**, 298–301 (1991).
7. Kindler, R. *et al.* Dissolved carbon leaching from soil is a crucial component of the net ecosystem carbon balance. *Glob. Chang. Biol.* **17**, 1167–1185 (2011).
8. Schlesinger, W. H. & Bernhardt, E. S. *Biogeochemistry: An analysis of global change.* *Biogeochemistry* (Elsevier, 2013). doi:10.1016/B978-0-12-385874-0.00007-8
9. Ramesh Reddy, K. & DeLaune, R. D. *Biogeochemistry of wetlands: science and applications.* (CRC Press, 2008).
10. Bridgman, S. D., Megonigal, J. P., Keller, J. K., Bliss, N. B. & Trettin, C. The carbon balance of North American wetlands. *Wetlands* **26**, 889–916 (2006).
11. Heikkinen, J. E. P., Elsakov, V. & Martikainen, P. J. Carbon dioxide and methane dynamics and annual carbon balance in tundra wetland in NE Europe, Russia. *Global Biogeochem. Cycles* **16**, 1115 (2002).
12. Corradi, C., Kolle, O., Walter, K., Zimov, S. A. & Schulze, E. D. Carbon dioxide and methane exchange of a north-east Siberian tussock tundra. *Glob. Chang. Biol.* **11**, 1910–1925 (2005).
13. Olefeldt, D., Turetsky, M. R., Crill, P. M. & McGuire, A. D. Environmental and physical controls on northern terrestrial methane emissions across permafrost zones. *Glob. Chang. Biol.* **19**, 589–603 (2013).
14. Klüber, H. D. & Conrad, R. Effects of nitrate, nitrite, NO and N₂O on methanogenesis and other redox processes in anoxic rice field soil. *FEMS Microbiol. Ecol.* **25**, 301–318 (1998).
15. Scheid, D., Stubner, S. & Conrad, R. Effects of nitrate- and sulfate-amendment on the methanogenic populations in rice root incubations. *FEMS Microbiol. Ecol.* **43**, 309–315

- (2003).
16. Schönheit, P., Kristjansson, J. K. & Thauer, R. K. Kinetic mechanism for the ability of sulfate reducers to out-compete methanogens for acetate. *Arch. Microbiol.* **132**, 285–288 (1982).
 17. Hope, D., Palmer, S. M., Billett, M. F. & Dawson, J. J. C. Variations in dissolved CO₂ and CH₄ in a first-order stream and catchment: an investigation of soil-stream linkages. *Hydrol. Process.* **18**, 3255–3275 (2004).
 18. Conrad, R. & Rothfuss, F. Methane oxidation in the soil surface layer of a flooded rice field and the effect of ammonium. *Biol. Fertil. Soils* **12**, 28–32 (1991).
 19. Le Mer, J. & Roger, P. Production, oxidation, emission and consumption of methane by soils: A review. *Eur. J. Soil Biol.* **37**, 25–50 (2001).
 20. Smith, K. A. *et al.* Oxidation of atmospheric methane in Northern European soils, comparison with other ecosystems, and uncertainties in the global terrestrial sink. *Glob. Chang. Biol.* **6**, 791–803 (2000).
 21. Born, M., Dorr, H. & Levin, I. Methane consumption in aerated soils of the temperate zone. *Tellus B* **42**, 2–8 (1990).
 22. Whalen, S. C. & Reeburgh, W. S. Consumption of atmospheric methane by tundra soils. *Nature* **346**, 160–162 (1990).
 23. White, M. A., Running, S. W. & Thornton, P. E. The impact of growing-season length variability on carbon assimilation and evapotranspiration over 88 years in the eastern US deciduous forest. *Int. J. Biometeorol.* **42**, 139–145 (1999).
 24. Baptist, F. & Choler, P. A simulation of the importance of length of growing season and canopy functional properties on the seasonal gross primary production of temperate alpine meadows. *Ann. Bot.* **101**, 549–559 (2008).
 25. Xia, J. *et al.* Joint control of terrestrial gross primary productivity by plant phenology and physiology. *Proc. Natl. Acad. Sci. U. S. A.* **112**, 2788–2793 (2015).
 26. Barr, A. G. *et al.* Inter-annual variability in the leaf area index of a boreal aspen-hazelnut forest in relation to net ecosystem production. *Agric. For. Meteorol.* **126**, 237–255 (2004).
 27. Vicca, S. *et al.* Fertile forests produce biomass more efficiently. *Ecol. Lett.* **15**, 520–526 (2012).
 28. Tucker, C. L., Bell, J., Pendall, E. & Ogle, K. Does declining carbon-use efficiency explain thermal acclimation of soil respiration with warming? *Glob. Chang. Biol.* **19**, 252–263 (2013).
 29. Lloyd, J. & Taylor, J. A. On the temperature dependence of soil respiration. *Funct. Ecol.* **8**, 315–323 (1994).
 30. Xu, L., Baldocchi, D. D. & Tang, J. How soil moisture, rain pulses, and growth alter the

response of ecosystem respiration to temperature. *Global Biogeochem. Cycles* **18**, GB4002 (2004).

31. Davidson, E. A., Belk, E. & Boone, R. D. Soil water content and temperature as independent or confounded factors controlling soil respiration in a temperate mixed hardwood forest. *Glob. Chang. Biol.* **4**, 217–227 (1998).
32. Bowden, R. D., Nadelhoffer, K. J., Boone, R. D., Melillo, J. M. & Garrison, J. B. Contributions of aboveground litter, belowground litter, and root respiration to total soil respiration in a temperate mixed hardwood forest. *Can. J. For. Res.* **23**, 1402–1407 (1993).
33. Chemidlin Prévost-Bouré, N. *et al.* Increase in aboveground fresh litter quantity overstimulates soil respiration in a temperate deciduous forest. *Appl. Soil Ecol.* **46**, 26–34 (2010).
34. Chapin, F. S., Matson, P. A. & Vitousek, P. M. in *Princ. Terr. Ecosyst. Ecol.* 183–228 (Springer New York, 2012). doi:10.1007/978-1-4419-9504-9
35. Turetsky, M. R. *et al.* A synthesis of methane emissions from 71 northern, temperate, and subtropical wetlands. *Glob. Chang. Biol.* **20**, 2183–2197 (2014).
36. Morrissey, L. A. & Livingston, G. P. Methane emissions from Alaska arctic tundra - an assessment of local spatial variability. *J. Geophys. Res.* **97**, 16661–16670 (1992).
37. King, J. Y., Reeburgh, W. S. & Regli, S. K. Methane emission and transport by arctic sedges in Alaska: Results of a vegetation removal experiment. *J. Geophys. Res.* **103**, 29083–29092 (1998).
38. Tsuyuzaki, S., Nakano, T., Kuniyoshi, S. & Fukuda, M. Methane flux in grassy marshlands near Kolyma River, north-eastern Siberia. *Soil Biol. Biochem.* **33**, 1419–1423 (2001).
39. Kutzbach, L., Wagner, D. & Pfeiffer, E.-M. Effect of microrelief and vegetation on methane emission from wet polygonal tundra, Lena Delta, Northern Siberia. *Biogeochemistry* **69**, 341–362 (2004).
40. von Fischer, J. C., Rhew, R. C., Ames, G. M., Fossdick, B. K. & von Fischer, P. E. Vegetation height and other controls of spatial variability in methane emissions from the Arctic coastal tundra at Barrow, Alaska. *J. Geophys. Res. Biogeosciences* **115**, G00I03 (2010).
41. McEwing, K. R., Fisher, J. P. & Zona, D. Environmental and vegetation controls on the spatial variability of CH₄ emission from wet-sedge and tussock tundra ecosystems in the Arctic. *Plant Soil* **388**, 37–52 (2015).
42. Knoblauch, C., Spott, O., Evgrafova, S., Kutzbach, L. & Pfeiffer, E.-M. Regulation of methane production, oxidation and emission by vascular plants and bryophytes in ponds of the northeast Siberian polygonal tundra. *J. Geophys. Res. Biogeosciences* **120**, 2525–2541 (2015).

43. Dunfield, P., Knowles, R., Dumont, R. & Moore, T. Methane production and consumption in temperate and subarctic peat soils: Response to temperature and pH. *Soil Biol. Biochem.* **25**, 321–326 (1993).
44. van Hulzen, J. B., Segers, R., van Bodegom, P. M. & Leffelaar, P. A. Temperature effects on soil methane production: an explanation for observed variability. *Soil Biol. Biochem.* **31**, 1919–1929 (1999).
45. Roy Chowdhury, T. *et al.* Stoichiometry and temperature sensitivity of methanogenesis and CO₂ production from saturated polygonal tundra in Barrow, Alaska. *Glob. Chang. Biol.* **21**, 722–737 (2015).
46. Whalen, S. C. & Reeburgh, W. S. Moisture and temperature sensitivity of CH₄ oxidation in boreal soils. *Soil Biol. Biochem.* **28**, 1271–1281 (1996).
47. McGuire, A. D. *et al.* Equilibrium responses of global net primary production and carbon storage to doubled atmospheric carbon dioxide: Sensitivity to changes in vegetation nitrogen concentration. *Global Biogeochem. Cycles* **11**, 173–189 (1997).
48. Chapin, F. S., Matson, P. A. & Vitousek, P. M. in *Princ. Terr. Ecosyst. Ecol.* 23–62 (Springer New York, 2012). doi:10.1007/978-1-4419-9504-9
49. Zhang, T., Barry, R. G., Knowles, K., Heginbottom, J. A. & Brown, J. Statistics and characteristics of permafrost and ground-ice distribution in the Northern Hemisphere. *Polar Geogr.* **23**, 132–154 (1999).
50. Tarnocai, C. in *Permafrost soils* 3–16 (Springer-Verlag Berlin Heidelberg, 2009). doi:10.1007/978-3-540-69371-0_1
51. Walker, D. A. A hierarchical tundra vegetation classification especially designed for mapping in Northern Alaska. in *Permafrost. Fourth Int. Conf. Proc.* 1332–1337 (1983).
52. Saugier, B., Roy, J. & Mooney, H. A. in *Terr. Glob. Product.* 543–557 (Elsevier, 2001). doi:10.1016/B978-012505290-0/50024-7
53. Hugelius, G. *et al.* Estimated stocks of circumpolar permafrost carbon with quantified uncertainty ranges and identified data gaps. *Biogeosciences* **11**, 6573–6593 (2014).
54. Schuur, E. A. G. *et al.* Climate change and the permafrost carbon feedback. *Nature* **520**, 171–179 (2015).
55. Tarnocai, C. *et al.* Soil organic carbon pools in the northern circumpolar permafrost region. *Global Biogeochem. Cycles* **23**, GB2023 (2009).
56. Batjes, N. H. Total carbon and nitrogen in the soils of the world. *Eur. J. Soil Sci.* **47**, 151–163 (1996).
57. Jobbágy, E. G. & Jackson, R. B. The vertical distribution of soil organic carbon and its relation to climate and vegetation. *Ecol. Appl.* **10**, 423–436 (2000).
58. Hartmann, D. L. *et al.* in *Clim. Chang. 2013 Phys. Sci. Basis. Contrib. Work. Gr. I to Fifth Assess. Rep. Intergov. Panel Clim. Chang.* (Cambridge University Press, 2013).

59. Serreze, M. C. & Barry, R. G. Processes and impacts of Arctic amplification: A research synthesis. *Glob. Planet. Change* **77**, 85–96 (2011).
60. Pithan, F. & Mauritsen, T. Arctic amplification dominated by temperature feedbacks in contemporary climate models. *Nat. Geosci.* **7**, 181–184 (2014).
61. Kirtman, B. *et al.* in *Clim. Chang. 2013 Phys. Sci. Basis. Contrib. Work. Gr. I to Fifth Assess. Rep. Intergov. Panel Clim. Chang.* (Stocker, T. F. *et al.*) 953–1028 (Cambridge University Press, 2013).
62. Collins, M. *et al.* in *Clim. Chang. 2013 Phys. Sci. Basis. Contrib. Work. Gr. I to Fifth Assess. Rep. Intergov. Panel Clim. Chang.* (Stocker, T. F. *et al.*) 1029–1136 (Cambridge University Press, 2013).
63. Overland, J. E., Wang, M., Walsh, J. E. & Stroeve, J. C. Future Arctic climate changes: Adaptation and mitigation time scales. *Earth's Futur.* **2**, 68–74 (2014).
64. Zimov, S. A., Schuur, E. A. G. & Chapin, F. S. Permafrost and the global carbon budget. *Science (80-)*. **312**, 1612–1613 (2006).
65. Jorgenson, M. T., Shur, Y. L. & Pullman, E. R. Abrupt increase in permafrost degradation in Arctic Alaska. *Geophys. Res. Lett.* **33**, L02503 (2006).
66. O'Donnell, J. A. *et al.* The effects of permafrost thaw on soil hydrologic, thermal, and carbon dynamics in an Alaskan peatland. *Ecosystems* **15**, 213–229 (2011).
67. Hopkins, D. M. Thaw lakes and thaw sinks in the Imuruk lake area, Seward Peninsula, Alaska. *J. Geol.* **57**, 119–131 (1949).
68. Brouchkov, A., Fukuda, M., Fedorov, A., Konstantinov, P. & Iwahana, G. Thermokarst as a short-term permafrost disturbance, Central Yakutia. *Permafrost. Periglac. Process.* **15**, 81–87 (2004).
69. Johnston, C. E. *et al.* Effect of permafrost thaw on CO₂ and CH₄ exchange in a western Alaska peatland chronosequence. *Environ. Res. Lett.* **9**, 085004 (2014).
70. Liljedahl, A. K. *et al.* Pan-Arctic ice-wedge degradation in warming permafrost and its influence on tundra hydrology. *Nat. Geosci.* **9**, 312–318 (2016).
71. Avis, C. A., Weaver, A. J. & Meissner, K. J. Reduction in areal extent of high-latitude wetlands in response to permafrost thaw. *Nat. Geosci.* **4**, 444–448 (2011).
72. Morgenstern, A. *et al.* Evolution of thermokarst in East Siberian ice-rich permafrost: A case study. *Geomorphology* **201**, 363–379 (2013).
73. Smith, L. C., Sheng, Y., MacDonald, G. M. & Hinzman, L. D. Disappearing Arctic lakes. *Science (80-)*. **308**, 1429 (2005).
74. Kattsov, V. M. & Walsh, J. E. Twentieth-century trends of Arctic precipitation from observational data and a climate model simulation. *J. Clim.* **13**, 1362–1370 (2000).
75. Bintanja, R. & Selten, F. M. Future increases in Arctic precipitation linked to local

- evaporation and sea-ice retreat. *Nature* **509**, 479–482 (2014).
76. Huntington, T. G. Evidence for intensification of the global water cycle: Review and synthesis. *J. Hydrol.* **319**, 83–95 (2006).
 77. Curtis, J., Wendler, G., Stone, R. & Dutton, E. Precipitation decrease in the western Arctic, with special emphasis on Barrow and Barter Island, Alaska. *Int. J. Climatol.* **18**, 1687–1707 (1998).
 78. Stafford, J. M., Wendler, G. & Curtis, J. Temperature and precipitation of Alaska: 50 year trend analysis. *Theor. Appl. Climatol.* **67**, 33–44 (2000).
 79. Myneni, R. B., Keeling, C. D., Tucker, C. J., Asrar, G. & Nemani, R. R. Increased plant growth in the northern high latitudes from 1981 to 1991. *Nature* **386**, 698–702 (1997).
 80. Xu, L. *et al.* Temperature and vegetation seasonality diminishment over northern lands. *Nat. Clim. Chang.* **3**, 581–586 (2013).
 81. Jia, G. J. Greening of arctic Alaska, 1981–2001. *Geophys. Res. Lett.* **30**, 2067 (2003).
 82. Epstein, H. E. *et al.* Dynamics of aboveground phytomass of the circumpolar Arctic tundra during the past three decades. *Environ. Res. Lett.* **7**, 015506 (2012).
 83. Davidson, E. A. & Janssens, I. A. Temperature sensitivity of soil carbon decomposition and feedbacks to climate change. *Nature* **440**, 165–173 (2006).
 84. Walter, K. M., Zimov, S. A., Chanton, J. P., Verbyla, D. & Chapin, F. S. Methane bubbling from Siberian thaw lakes as a positive feedback to climate warming. *Nature* **443**, 71–75 (2006).
 85. Koven, C. D. *et al.* Permafrost carbon-climate feedbacks accelerate global warming. *Proc. Natl. Acad. Sci. U. S. A.* **108**, 14769–14774 (2011).
 86. Schuur, E. A. G. *et al.* Vulnerability of permafrost carbon to climate change: Implications for the global carbon cycle. *Bioscience* **58**, 701–714 (2008).
 87. Abbott, B. W. *et al.* Biomass offsets little or none of permafrost carbon release from soils, streams, and wildfire: an expert assessment. *Environ. Res. Lett.* **11**, 034014 (2016).
 88. Belshe, F., Schuur, E. A. G. & Bolker, B. M. Tundra ecosystems observed to be CO₂ sources due to differential amplification of the carbon cycle. *Ecol. Lett.* **16**, 1307–1315 (2013).
 89. Forkel, M. *et al.* Enhanced seasonal CO₂ exchange caused by amplified plant productivity in northern ecosystems. *Science* **351**, 696–699 (2016).
 90. Goetz, S. J., Bunn, A. G., Fiske, G. J. & Houghton, R. A. Satellite-observed photosynthetic trends across boreal North America associated with climate and fire disturbance. *Proc. Natl. Acad. Sci. U. S. A.* **102**, 13521–13525 (2005).
 91. Elmendorf, S. C. *et al.* Plot-scale evidence of tundra vegetation change and links to recent summer warming. *Nat. Clim. Chang.* **2**, 453–457 (2012).

92. Natali, S. M., Schuur, E. A. G., Webb, E. E., Pries, C. E. H. & Crummer, K. G. Permafrost degradation stimulates carbon loss from experimentally warmed tundra. *Ecology* **95**, 602–608 (2014).
93. Natali, S. M. *et al.* Effects of experimental warming of air, soil and permafrost on carbon balance in Alaskan tundra. *Glob. Chang. Biol.* **17**, 1394–1407 (2011).
94. Dorrepaal, E. *et al.* Carbon respiration from subsurface peat accelerated by climate warming in the subarctic. *Nature* **460**, 616–619 (2009).
95. Hicks Pries, C. E., Schuur, E. A. G. & Crummer, K. G. Thawing permafrost increases old soil and autotrophic respiration in tundra: partitioning ecosystem respiration using $\delta(13)C$ and $\Delta(14)C$. *Glob. Chang. Biol.* **19**, 649–661 (2013).
96. Hicks Pries, C. E., Schuur, E. A. G., Natali, S. M. & Crummer, K. G. Old soil carbon losses increase with ecosystem respiration in experimentally thawed tundra. *Nat. Clim. Chang.* **6**, 214–218 (2016).
97. Schuur, E. A. G. *et al.* The effect of permafrost thaw on old carbon release and net carbon exchange from tundra. *Nature* **459**, 556–559 (2009).
98. Natali, S. M. *et al.* Permafrost thaw and soil moisture drive CO₂ and CH₄ release from upland tundra. *J. Geophys. Res. Biogeosciences* **120**, 525–537 (2015).
99. Christensen, T. R. *et al.* Trace gas exchange in a high-Arctic valley: 1. Variations in CO₂ and CH₄ flux between tundra vegetation types. *Global Biogeochem. Cycles* **14**, 701–713 (2000).
100. Kim, Y. Effect of thaw depth on fluxes of CO₂ and CH₄ in manipulated Arctic coastal tundra of Barrow, Alaska. *Sci. Total Environ.* **505**, 385–389 (2015).
101. Oechel, W. C., Vourlitis, G. L., Hastings, S. J., Ault, R. P. & Bryant, P. The effects of water table manipulation and elevated temperature on the net CO₂ flux of wet sedge tundra ecosystems. *Glob. Chang. Biol.* **4**, 77–90 (1998).
102. Olivas, P. C., Oberbauer, S. F., Tweedie, C. E., Oechel, W. C. & Kuchy, A. Responses of CO₂ flux components of Alaskan Coastal Plain tundra to shifts in water table. *J. Geophys. Res.* **115**, G00I05 (2010).
103. Zona, D., Lipson, D. A., Zulueta, R. C., Oberbauer, S. F. & Oechel, W. C. Microtopographic controls on ecosystem functioning in the Arctic Coastal Plain. *J. Geophys. Res.* **116**, G00I08 (2011).
104. Huemmrich, K. F. *et al.* Tundra carbon balance under varying temperature and moisture regimes. *J. Geophys. Res.* **115**, G00I02 (2010).
105. Merbold, L. *et al.* Artificial drainage and associated carbon fluxes (CO₂/CH₄) in a tundra ecosystem. *Glob. Chang. Biol.* **15**, 2599–2614 (2009).
106. Rhew, R. C., Teh, Y. A. & Abel, T. Methyl halide and methane fluxes in the northern Alaskan coastal tundra. *J. Geophys. Res. Biogeosciences* **112**, G02009 (2007).

107. van der Molen, M. K. *et al.* The growing season greenhouse gas balance of a continental tundra site in the Indigirka lowlands, NE Siberia. *Biogeosciences* **4**, 985–1003 (2007).
108. Sturtevant, C. S., Oechel, W. C., Zona, D., Kim, Y. & Emerson, C. E. Soil moisture control over autumn season methane flux, Arctic Coastal Plain of Alaska. *Biogeosciences* **9**, 1423–1440 (2012).
109. Lee, H., Schuur, E. A. G., Inglett, K. S., Lavoie, M. & Chanton, J. P. The rate of permafrost carbon release under aerobic and anaerobic conditions and its potential effects on climate. *Glob. Chang. Biol.* **18**, 515–527 (2012).
110. Coyne, P. I. & Kelley, J. J. Release of carbon dioxide from frozen soil to the Arctic atmosphere. *Nature* **234**, 407–408 (1971).
111. Kelley, J. J., Weaver, D. F. & Smith, B. P. The variation of carbon dioxide under the snow in the Arctic. *Ecology* **49**, 358–361 (1968).
112. Panikov, N. S. & Dedysh, S. N. Cold season CH₄ and CO₂ emission from boreal peat bogs (West Siberia): Winter fluxes and thaw activation dynamics. *Global Biogeochem. Cycles* **14**, 1071–1080 (2000).
113. Webb, E. E. *et al.* Increased wintertime CO₂ loss as a result of sustained tundra warming. *J. Geophys. Res.* **121**, 249–265 (2016).
114. Zimov, S. A. *et al.* Wintertime CO₂ emission from soils of northeastern Siberia. *Arctic* **46**, 197–204 (1993).
115. Zimov, S. A. *et al.* Siberian CO₂ efflux in winter as a CO₂ source and cause of seasonality in atmospheric CO₂. *Clim. Change* **33**, 111–120 (1996).
116. Wille, C., Kutzbach, L., Sachs, T., Wagner, D. & Pfeiffer, E. M. Methane emission from Siberian arctic polygonal tundra: eddy covariance measurements and modeling. *Glob. Chang. Biol.* **14**, 1395–1408 (2008).
117. Mastepanov, M. *et al.* Large tundra methane burst during onset of freezing. *Nature* **456**, 628–630 (2008).
118. Mastepanov, M. *et al.* Revisiting factors controlling methane emissions from high-Arctic tundra. *Biogeosciences* **10**, 5139–5158 (2013).
119. Whalen, S. C. & Reeburgh, W. S. Interannual variations in tundra methane emission: A 4-year time series at fixed sites. *Global Biogeochem. Cycles* **6**, 139–159 (1992).
120. Zona, D. *et al.* Cold season emissions dominate the Arctic tundra methane budget. *Proc. Natl. Acad. Sci. U. S. A.* **113**, 40–45 (2015).
121. Johnson, L. C. *et al.* Effects of drainage and temperature on carbon balance of tussock tundra microcosms. *Oecologia* **108**, 737–748 (1996).
122. Billings, W. D., Luken, J. O., Mortensen, D. A. & Peterson, K. M. Arctic tundra a source or sink for atmospheric carbon dioxide in a changing environment? *Oecologia*

53, 7–11 (1982).

123. Peterson, K. M., Billings, W. D. & Reynolds, D. N. Influence of water-table and atmospheric CO₂ concentration on the carbon balance of Arctic tundra. *Arct. Alp. Res.* **16**, 331–335 (1984).
124. Christiansen, J. R. *et al.* Methane fluxes and the functional groups of methanotrophs and methanogens in a young Arctic landscape on Disko Island, West Greenland. *Biogeochemistry* **122**, 15–33 (2015).
125. Nakano, T., Kuniyoshi, S. & Fukuda, M. Temporal variation in methane emission from tundra wetlands in a permafrost area, northeastern Siberia. *Atmos. Environ.* **34**, 1205–1213 (2000).
126. McCalley, C. K. *et al.* Methane dynamics regulated by microbial community response to permafrost thaw. *Nature* **514**, 478–481 (2014).
127. Høj, L., Rusten, M., Haugen, L. E., Olsen, R. A. & Torsvik, V. L. Effects of water regime on archaeal community composition in Arctic soils. *Environ. Microbiol.* **8**, 984–996 (2006).
128. Christensen, T. R., Jonasson, S., Callaghan, T. V. & Havström, M. Spatial variation in high-latitude methane flux along a transect across Siberian and European tundra environments. *J. Geophys. Res.* **100**, 21035 (1995).
129. Wagner, D., Kobabe, S., Pfeiffer, E.-M. M. & Hubberten, H.-W. W. Microbial controls on methane fluxes from a polygonal tundra of the Lena Delta, Siberia. *Permafrost. Periglac. Process.* **14**, 173–185 (2003).
130. Richards, J. A. & Xiuping, J. in *Remote Sens. Digit. image Anal. an Introd.* 181–222 (Springer-Verlag Berlin Heidelberg, 1999). doi:10.1007/978-3-662-03978-6
131. Parkin, T. B. & Venterea, R. T. in *Sampl. Protoc.* (Follett, R. F.) 3.1–3.39 (2010).
132. Höglberg, P. *et al.* Large-scale forest girdling shows that current photosynthesis drives soil respiration. *Nature* **411**, 789–792 (2001).
133. Rochette, P. & Hutchinson, G. L. in *Micrometeorology Agric. Syst.* 247–286 (American Society of Agronomy, 2005).
134. Luus, K. A. & Lin, J. C. The Polar Vegetation Photosynthesis and Respiration Model: a parsimonious, satellite-data-driven model of high-latitude CO₂ exchange. *Geosci. Model Dev.* **8**, 2655–2674 (2015).
135. Mahadevan, P. *et al.* A satellite-based biosphere parameterization for net ecosystem CO₂ exchange: Vegetation Photosynthesis and Respiration Model (VPRM). *Global Biogeochem. Cycles* **22**, GB2005 (2008).
136. R Development Core Team. R: a language and environment for statistical computing. (2013). at <<http://www.r-project.org>>
137. Zhou, T., Shi, P., Hui, D. & Luo, Y. Global pattern of temperature sensitivity of soil

- heterotrophic respiration (Q10) and its implications for carbon-climate feedback. *J. Geophys. Res.* **114**, G02016 (2009).
138. Bauer, J. E., Williams, P. M. & Druffel, E. R. M. Recovery of submilligram quantities of carbon dioxide from gas streams by molecular sieve for subsequent determination of isotopic carbon-13 and carbon-14 natural abundances. *Anal. Chem.* **64**, 824–827 (1992).
 139. Reimer, P. J., Brown, T. A. & Reimer, R. W. Discussion: Reporting and calibration of post-bomb ^{14}C data. *Radiocarbon* **46**, 1299–1304 (2004).
 140. Schuur, E. A. G. & Trumbore, S. E. Partitioning sources of soil respiration in boreal black spruce forest using radiocarbon. *Glob. Chang. Biol.* **12**, 165–176 (2006).
 141. Bracho, R. *et al.* Temperature sensitivity of organic matter decomposition of permafrost-region soils during laboratory incubations. *Soil Biol. Biochem.* **97**, 1–14 (2016).
 142. Hicks Pries, C. E. *et al.* Decadal warming causes a consistent and persistent shift from heterotrophic to autotrophic respiration in contrasting permafrost ecosystems. *Glob. Chang. Biol.* **21**, 4508–4519 (2015).
 143. Parnell, A. C., Inger, R., Bearhop, S. & Jackson, A. L. Source partitioning using stable isotopes: coping with too much variation. *PLoS One* **5**, e9672 (2010).
 144. Phillips, D. L. & Gregg, J. W. Source partitioning using stable isotopes: coping with too many sources. *Oecologia* **136**, 261–269 (2003).
 145. Caporaso, J. G. *et al.* Global patterns of 16S rRNA diversity at a depth of millions of sequences per sample. *Proc. Natl. Acad. Sci. U. S. A.* **108**, 4516–4522 (2011).
 146. Caporaso, J. G. *et al.* Ultra-high-throughput microbial community analysis on the Illumina HiSeq and MiSeq platforms. *ISME J.* **6**, 1621–1624 (2012).
 147. Gilbert, J. A. *et al.* The Earth Microbiome Project: successes and aspirations. *BMC Biol.* **12**, 69 (2014).
 148. Earth Microbiome Project. at <<http://www.earthmicrobiome.org/emp-standard-protocols/16s/>>
 149. Schloss, P. D. P. *et al.* Introducing mothur: Open-source, platform-independent, community-supported software for describing and comparing microbial communities. *Appl. Environ. Microbiol.* **75**, 7537–7541 (2009).
 150. Edgar, R. C., Haas, B. J., Clemente, J. C., Quince, C. & Knight, R. UCHIME improves sensitivity and speed of chimera detection. *Bioinformatics* **27**, 2194–2200 (2011).
 151. DeLong, E. F. Archaea in coastal marine environments. *Proc. Natl. Acad. Sci. U. S. A.* **89**, 5685–5689 (1992).
 152. Takai, K. & Horikoshi, K. Rapid detection and quantification of members of the archaeal community by quantitative PCR using fluorogenic probes. *Appl. Environ. Microbiol.* **66**, 5066–5072 (2000).

153. Daims, H., Brühl, A., Amann, R., Schleifer, K.-H. & Wagner, M. The domain-specific probe EUB338 is insufficient for the detection of all bacteria: Development and evaluation of a more comprehensive probe set. *Syst. Appl. Microbiol.* **22**, 434–444 (1999).
154. Loy, A. *et al.* Oligonucleotide microarray for 16S rRNA gene-based detection of all recognized lineages of sulfate-reducing prokaryotes in the environment. *Appl. Environ. Microbiol.* **68**, 5064–5081 (2002).
155. Herrmann, M., Hädrich, A. & Küsel, K. Predominance of thaumarchaeal ammonia oxidizer abundance and transcriptional activity in an acidic fen. *Environ. Microbiol.* **14**, 3013–3025 (2012).
156. Lumley, T. *Regression subset selection.* (2015).
157. Ripley, B. *et al.* *Support functions and datasets for Venables and Ripley's MASS.* (2015).
158. Ferreira, C. Gene expression programming: a new adaptive algorithm. in *6th Online World Conf. Soft Comput. Ind. Appl.* (2001).
159. Hansen, N., Müller, S. D. & Koumoutsakos, P. Reducing the time complexity of the derandomized evolution strategy with covariance matrix adaptation (CMA-ES). *Evol. Comput.* **11**, 1–18 (2003).
160. Ilie, I., Dittrich, P., Jung, M., Carvalhais, N. & Mahecha, M. Evolving compact symbolic expressions by a GEP CMA-ES hybrid approach. *Prep.*
161. Coello, C. A. & Montes, E. M. Constraint-handling in genetic algorithms through the use of dominance-based tournament selection. *Adv. Eng. Informatics* **16**, 193–203 (2002).
162. Bonin, A. S. & Boone, D. R. in *The Prokaryotes* (Dworkin, M., Falkow, S., Rosenberg, E., Schleifer, K.-H. & Stackebrandt, E.) 231–243 (Springer New York, 2006). doi:10.1007/0-387-30743-5_11
163. Whitman, W. B., Bowen, T. L. & Boone, D. R. in *The Prokaryotes* (Dworkin, M., Falkow, S., Rosenberg, E., Schleifer, K.-H. & Stackebrandt, E.) 165–207 (Springer New York, 2006). doi:10.1007/0-387-30743-5
164. Hedderich, R. & Whitman, W. B. in *The Prokaryotes* (Rosenberg, E., DeLong, E. F., Lory, S., Stackebrandt, E. & Thompson, F.) 635–662 (Springer Berlin Heidelberg, 2013).
165. Bräuer, S. L., Cadillo-Quiroz, H., Yashiro, E., Yavitt, J. B. & Zinder, S. H. Isolation of a novel acidiphilic methanogen from an acidic peat bog. *Nature* **442**, 192–194 (2006).
166. Kendall, M. M. & Boone, D. R. in *The Prokaryotes* (Dworkin, M., Falkow, S., Rosenberg, E., Schleifer, K.-H. & Stackebrandt, E.) 244–256 (Springer New York, 2006). doi:10.1007/0-387-30743-5_12
167. Garcia, J.-L., Ollivier, B. & Whitman, W. B. in *The Prokaryotes* (Dworkin, M., Falkow,

- S., Rosenberg, E., Schleifer, K.-H. & Stackebrandt, E.) 208–230 (Springer New York, 2006). doi:10.1007/0-387-30743-5_10
168. Großkopf, R., Stubner, S. & Liesack, W. Novel euryarchaeotal lineages detected on rice roots and in the anoxic bulk soil of flooded rice microcosms. *Appl. Environ. Microbiol.* **64**, 4983–4989 (1998).
 169. Mondav, R. *et al.* Discovery of a novel methanogen prevalent in thawing permafrost. *Nat. Commun.* **5**, 3212 (2014).
 170. Baani, M. & Liesack, W. Two isozymes of particulate methane monooxygenase with different methane oxidation kinetics are found in *Methylocystis* sp. strain SC2. *Proc. Natl. Acad. Sci. U. S. A.* **105**, 10203–10208 (2008).
 171. Bowman, J. in *The Prokaryotes* (Dworkin, M., Falkow, S., Rosenberg, E., Schleifer, K.-H. & Stackebrandt, E.) 266–289 (Springer New York, 2006). doi:10.1007/0-387-30745-1_15
 172. Dunfield, P. F. *et al.* Isolation of a *Methylocystis* strain containing a novel *pmoA*-like gene. *FEMS Microbiol. Ecol.* **41**, 17–26 (2002).
 173. Hanson, R. S. & Hanson, T. E. Methanotrophic bacteria. *Microbiol. Rev.* **60**, 439–471 (1996).
 174. Yimiga, M. T., Dunfield, P. F., Ricke, P., Heyer, J. & Liesack, W. Wide distribution of a novel *pmoA*-like gene copy among type II methanotrophs, and its expression in *Methylocystis* strain SC2. *Appl. Environ. Microbiol.* **69**, 5593–5602 (2003).
 175. Danilova, O. V. *et al.* *Methylomonas paludis* sp. nov., the first acid-tolerant member of the genus *Methylomonas*, from an acidic wetland. *Int. J. Syst. Evol. Microbiol.* **63**, 2282–2289 (2013).
 176. Dedysh, S. N. *et al.* *Methylocella palustris* gen. nov., sp. nov., a new methane-oxidizing acidophilic bacterium from peat bogs, representing a novel subtype of serine-pathway methanotrophs. *Int. J. Syst. Evol. Microbiol.* **50**, 955–969 (2000).
 177. Dedysh, S. N. *et al.* *Methylocella tundrae* sp. nov., a novel methanotrophic bacterium from acidic tundra peatlands. *Int. J. Syst. Evol. Microbiol.* **54**, 151–156 (2004).
 178. Dunfield, P. F., Khmelenina, V. N., Suzina, N. E., Trotsenko, Y. A. & Dedysh, S. N. *Methylocella silvestris* sp. nov., a novel methanotroph isolated from an acidic forest cambisol. *Int. J. Syst. Evol. Microbiol.* **53**, 1231–1239 (2003).
 179. Schwarz, P. A., Fahey, T. J. & Dawson, T. E. Seasonal air and soil temperature effects on photosynthesis in red spruce (*Picea rubens*) saplings. *Tree Physiol.* **17**, 187–194 (1997).
 180. Lawrence, W. T. & Oechel, W. C. Effects of soil temperature on the carbon exchange of taiga seedlings. II. Photosynthesis, respiration, and conductance. *Can. J. For. Res.* **13**, 850–859 (1983).
 181. Boone, R. D., Nadelhoffer, K. J., Canary, J. D. & Kaye, J. P. Roots exert a strong

- influence on the temperature sensitivity of soil respiration. *Nature* **396**, 570–572 (1998).
182. Chanton, J. P., Whiting, G. J., Happell, J. D. & Gerard, G. Contrasting rates and diurnal patterns of methane emission from emergent aquatic macrophytes. *Aquat. Bot.* **46**, 111–128 (1993).
 183. Atanasiu, L. Photosynthesis and respiration of three mosses at winter low temperatures. *Bryologist* **74**, 23–27 (1971).
 184. Tokida, T. *et al.* Falling atmospheric pressure as a trigger for methane ebullition from peatland. *Global Biogeochem. Cycles* **21**, GB2003 (2007).
 185. Mattson, M. D. & Likens, G. E. Air pressure and methane fluxes. *Nature* **347**, 718–719 (1990).
 186. Green, J. C. Modelling flow resistance in vegetated streams: review and development of new theory. *Hydrol. Process.* **19**, 1245–1259 (2005).
 187. Allan, J. D. in *Stream Ecol. Struct. Funct. Run. Waters* 1–22 (Chapman and Hall, 1995). doi:10.1007/978-1-4020-5583-6
 188. Lakshmi, V., Jackson, T. J. & Zehrhuhs, D. Soil moisture-temperature relationships: results from two field experiments. *Hydrol. Process.* **17**, 3041–3057 (2003).
 189. Reginato, R. J. *et al.* Soil water content and evaporation determined by thermal parameters obtained from ground-based and remote measurements. *J. Geophys. Res.* **81**, 1617–1620 (1976).
 190. Idso, S. B., Schugge, T. J., Jackson, R. D. & Reginato, R. J. The utility of surface temperature measurements for the remote sensing of surface soil water status. *J. Geophys. Res.* **80**, 3044–3049 (1975).
 191. Abu-Hamdeh, N. H. Thermal properties of soils as affected by density and water content. *Biosyst. Eng.* **86**, 97–102 (2003).
 192. Rouse, W. R., Carlson, D. W. & Weick, E. J. Impacts of summer warming on the energy and water balance of wetland tundra. *Clim. Change* **22**, 305–326 (1992).
 193. Blok, D. *et al.* Shrub expansion may reduce summer permafrost thaw in Siberian tundra. *Glob. Chang. Biol.* **16**, 1296–1305 (2010).
 194. Bonfils, C. J. W. *et al.* On the influence of shrub height and expansion on northern high latitude climate. *Environ. Res. Lett.* **7**, 015503 (2012).
 195. Chapin, F. S., Matson, P. A. & Vitousek, P. M. in *Princ. Terr. Ecosyst. Ecol.* 339–367 (Springer New York, 2012). doi:10.1007/978-1-4419-9504-9
 196. Niinemets, Ü. Responses of forest trees to single and multiple environmental stresses from seedlings to mature plants: Past stress history, stress interactions, tolerance and acclimation. *For. Ecol. Manage.* **260**, 1623–1639 (2010).
 197. Shaver, G. R. & Jonasson, S. in *Terr. Glob. Product.* 189–210 (Elsevier, 2001).

doi:10.1016/B978-012505290-0/50024-7

198. Hobbie, S. E. Temperature and plant species control over litter decomposition in Alaskan tundra. *Ecol. Monogr.* **66**, 503–522 (2008).
199. Schädel, C. *et al.* Circumpolar assessment of permafrost C quality and its vulnerability over time using long-term incubation data. *Glob. Chang. Biol.* **20**, 641–652 (2014).
200. Tape, K., Sturm, M. & Racine, C. The evidence for shrub expansion in Northern Alaska and the Pan-Arctic. *Glob. Chang. Biol.* **12**, 686–702 (2006).
201. Myers-Smith, I. H. *et al.* Climate sensitivity of shrub growth across the tundra biome. *Nat. Clim. Chang.* **5**, 887–891 (2015).
202. Colmer, T. D. Long-distance transport of gases in plants: a perspective on internal aeration and radial oxygen loss from roots. *Plant, Cell Environ.* **26**, 17–36 (2003).
203. Vartapetian, B. B. in *Interact. Stress. Plants a Chang. Clim.* (Jackson, M. B. & Black, C. R.) 231–241 (Springer Science & Business Media, 2013).
204. Westermann, P. Temperature regulation of methanogenesis in wetlands. *Chemosphere* **26**, 321–328 (1993).
205. Yvon-Durocher, G. *et al.* Methane fluxes show consistent temperature dependence across microbial to ecosystem scales. *Nature* **507**, 488–491 (2014).
206. Chanton, J. P. & Dacey, J. W. H. in *Trace gas Emiss. by plants* (Sharkey, T. D., Holland, E. A. & Mooney, H. A.) 65–92 (Academic Press, Inc., 1991).
207. Liebner, S. & Wagner, D. Abundance, distribution and potential activity of methane oxidizing bacteria in permafrost soils from the Lena Delta, Siberia. *Environ. Microbiol.* **9**, 107–117 (2007).
208. Hultman, J. *et al.* Multi-omics of permafrost, active layer and thermokarst bog soil microbiomes. *Nature* **521**, 208–212 (2015).
209. Tveit, A. T., Urich, T., Frenzel, P. & Svenning, M. M. Metabolic and trophic interactions modulate methane production by Arctic peat microbiota in response to warming. *Proc. Natl. Acad. Sci. U. S. A.* **112**, E2507–E2516 (2015).
210. Kravchenko, I. K., Kizilova, A. K., Bykova, S. A., Men’ko, E. V. & Gal’chenko, V. F. Molecular analysis of high-affinity methane-oxidizing enrichment cultures isolated from a forest biocenosis and agrocenoses. *Microbiology* **79**, 106–114 (2010).
211. Rivkina, E. *et al.* Microbial life in permafrost. *Adv. Sp. Res. Off. J. Comm. Sp. Res.* **33**, 1215–1221 (2004).
212. Rivkina, E. *et al.* Biogeochemistry of methane and methanogenic archaea in permafrost. *FEMS Microbiol. Ecol.* **61**, 1–15 (2007).
213. Schimel, J. P. *et al.* Cold-season production of CO₂ in Arctic soils: Can laboratory and field estimates be reconciled through a simple modeling approach? *Arctic, Antarct. Alp.*

Res. **38**, 249–256 (2006).

214. Friborg, T., Christensen, T. R. & Søgaard, H. Rapid response of greenhouse gas emission to early spring thaw in a subarctic mire as shown by micrometeorological techniques. *Geophys. Res. Lett.* **24**, 3061–3064 (1997).
215. Winston, G. C., Sundquist, E. T., Stephens, B. B. & Trumbore, S. E. Winter CO₂ fluxes in a boreal forest. *J. Geophys. Res. Atmos.* **102**, 28795–28804 (1997).
216. Smith, K. ., Thomson, P. ., Clayton, H., McTaggart, I. . & Conen, F. Effects of temperature, water content and nitrogen fertilisation on emissions of nitrous oxide by soils. *Atmos. Environ.* **32**, 3301–3309 (1998).
217. Moosavi, S. C., Crill, P. M., Pullman, E. R., Funk, D. W. & Peterson, K. M. Controls on CH₄ flux from an Alaskan boreal wetland. *Global Biogeochem. Cycles* **10**, 287–296 (1996).
218. Matthias, A. D., Yarger, D. N. & Weinbeck, R. S. A numerical evaluation of chamber methods for determining gas fluxes. *Geophys. Res. Lett.* **5**, 765–768 (1978).
219. Hutchinson, G. L., Livingston, G. P., Healy, R. W. & Striegl, R. G. Chamber measurement of surface-atmosphere trace gas exchange: Numerical evaluation of dependence on soil, interfacial layer, and source/sink properties. *J. Geophys. Res.* **105**, 8865–8875 (2000).
220. Kutzbach, L. *et al.* CO₂ flux determination by closed-chamber methods can be seriously biased by inappropriate application of linear regression. *Biogeosciences* **4**, 1005–1025 (2007).
221. Fry, B. in *Stable Isot. Ecol.* 40–75 (Springer-Verlag New York, 2006). doi:10.1007/0-387-33745-8
222. Attendorn, H. G. & Bowen, R. N. C. in *Radioact. Stable Isot. Geol.* 244–267 (Springer Netherlands, 1997). doi:10.1007/978-94-011-5840-4
223. Boström, B., Comstedt, D. & Ekblad, A. Isotope fractionation and ¹³C enrichment in soil profiles during the decomposition of soil organic matter. *Oecologia* **153**, 89–98 (2007).
224. Nadelhoffer, K. J. & Fry, B. Controls on natural nitrogen-15 and carbon-13 abundances in forest soil organic matter. *Soil Sci. Soc. Am. J.* **52**, 1633–1640 (1988).
225. Wynn, J. G., Bird, M. I. & Wong, V. N. L. Rayleigh distillation and the depth profile of ¹³C/¹²C ratios of soil organic carbon from soils of disparate texture in Iron Range National Park, Far North Queensland, Australia. *Geochim. Cosmochim. Acta* **69**, 1961–1973 (2005).
226. Bowling, D. R., Pataki, D. E. & Randerson, J. T. Carbon isotopes in terrestrial ecosystem pools and CO₂ fluxes. *New Phytol.* **178**, 24–40 (2008).
227. Pataki, D. E. *et al.* The application and interpretation of Keeling plots in terrestrial carbon cycle research. *Global Biogeochem. Cycles* **17**, 1022 (2003).

228. Chanton, J., Chaser, L., Glasser, P. & Siegel, D. in *Stable Isot. Biosph. Interact.* (Flanagan, L. B., Ehleringer, J. R. & Pataki, D. E.) 85–105 (Elsevier, 2005).
229. Ramette, A. & Tiedje, J. M. Multiscale responses of microbial life to spatial distance and environmental heterogeneity in a patchy ecosystem. *Proc. Natl. Acad. Sci. U. S. A.* **104**, 2761–2766 (2007).
230. Horner-Devine, M. C., Lage, M., Hughes, J. B. & Bohannon, B. J. M. A taxa-area relationship for bacteria. *Nature* **432**, 750–753 (2004).
231. Haichar, F. Z. *et al.* Plant host habitat and root exudates shape soil bacterial community structure. *ISME J.* **2**, 1221–1230 (2008).
232. Shi, S. *et al.* Effects of selected root exudate components on soil bacterial communities. *FEMS Microbiol. Ecol.* **77**, 600–610 (2011).
233. Wang, W. ., Dalal, R. ., Moody, P. . & Smith, C. . Relationships of soil respiration to microbial biomass, substrate availability and clay content. *Soil Biol. Biochem.* **35**, 273–284 (2003).
234. Rochette, P. & Gregorich, E. G. Dynamics of soil microbial biomass C, soluble organic C and CO₂ evolution after three years of manure application. *Can. J. Soil Sci.* **78**, 283–290 (1998).
235. Allison, S. D., Wallenstein, M. D. & Bradford, M. A. Soil-carbon response to warming dependent on microbial physiology. *Nat. Geosci.* **3**, 336–340 (2010).
236. Schimel, J. P., Gullledge, J. M., Clein-Curley, J. S., Lindstrom, J. E. & Braddock, J. F. Moisture effects on microbial activity and community structure in decomposing birch litter in the Alaskan taiga. *Soil Biol. Biochem.* **31**, 831–838 (1999).
237. Ratering, S. & Conrad, R. Effects of short-term drainage and aeration on the production of methane in submerged rice soil. *Glob. Chang. Biol.* **4**, 397–407 (1998).
238. Waddington, J. M. & Day, S. M. Methane emissions from a peatland following restoration. *J. Geophys. Res. Biogeosciences* **112**, G03018 (2007).
239. Komulainen, V.-M., Nykänen, H., Martikainen, P. J. & Laine, J. Short-term effect of restoration on vegetation change and methane emissions from peatlands drained for forestry in southern Finland. *Can. J. For. Res.* **28**, 402–411 (1998).
240. Christensen, T. R. & Cox, P. Response of methane emission from Arctic tundra to climate change: results from a model simulation. *Tellus* **47B**, 301–309 (1995).
241. Oberbauer, S. F., Starr, G. & Pop, E. W. Effects of extended growing season and soil warming on carbon dioxide and methane exchange of tussock tundra in Alaska. *J. Geophys. Res.* **103**, 29075–29082 (1998).
242. Chapin, F. S. Direct and indirect effects of temperature on arctic plants. *Polar Biol.* **2**, 47–52 (1983).
243. Tieszen, L. L. Photosynthesis and respiration in Arctic tundra grasses: Field light

- intensity and temperature responses. *Arct. Alp. Res.* **5**, 239–251 (1973).
244. Feller, G. & Gerday, C. Psychrophilic enzymes: hot topics in cold adaptation. *Nat. Rev. Microbiol.* **1**, 200–208 (2003).
 245. Bond-Lamberty, B. & Thomson, A. Temperature-associated increases in the global soil respiration record. *Nature* **464**, 579–582 (2010).
 246. Keeling, C. D., Chin, J. F. S. & Whorf, T. P. Increased activity of northern vegetation inferred from atmospheric CO₂ measurements. *Nature* **382**, 146–149 (1996).
 247. Randerson, J. T., Thompson, M. V., Conway, T. J., Fung, I. Y. & Field, C. B. The contribution of terrestrial sources and sinks to trends in the seasonal cycle of atmospheric carbon dioxide. *Global Biogeochem. Cycles* **11**, 535–560 (1997).
 248. Graven, H. D. *et al.* Enhanced seasonal exchange of CO₂ by northern ecosystems since 1960. *Science* (80-.). **341**, 1085–1089 (2013).
 249. Forkel, M. *et al.* Codominant water control on global interannual variability and trends in land surface phenology and greenness. *Glob. Chang. Biol.* **21**, 3414–3435 (2015).

Acknowledgement

I would like to express my gratitude to everyone who made this work possible.

I would like to express my appreciation to my advisor, Dr. Mathias Göckede, and co-advisors, Prof. Dr. Martin Heimann, Prof. Dr. Kirsten Küsel, and Prof. Dr. Edward A. G. Schuur, for their great support and guidance. I have learned a lot from them not only academically but also personally.

I would like to thank my Russian family, the Zimovs. Sergey, Galya, Nikita and Nastya provided wonderful hospitality, and I would not be able to carry out this research without them. I thank Vladimir Tatayev and many other staff members at NESS as well.

Whenever I needed help, a lot of people at MPI supported me: Steffi Rothhardt, John Schmidt, and Anna Görner always gave a big hand; Olaf Kolle, Martin Hertel, Karl Kübler, Agnes Fastnacht, Nadine Hempel, Kerstin Hippler, Axel Steinhof, Frank Voigt, Waldemar Ziegler, Ines Hilke, Willi A. Brand, and many others greatly supported me. I would like to thank the group members as well, Karel Castro-Morales, Ina Burjack, Sandra Bölck, Fanny Kittler, and Friedemann Reum.

I would like to gratefully thank my family and friends:아빠, 엄마, 오빠 for being my family; Sebastian Heynold, Talie Musavi, Ina Burjack, Iulia Ilie, Gaurav Sharma, Johannes Meyerholt, Martin Kunz, Mirco Migliavacca, Sabrina Arnold, John H. Kim, Fabio Boschetti, Sung-Bin Park, Shreeya Verma, Chirag Dhara, and many other warm-hearted people; and additionally, Ina Burjack and Sebastian Heynold for translating the summary into German.

This work has been financially supported by the European Commission (FP7-ENV-2011, Grant Agreement No. 282700), German Ministry of Education and Research (CarboPerm-Project, BMBF Grant No. 03G0836G), and the International Max Planck Research School for Global Biogeochemical Cycles (IMPRS-gBGC).

Contributions of others: Felix Beulig advised on microbial analysis, processed sequence data, and wrote the method section for microbial analysis; Iulia Ilie conducted CMAGEP analysis and wrote the related method section; Miguel D. Mahecha advised on CMAGEP analysis and wrote the method section of it; Marcus Wildner assisted with field work in 2014 and estimated the proportion of ebullition; Joel E. Kostka carried out Illumina sequencing and wrote the method section for sequencing; Ines Hilke carried out soil analysis in Jena; Olaf Kolle set up the field experiment; Lutz Merbold advised on designing and conducting the experiment; Kristina A. Luus advised on CO₂ flux interpolation; Caitlin Hicks Pries advised on partitioning and statistical analyses; Axel Steinhof carried out radiocarbon analysis; and Martin Heimann, Kirsten Küsel, Edward A. G. Schuur, Mathias Göckede, Nikita Zimov, and Sergey A. Zimov advised on designing and conducting the experiment throughout the project.

Declaration of independent completion of dissertation

I hereby declare that this thesis is the result of my own investigation under the supervision of Prof. Dr. Martin Heimann, Prof. Dr. Kirsten Küsel, Prof. Dr. Edward A. G. Schuur, and Dr. Mathias Göckede. Contributions of others are mentioned and indicated in the acknowledgement.

I confirm that I have read the “Course of Examination for Doctoral Candidates (Promotionsordnung)” issued by the Faculty of Biology and Pharmacy of the Friedrich-Schiller University. Neither doctoral consultants (Promotionsberater) nor third parties assisted with writing this dissertation or received direct or indirect financial rewards in relation with this dissertation. In addition, this dissertation has not been submitted as thesis for scientific examination to the Friedrich-Schiller University or any other university.

Jena, 28.11.2016

Minjung Kwon

Published or pending manuscripts

Materials on CO₂ fluxes: Min Jung Kwon, Martin Heimann, Olaf Kolle, Kristina A. Luus, Edward A. G. Schuur, Nikita Zimov, Sergey A. Zimov, Mathias Göckede. Long-term drainage reduces CO₂ uptake and increases CO₂ emission on a Siberian floodplain due to shifts in vegetation community and soil thermal characteristics. *Biogeosciences* 13: 4219–4235.

Materials on R_{eco} partitioning: Min Jung Kwon, Axel Steinhof, Susan M. Natali, Caitlin Hicks Pries, Edward A. G. Schuur, K. G. Crummer, Nikita Zimov, Sergey A. Zimov, Martin Heimann, Olaf Kolle, Mathias Göckede. Drainage decreases deep soil contributions to ecosystem respiration in tundra ecosystems. This manuscript is planned to be submitted to *Environmental Research Letters* (in preparation).

Materials on CH₄ fluxes: Min Jung Kwon, Felix Beulig, Iulia Ilie, Marcus Wildner, Kirsten Küsel, Lutz Merbold, Miguel D. Mahecha, Nikita Zimov, Sergey A. Zimov, Martin Heimann, Edward A. G. Schuur, Joel E. Kostka, Olaf Kolle, Ines Hilke, Mathias Göckede. Plants, microorganisms and soil temperatures contribute to a decrease in methane fluxes on a drained Arctic floodplain. *Global Change Biology* (doi: 10.1111/gcb.13558).